

SYNTHESIS AND CHARACTERIZATION OF
ELECTROACTIVE ORGANOSILANES

by

David Allen Lee

A thesis submitted to the faculty of
The University of North Carolina at Charlotte
in partial fulfillment of the requirements
for the degree of Master of Science in
Chemistry

Charlotte

2015

Approved by:

Dr. Thomas A. Schmedake

Dr. Daniel S. Jones

Dr. Michael G. Walter

Dr. Maciej A. Noras

©2015
David Allen Lee
ALL RIGHTS RESERVED

ABSTRACT

DAVID ALLEN LEE. Synthesis and characterization of electroactive organosilanes.
(Under the direction of DR. THOMAS A. SCHMEDAKE)

Siloles, or silacyclopentadienes, have unique electronic properties due to interaction between the butadiene π^* orbital and the silylene σ^* orbital. Consequently they have drawn interest for use in a variety of organic electronic interactions. A silylene bridged viologen has been synthesized for use in electrochromic applications. Lithiation of 3,3'-dibromo-4,4'-bipyridine and subsequent reaction with dichlorodimethylsilane leads to the corresponding dipyridinosilole. The dipyridinosilole can be converted to the methyl viologen analogue by reaction with methyl triflate. It is stable and can be isolated but hydrolyses upon exposure to air. Its electrochemical, spectroelectrochemical, and spectroscopic properties have been investigated.

Similar chemistry was exploited to synthesize spiro-linked siloles for use in electronic applications. Lithiation of dibromo-2,2'-diiodobiphenyls followed by reaction with SiCl_4 leads to the corresponding tetrabromospirosilabifluorenes. The tetrabromospirosilabifluorenes were explored for their suitability toward Buchwald-Hartwig amination and Suzuki coupling, but the spiro linkage was found to cleave under basic conditions.

ACKNOWLEDGEMENTS

First and foremost, I would like to thank Dr. Schmedake for all his help and guidance over the past four years. I have learned an enormous amount under his instruction and grown greatly as a researcher. Dr. Jones and his research group for their hard work in solving all the crystal structures. Dr. Walter and Dr. Noras for their time and being part of my thesis committee. Dr. Merkert for running the CVs. Dr. Carlin for keeping all the departmental instruments running, without which research could not progress. The many professors in the chemistry department I have had over the years who have stimulated my interest in and expanded my knowledge of chemistry, of whom there are too many to list here. Finally, I would like to thank the rest of the Schmedake group for their continual advice and support in the lab.

TABLE OF CONTENTS

LIST OF EQUATIONS	viii
LIST OF FIGURES	ix
LIST OF SCHEMES	xi
LIST OF COMPOUNDS	xii
LIST OF ABBREVIATIONS	xiii
CHAPTER 1: INTRODUCTION	1
1.1 Overview of Electroactive Silicon Compounds	1
1.1.1 Polysilanes	2
1.1.2 Siloles	3
1.1.3 Porphyrins	5
1.1.4 Polypyridyl Silanes	5
1.2 Introduction to Electrochemistry	6
1.2.1 Cyclic Voltammetry	6
1.2.2 Spectroelectrochemistry	7
CHAPTER 2: VIOLOGENS	9
2.1 Background	9
2.2 Dimethyldipyridosilole	11
2.2.1 Synthesis and Structure	11
2.2.2 3,5-Dibromo-4,4-Bipyridine	14
2.3 Siloloviologen	15
2.3.1 Synthesis and Structure	15
2.3.2 Hydrolysis Kinetics	18

2.3.3	Electrochemistry and Spectroscopy	21
2.4	Experimental	26
2.4.1	Instrumentation and General Methods	26
2.4.2	Synthetic Details	27
2.5	Discussion	30
CHAPTER 3: SPIROSILABIFLUORENES		34
3.1	Background	34
3.1.1	Spirobifluorenes	34
3.1.2	Spirosilabifluorenes	40
3.2	Spiro-sila-OMeTAD	44
3.2.1	Tetrabromospirosilabifluorenes	45
3.2.2	Cross Coupling Reactions	48
3.3	Experimental	52
3.3.1	Instrumentation and General Methods	52
3.3.2	Synthetic Details	54
3.4	Discussion	60
CHAPTER 4: CONCLUSION AND FUTURE WORK		62
REFERENCES		65
APPENDIX A: CRYSTALLOGRAPHIC DATA		72
APPENDIX B: DIMETHYLDIPYRIDOSILOLE SPECTRA		73
APPENDIX C: SILOLOVIOLOGEN SPECTRA		77
APPENDIX D: SILOLOVIOLOGEN HYDROLYSIS DATA		81
APPENDIX E: 3,5-DIBROMO-4-4'-BIPYRIDINE SPECTRA		82

APPENDIX F: 3,3',6,6'-TETRABROMOSPIROSILABIFLUORENE SPECTRA 85

APPENDIX G: 2,2',7,7'-TETRABROMOSPIROSILABIFLUORENE SPECTRA 89

LIST OF EQUATIONS

EQUATION 1: The Randles-Sevcik equation at 25 °C	7
EQUATION 2: Second order rate equation and first order approximation	18
EQUATION 3: Integral representation of the first order rate equation	18
EQUATION 4: Intermolecular hopping rate as a function of temperature, overlap integral, and reorganization energy	43
EQUATION 5: Calculation of hole reorganization energy	44

LIST OF FIGURES

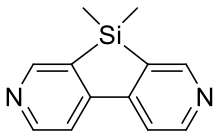
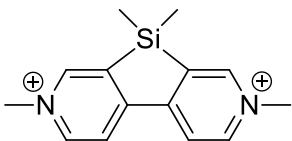
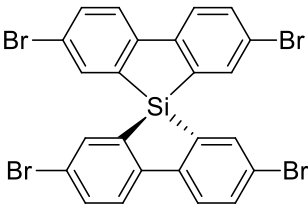
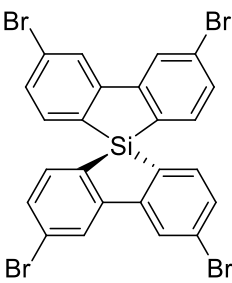
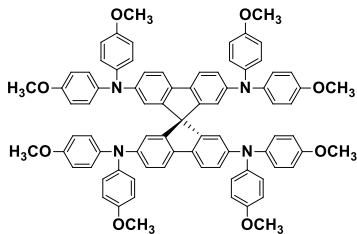
FIGURE 1: Effect of dihedral angle ω on σ and σ^* orbital energies of polysilanes	3
FIGURE 2: Delocalization of the LUMO of silole due to $\sigma^*-\pi^*$ conjugation	4
FIGURE 3: The redox states of methyl viologen	9
FIGURE 4: Heteroatom bridged methyl viologens and bipyridines	10
FIGURE 5: ORTEP representation of dimethyldipyridosilole	13
FIGURE 6: UV-Vis absorbance of dimethyldipyridosilole	14
FIGURE 7: ORTEP representation of 3,5-dibromo-4,4'-bipyridine	15
FIGURE 8: ORTEP representation of hydrolyzed siloloviologen iodide	16
FIGURE 9: ORTEP representation of siloloviologen with triflate counterions removed	16
FIGURE 10: Attempted ESI-MS of SiMV with assigned species	17
FIGURE 11: Pseudo first order kinetics plot of the hydrolysis of SiMV in acetonitrile- d_3	19
FIGURE 12: $^1\text{H-NMR}$ of SiMV with H_2O in CD_3CN after 15.5 days	19
FIGURE 13: Pseudo first order kinetics plot of the hydrolysis of SiMV in D_2O	20
FIGURE 14: CV of SiMV in CH_3CN	21
FIGURE 15: Plots of peak forward current versus scan rate for the first and second reductions of SiMV	22
FIGURE 16: UV-Vis absorbance of 10^{-5} M SiMV in CH_3CN	22
FIGURE 17: Spectroelectrochemistry of SiMV in CH_3CN	24
FIGURE 18: Fluorescence excitation and emission spectra of SiMV	25
FIGURE 19: Emission of fresh sample of SiMV superimposed on a sample after repeated irradiation	25
FIGURE 20: Spirobifluorene	35

FIGURE 21: The many uses of spirobifluorene derivatives	36
FIGURE 22: The DSSC	37
FIGURE 23: Common OLED architectures	40
FIGURE 24: Spirosilabifluorenes studied by Kawashima et al.	42
FIGURE 25: Tetrakis(dimethylamine)spirobifluorenes modeled by DFT	44
FIGURE 26: ORTEP representations of 3,3',6,6'-tetrabromospirosilabifluorene and 2,2',7,7'-tetrabromospirosilabifluorene	47
FIGURE 27: UV-Vis absorbance spectra of tetrabromospirobifluorenes	48
FIGURE 28: MALDI-TOF-MS of spiro-sila-OMeTAD reaction product	49
FIGURE 29: MALDI-TOF-MS of tetratolyl spirosilabifluorene reaction product	51
FIGURE 30: MALDI-TOF-MS of tetratolyl spirobifluorene	52

LIST OF SCHEMES

SCHEME 1: Synthesis of dimethyldipyridosilole	12
SCHEME 2: Synthesis of 3,5-dibromo-4,4'-bipyridine	14
SCHEME 3: Methylation of dimethyldipyridosilole	15
SCHEME 4: Pyridone formation from methyl viologen	32
SCHEME 5: Comparison of synthetic routes to tetrasubstituted spirobifluorenes and spirosilabifluorenes	41
SCHEME 5: Synthetic approach toward spiro-sila-OMeTADs	45
SCHEME 6: Synthesis of 5,5'-dibromo-2,2'-diiodobiphenyl	46
SCHEME 7: Synthesis of 4,4'-dibromo-2,2'-diiodobiphenyl	47
SCHEME 8: Attempted synthesis of 3,3',6,6'-tetratolylspirosilabifluorene	50
SCHEME 9: Summary of the reactivity of 3,3',6,6'-tetrabromo-spirosilabifluorene	61
SCHEME 10: Proposed alternative synthesis of 3,3',6,6'-spiro-sila-OMeTAD	63

LIST OF COMPOUNDS

Structure	Name	Abbreviation
	dimethyldipyridosilole	DPS
	methyl siloloviologen	SiMV
	2,2',7,7'-tetrabromo-spirosilabifluorene	27-tbssbf
	3,3',6,6'-tetrabromo-spirosilabifluorene	36-tbssbf
	2,2',7,7'-tetrakis(N,N-di-p-methoxy phenylamino)-9,9'-spirobifluorene	Spiro-OMeTAD

LIST OF ABBREVIATIONS

CV	cyclic voltammetry
DFT	density functional theory
DMF	dimethylformamide
dppf	1,1'-Bis(diphenylphosphino)ferrocene
DSSC	dye-sensitized solar cell
EI-MS	electron impact mass spectrometry
ESI-MS	electrospray ionization mass spectrometry
EtOH	ethanol
HOMO	highest occupied molecular orbital
HTM	hole transport material
LDA	lithium diisopropylamide
LUMO	lowest unoccupied molecular orbital
MALDI	matrix-assisted light desorption/ionization
n-BuLi	n-butyl lithium
NMR	nuclear magnetic resonance spectroscopy
OLED	organic light emitting diode
ORTEP	Oak Ridge thermal ellipsoid plot
t-BuONa	sodium tert-butoxide
T _g	glass transition temperature
THF	tetrahydrofuran
TOF-MS	time-of-flight mass spectrometry

CHAPTER 1: INTRODUCTION

1.1 Overview of Electroactive Silicon Compounds

For over half a century silicon has been synonymous with the electronics industry. Terms such as “silicon valley” and the “silicon age” have long since entrenched themselves in the modern vernacular. It’s not hyperbole to suggest that silicon has fundamentally impacted mankind to an extent few elements have. The development of the silicon transistor in the 1950’s was followed by rapid improvements in digital computers.¹ Silicon semiconductor technology has consequently formed the basis of our information and communication technology. Today computers and other electronic devices, all containing silicon, are ubiquitous in modern society.

These devices of course use silicon in its crystalline forms. Organosilicon materials, those containing silicon-carbon bonds, have in contrast received relatively little fanfare. Commercially they are most important in the form of silicones, whose electronic applications are limited to sealing and encapsulating electronic components.

Organosilicon compounds capable of playing an active role in electronics are less common, and at this stage are more of academic interest than practical use. That this academic interest exists however is a hint at their potential. The field of organic electronics has grown greatly in recent decades, in part because of the unique properties and tunability afforded by the inclusion of heteroatoms such as silicon in carbon-based molecules. Siloles are the focus of this work, but the potential of organosilicon

compounds for electronic applications extends to polysilanes and hypervalent silicon species.

1.1.1 Polysilanes

Polysilanes, polymers consisting of an all silicon backbone, have been known since the 1920's. However, it wasn't until the late 1970's that this class of compounds began to garner serious scientific interest. In addition to having excellent thermal and mechanical properties, polysilanes are unique in that in contrast to their carbon analogues the σ -backbone is highly delocalized.² This leads to a relatively small HOMO-LUMO gap of around 4 eV and strong near UV absorbance. Polysilanes are typically synthesized by Wurtz-type reductive couplings of dichloro-organosilanes.³

While intrinsic insulators, polysilanes can be doped to sufficient levels to act as semiconductors with p-type charge transport. Doping with C_{60} has been shown to increase the photoconductivity.^{4,5} The hole transporting ability of simple polysilanes such as poly(methylphenylsilane) is sufficient to serve as the hole transporting material of organic light emitting diodes.⁶ Furthermore, diaryl polysilanes display enhanced electroluminescence properties and have been used as emitters in OLEDs.⁶

A unique property of polysilanes is that their electronic spectra change dramatically as a result of conformational backbone changes. Conformers with large SiSiSiSi dihedral angles strongly show the effects of σ conjugation, while small dihedral angles behave as defects which suppress conjugation.⁷ One consequence of this is thermochromism. Solutions of poly(di-n-hexylsilylene) were found to exhibit a broad absorption around 320 nm at room temperature.⁸ As the temperature was decreased to -55

°C, this peak disappeared and was replaced by new bands at 357 and 368 nm. These are attributed to an unwinding of the polymer chain as the temperature is decreased.

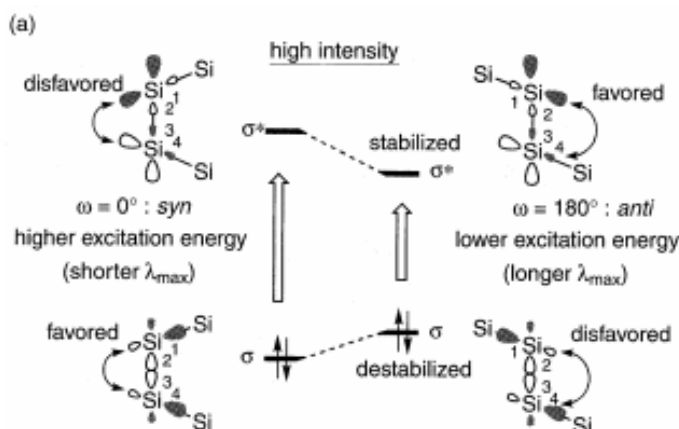


Figure 1: Effect of dihedral angle ω on σ and σ^* orbital energies of polysilanes.⁹

1.1.2 Siloles

Siloles, silacyclopentadiene derivatives, have unique electronic properties due to $\sigma^*-\pi^*$ conjugation stemming from interaction between the exocyclic silylene σ^* orbital and the π^* orbital of the butadiene fragment.¹⁰ The σ^* orbitals are forced to be orthogonal to the plane of the π system and have the correct symmetry and energy to interact with the π^* orbital, causing the LUMO to be further delocalized. Analogous conjugation is absent in cyclopentadiene as the energy of the σ^* orbital is too high to permit significant interaction. This LUMO stabilization makes siloles excellent electron acceptors, and siloles have been studied extensively as electron transporting and emissive materials.

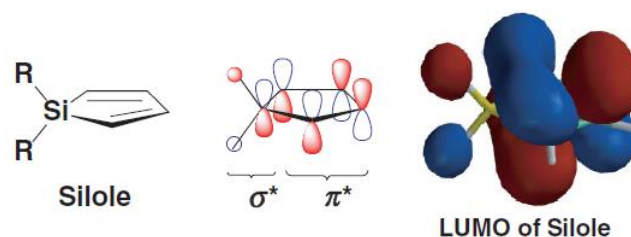


Figure 2: Delocalization of the LUMO of silole due to σ^* - π^* conjugation.¹¹

Aggregation induced emission has been demonstrated in 1,1-disubstituted 2,3,4,5-tetraphenyl siloles and their polymers.¹² These compounds are weak emitters in solution but exhibit an improvement in photoluminescence by up to two orders of magnitude in the solid state. This is contrary to most organic chromophores which form less emissive species such as excimers upon aggregation- an undesirable effect in thin film devices such as OLEDs. Aggregation induced emission is attributed to suppression of nonradiative vibrational and rotational relaxation pathways in the solid state. This phenomenon has been exploited by using these compounds as sensors for pH, vapors, explosives, and biomacromolecules.¹³

Dibenzosiloles, or silafluorenes, are promising candidates to replace fluorenes in organic electronics.¹⁴ Fluorenes and polyfluorenes have received much interest for use as blue emitters in organic light emitting diodes (OLEDs). Polyfluorene derivatives show good conductivity, high luminescence quantum yields, and high solubility in organic solvents allowing solution processability. However their use is limited by thermal instability attributed to oxidation of the bridging carbon, e.g. the formation of fluorenones, leading to the emergence of a green emission band. Polyfluorene analogues replacing the bridging atom with nitrogen, sulfur, or phosphorous have shown stable blue

emission but reduced solubility. Polysilafluorenes achieve this oxidative stability while retaining similar processability and optical properties to polyfluorenes.¹⁵

Fused siloles have been used in efficient bulk heterojunction solar cells. Chu et al. reported a thieno-dithioenosilole copolymer which achieved a power conversion efficiency of 7.3% when blended with PCBM.¹⁶

1.1.3 Porphyrins

Porphyrins are macrocyclic, tetradentate ligands comprised of four interconnected pyrrole subunits. Metalloporphyrin complexes exist for a wide range of metallic and pseudometallic elements.¹⁷ Porphyrins are widely found in nature, with porphyrins making up many important compounds such as heme and chlorophyll. Synthetic porphyrins are used in catalysis, sensing,

Introduction of silicon into porphyrins allows incorporation of axial ligands into the hexacoordinate complexes. This can help prevent aggregation, and has been used in dye sensitized solar cells to anchor porphyrin-based photosensitizers to electrode surfaces.¹⁸ To accommodate the relatively small silicon atom, the porphyrin adopts a ruffled geometry.¹⁹

1.1.4 Polypyridyl Silanes

Another class of hexacoordinate silicon complexes include those with polypyridyl ligands. These complexes have been found to be hydrolytically stable and can undergo multiple single electron reductions.²⁰⁻²² These reductions are often associated with a change in the UV-Vis absorbance of the complexes, giving them potential use as electrochromic materials.

1.2 Introduction to Electrochemistry

The rational design of organic electronic devices requires knowledge of the relative HOMO and LUMO energy levels of the constituent materials. The driving force of charge transfer in these systems is the energetic offset between orbitals of adjacent layers. The most direct method of obtaining the HOMO energy is ultraviolet photoemission spectroscopy (UPS). In UPS a thin film is irradiated with UV light and the kinetic energy of the ejected electrons measured, the electrons from the HOMO having the highest kinetic energy.²³ The principle disadvantage of this method is the relatively high cost and complexity of the instruments. A simpler alternative is to indirectly determine the HOMO level from oxidation potentials found using cyclic voltammetry.²⁴

1.2.1 Cyclic Voltammetry

Voltammetry is an electrochemical method in which the current of an electrochemical cell is measured as a function of an applied potential. In cyclic voltammetry (CV), the current is ramped linearly to a set potential and then ramped in the opposite direction back to the initial potential. CV utilizes a three-electrode cell consisting of a working electrode, counter electrode, and reference electrode.²⁵ The working electrode is where the redox reaction of interest occurs, the counter electrode conducts electricity to balance the working electrode, and the reference electrode maintains a constant potential against which to measure the potential of the working electrode. A nonreactive supporting electrolyte maintains conductivity.

When the applied potential is sufficient to oxidize the analyte in solution, a current develops. As the analyte at the electrode surface oxidizes, the current quickly reaches a peak anionic current at which point it drops as it becomes diffusion limited. As the

potential ramps in the opposite direction, the current goes to zero and then becomes cathodic as the oxidized analyte which has accumulated near the electrode surface is reduced back. For a reversible process the difference between the peak cathodic and anionic currents is equal to $59.2 \text{ mV}/n$ where n is the number of electrons involved in the half reaction, and the ratio of the magnitude of the two peak currents is 1.²⁶ In this case, the standard oxidation potential (E°_{ox}) can be approximated as the average of the peak anionic and cathodic currents. The energy of the HOMO level can then be calculated by adding the ionization potential of the reference electrode to the determined oxidation potential.

The peak current (i_{pr}) for the forward sweep of a reversible reaction follows equation 1, where n is the number of electrons in the half reaction, A is the area of the electrode, C is the concentration, D is the diffusion coefficient of the electroactive species, and ν is the sweep rate. Therefore the reversibility of a reaction can be gauged by the linearity of a plot of i_{pr} vs. $\nu^{1/2}$.

$$i_{pc} = (2.69 \times 10^8) n^{3/2} A C D^{1/2} \nu^{1/2}$$

Equation 1: The Randles-Sevcik equation at 25 °C.

1.2.2 Spectroelectrochemistry

Electrochemical techniques can be combined with spectroscopic ones in what is called spectroelectrochemistry. This provides information about the various redox states beyond their associated redox potentials. These techniques can involve UV-Vis and IR absorption, Raman, NMR, EPR, XAS, or luminescence spectroscopies. In the case of

UV-Vis absorption spectroscopy, spectroelectrochemistry allows for spectra to be obtained while the different redox states are formed via bulk electrolysis. The emergence and disappearance of absorptions can be observed.²⁷

While the electrochemical cell for spectroelectrochemistry is fundamentally the same as for conventional electrochemistry, i.e. use of a three-electrode cell, the physical design of the cell must account for use with a spectrometer. At least part of it must be optically transparent in the desired spectrum and the path length must be sufficient for adequate band intensity.

CHAPTER 2: VIOLOGENS

2.1 Background

Viologens, quaternized salts of 4,4'-bipyridine, have attracted widespread interest due to their reversible and accessible redox chemistry. The dicationic species can undergo a reversible single electron reduction to yield the radical cation, which is chemically extremely stable due to delocalization of the radical electron throughout the π -system. Further reduction yields the neutral species.²⁸ These changes in redox states are accompanied by dramatic changes in color, from the colorless dication to the blue/violet radical cation and yellow/orange neutral compound.²⁹ Furthermore, these electronic properties can be fine-tuned by modification of the N-substituent.³⁰

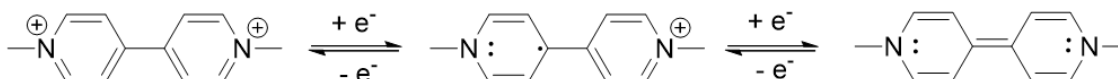


Figure 3: The redox states of methyl viologen: dication (left), radical cation (center), neutral compound (right).

These unique properties have made viologens useful for a wide range of applications. Viologens have been used as biological probes,³¹ redox indicators,³² and electron shuttles.^{33–35} These features have also made them particularly interesting for electrochromic applications such as anti-glare mirrors,³⁶ displays,³⁷ and smart windows.³⁸ Much recent research into electrochromic displays has focused on the deposition of electrochromic materials onto nanostructured electrodes.³⁷ The high surface area of the

electrode allows for high loading of small electrochromic molecules and consequently high color contrast and fast switching times.³⁹ Viologens are useful for this in part because they can be functionalized, usually through the N-substituent, to be covalently tethered to the electrode surface.⁴⁰

Substitution at the 3,3' positions is less common and has only recently begun to be studied in greater detail. Incorporation of a bridge between these positions serves to enforce planarity, as with fluorenes and silafluorenes. In 1985 Summers et al. described the synthesis⁴¹ of a sulphur-bridged methyl viologen, and later reported its use for the photoreduction of water.⁴² More recently, in 2011, Baumgartner reported the synthesis of a phosphorus-bridged methyl viologen.⁴³ It was found that the phosphorus bridge significantly increased the electron-accepting character of the compound, attributed to $\sigma^*-\pi^*$ conjugation. This report was followed up by a more detailed study demonstrating the tunability of the system by using a series of p-benzyl derivatives as N-substituents.⁴⁴ Interestingly the electron donating ability of the nitrogens was reduced so much relative to 4,4'-bipyridine that it would not completely react with the benzyl bromides in solution and instead neat reactions had to be carried out over a period of days.

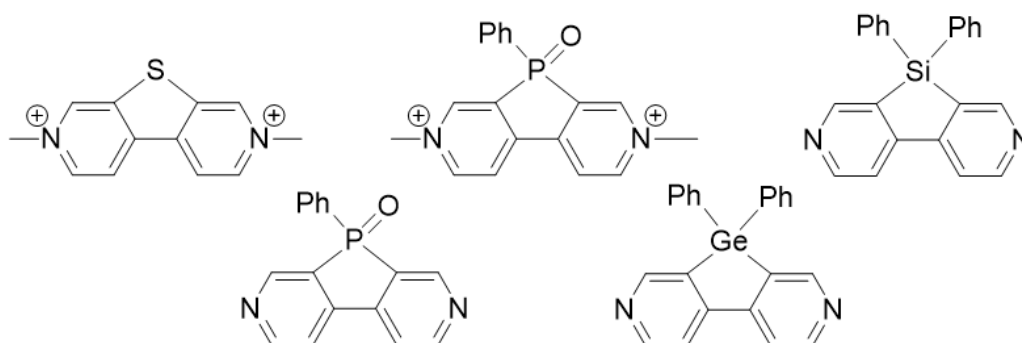


Figure 4: Heteroatom bridged methyl viologens and bipyridines. Thienoviologen⁴² (top left), phosphaviologen⁴³ (top center), diphenyldipyridosilole⁴⁵ (top right), phenyl dipyridophosphole oxide⁴³ (bottom left), and diphenyldipyridogermole⁴⁵ (bottom right).

Analogous silicon bridged viologens have not been reported in the literature. An increase in electron accepting character as with the phosphaviologens is expected owing to increased planarity and σ^* - π^* conjugation. Silicon bridged 4,4'-bipyridines, or dipyridosiloles, containing phenyl or p-methoxyphenyl substituents have been synthesized by Ohshita et al.⁴⁵ Comparing UV-Vis absorption maxima, they reported that ring conjugation was enhanced relative to 4,4'-bipyridine but less than for dipyridophosphole oxide. They also investigated the emissive properties of the siloles and found that they were nonfluorescent in chloroform solutions, but fluoresced in the solid state at room temperature and exhibited enhanced phosphorescence at low temperatures.

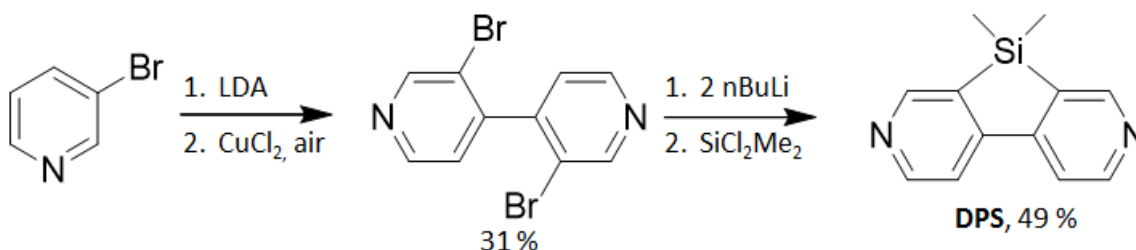
2.2 Dimethyldipyridosilole

Previous attempts by our group to synthesize dipyridosiloles via intramolecular ring closing reactions with bis(halopyridyl)silanes were unsuccessful. Our new strategy was to instead couple the pyridines together first, and then attach to the silicon atom, an adaptation of the approach developed by Baumgartner and later used by Ohshita. The silicon bridged viologen, or siloloviologen, could then be synthesized through standard alkylation conditions. Methyl substituents on both the silicon bridge and for the N-alkylation were chosen for their simplicity.

2.2.1 Synthesis and Structure

The precursor, 3,3'-dibromo-4,4'-bipyridine was synthesized according to a procedure developed by Baumgartner et al.⁴³ Reaction of 3-bromopyridine with lithium diisopropylamide (LDA) selectively deprotonates the pyridine at the more acidic 4 position. Addition of CuCl_2 in an Ullman type reaction results in 3,3'-dibromo-4,4'-

bipyridine in a modest yield. The crude product is a mixture of compounds and must be purified by column chromatography on silica gel.



Scheme 1: Synthesis of dimethyldipyridosilole (DPS)

Lithiation of 3,3'-dibromo-4,4'-bipyridine with two equivalents of n-butyl lithium at $-85\text{ }^{\circ}\text{C}$ followed by reaction with dichlorodimethylsilane affords dimethyldipyridosilole (DPS) in a 49% yield after purification by column chromatography on silica gel. This is a significantly higher yield than that reported by Ohshita et al.⁴⁵ for similarly synthesized dipyridosiloles containing phenyl and methoxyphenyl substituents (11 and 13% respectively). X-ray quality crystals were grown by slow evaporation of a saturated diethyl ether solution. Repeated attempts to obtain passing EA results through both recrystallization and sublimation were unsuccessful.

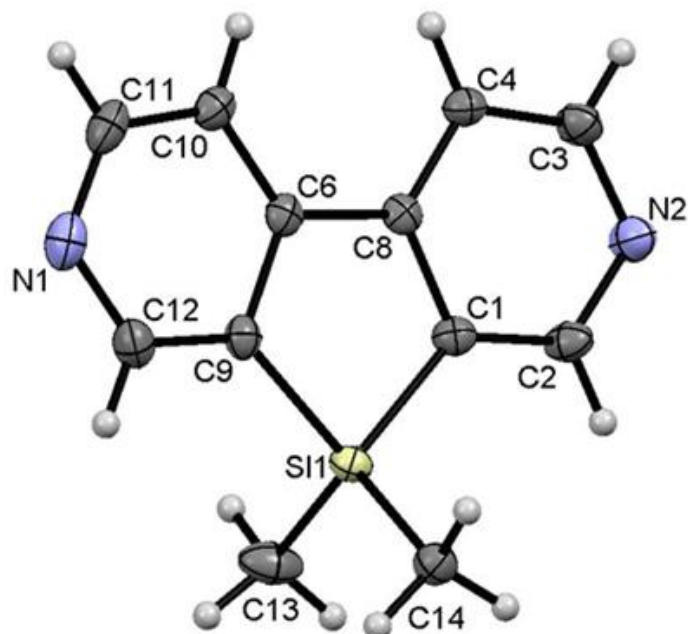


Figure 5: ORTEP representation of dimethyldipyridosilole (DPS). (R = 5.1%)

The crystal structure confirms the co-planar conformation of the rings. This is demonstrated in the UV-vis spectrum, which in chloroform showed an absorption in the UV with $\lambda_{\text{max}} = 273 \text{ nm}$ and an extinction coefficient of $11\,000 \text{ cm}^{-1} \text{ M}^{-1}$. This is a significant red shift from 4,4'-bipyridine, with a $\lambda_{\text{max}} = 237 \text{ nm}$ ⁴⁶, demonstrating the effect of increased conjugation due to the silicon bridge. These results are similar to those of Ohshita et al.⁴⁵, whose diphenyl and dimethoxyphenyl dipyridosilole derivatives also exhibited absorbance maxima of 273 nm.

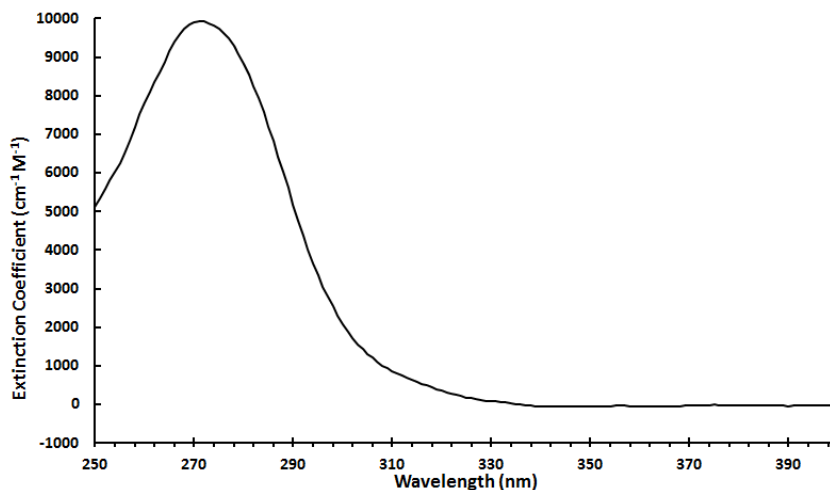
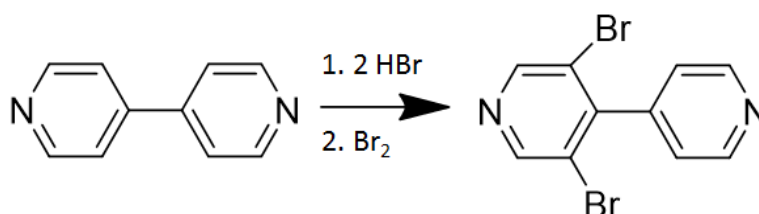


Figure 6: UV-Vis absorbance of dimethyldipyridosilole. (10^{-4} M, CHCl_3)

2.2.2 3,5-Dibromo-4,4'-Bipyridine

In an effort to find an easier route to synthesize 3,3'-dibromo-4,4'-bipyridine, a direct bromination of 4,4'-bipyridine was attempted, following the example of D'Souza et al.⁴⁷ The major product of this reaction was instead found to be 3,5-dibromo-4,4'-bipyridine. While not the desired outcome, this new compound may prove to be a useful starting material for other targets.



Scheme 2: Synthesis of 3,5-dibromo-4,4'-bipyridine

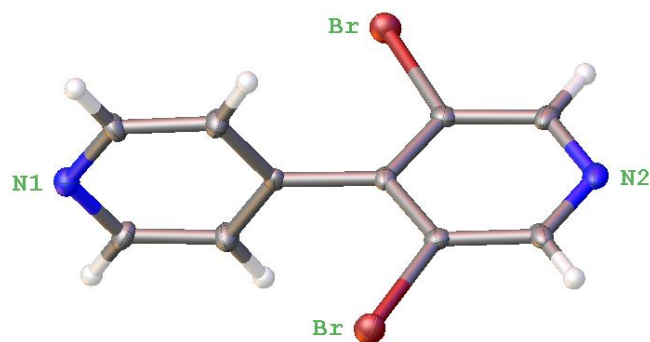
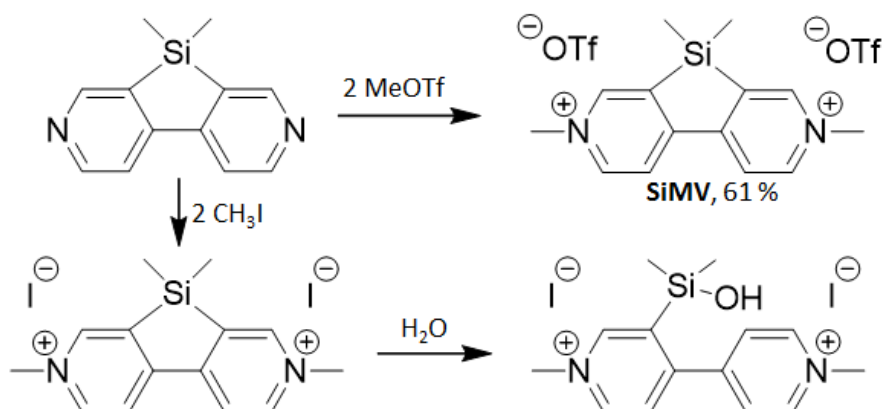


Figure 7: ORTEP representation of 3,5-dibromo-4,4'-bipyridine. ($R = 3.2\%$)

2.3 Siloloviologen

2.3.1 Synthesis and Structure

Addition of methyl iodide to a solution of DPS in acetonitrile- d_3 resulted in a red precipitate and an NMR consistent with the desired siloloviologen. The intense color of the dication is attributed to charge transfer with the iodide counter ion. Slow evaporation of the supernatant yielded crystals which were analyzed by x-ray crystallography. The structure was found to be that of the hydrolyzed compound, indicating a significant increase in hydrolytic instability upon alkylation. The hydrolyzed siloloviologen was characterized by ^1H and ^{13}C NMR (see appendix).



Scheme 3: Methylation of DPS. Synthesis of siloloviologen iodide and subsequent hydrolysis (bottom), synthesis of siloloviologen triflate (top right).

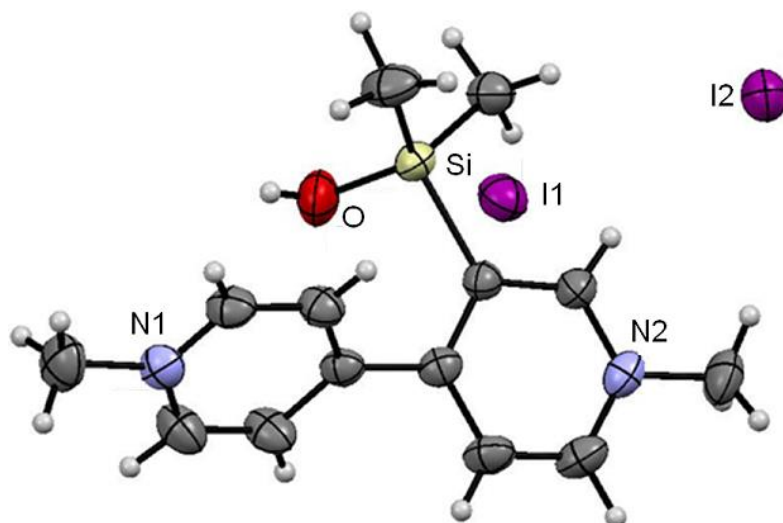


Figure 8: ORTEP representation of hydrolyzed siloloviologen iodide (R = 3.5%).

Reaction of dipyridosilole with methyl triflate in acetonitrile resulted in a colorless solution. Crystals suitable for x-ray diffraction were grown via ether diffusion showing the unhydrolyzed methyl siloloviologen. The compound was characterized by ^1H , ^{13}C , and ^{29}Si NMR. Passing elemental analysis results were obtained after repeated recrystallization.



Figure 9: ORTEP representation of siloloviologen (SiMV) with triflate counter-ions removed. (R = 4.1%)

Attempts to obtain ESI-MS data were unsuccessful. Fresh, pure samples dissolved in HPLC grade acetonitrile gave three identifiable peaks in the mass spectrum, however all masses were consistent with species containing no silicon atom. This result is surprising. It seems very unlikely that the entire sample could degrade to methyl viologen in the short time between sample preparation to sample injection, given the relative stability shown by NMR solutions of the compound in CD₃CN. It therefore seems that even a soft ionization technique such as ESI is enough to completely fragment the sample. This provides more evidence of the relatively labile nature of the Si-C bond in these compounds.

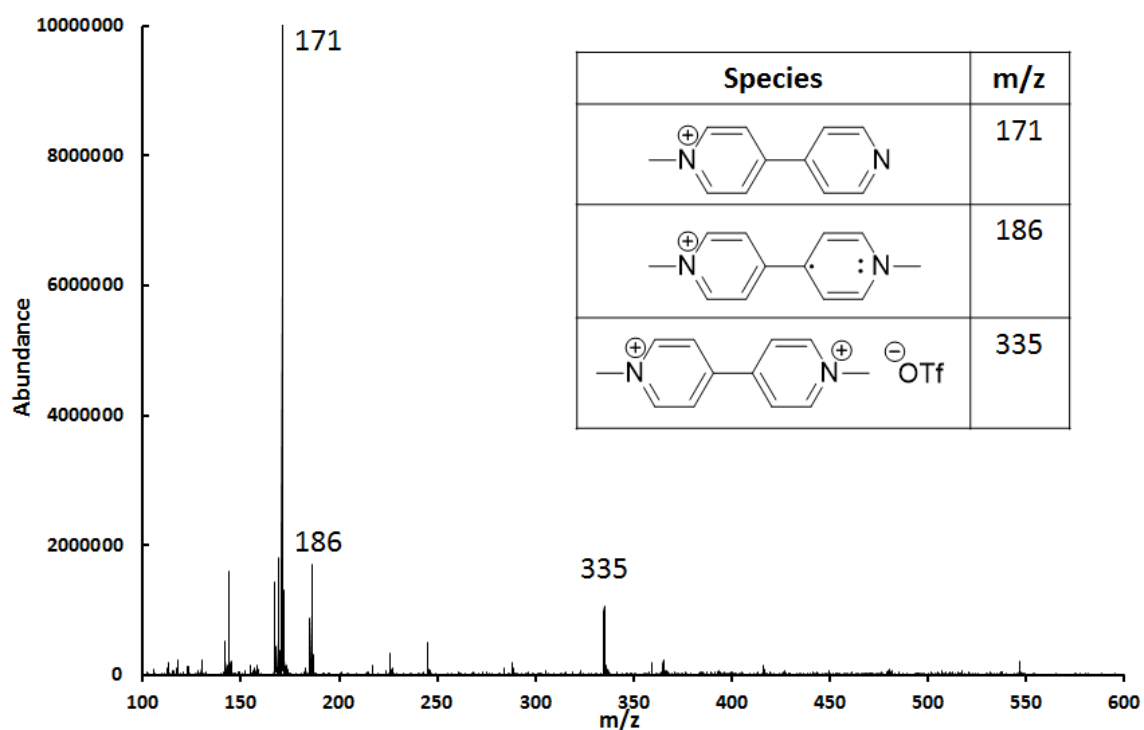


Figure 10: Attempted ESI-MS of SiMV with assigned species (inset).

2.3.2 Hydrolysis Kinetics

To better characterize the sensitivity of SiMV toward hydrolysis, kinetic studies of the triflate salt were carried out in CD₃CN and D₂O. 14 mg H₂O was added to a solution of 24 mg SiMV in 1.27 mL CD₃CN in an NMR tube. The solution was stored at room temperature and monitored by ¹H NMR over a period of a month. The N-methyls were observed to decay from a single peak at 4.37 ppm to two distinct peaks at 4.40 and 4.39 ppm as the symmetry of the compound was broken. The two methyls attached to the silicon atom, the 9 position, were observed to shift from 0.70 to 0.27 ppm. These latter two peaks were the most clearly resolved and therefore integrated to follow the changing concentration. The reaction was assumed to be first order with respect to both SiMV and H₂O. By having a large excess of H₂O it can be assumed the H₂O concentration is effectively constant and consequently the reaction can be approximated as pseudo-first order. The differential form of the pseudo first order rate equation (equation 2) can be integrated to give equation 3.

$$rate = k[H_2O][SiMV] = k'[SiMV]$$

Equation 2: Second order rate equation and first order approximation.

$$\ln[SiMV] = -k't + \ln[SiMV]_0$$

Equation 3: Integral representation of the first order rate equation.

The natural log of SiMV concentration was plotted as a function of time as according to equation 3 and found to be linear over the observed period ($R^2 = 0.994$), indicating the validity of the first order approximation. The rate constant for the

hydrolysis of SiMV in acetonitrile at approximately 23 °C was calculated to be $3.21 \pm 0.35 \times 10^{-7} \text{ M}^{-1} \text{ s}^{-1}$.

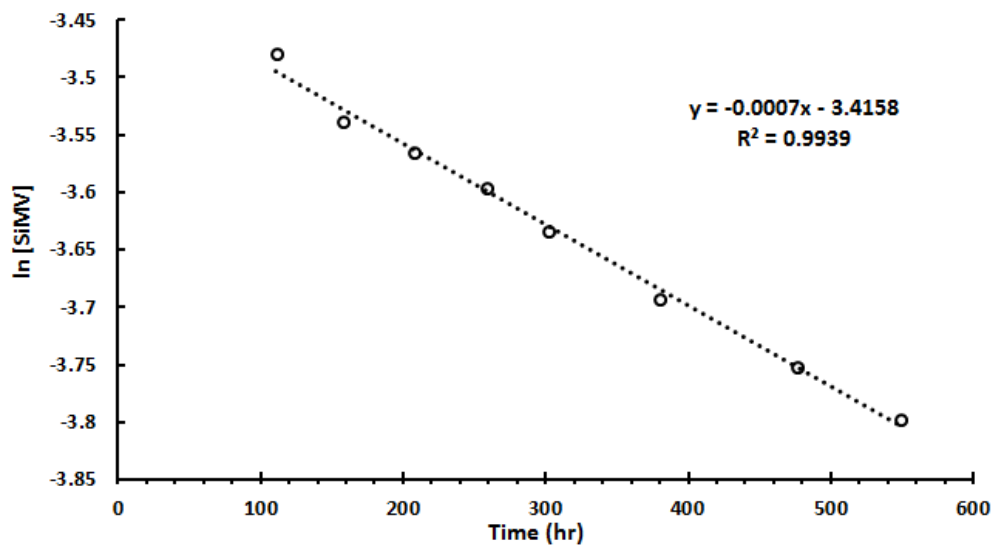


Figure 11: Pseudo first order kinetics plot of the hydrolysis of SiMV in acetonitrile- d_3 .

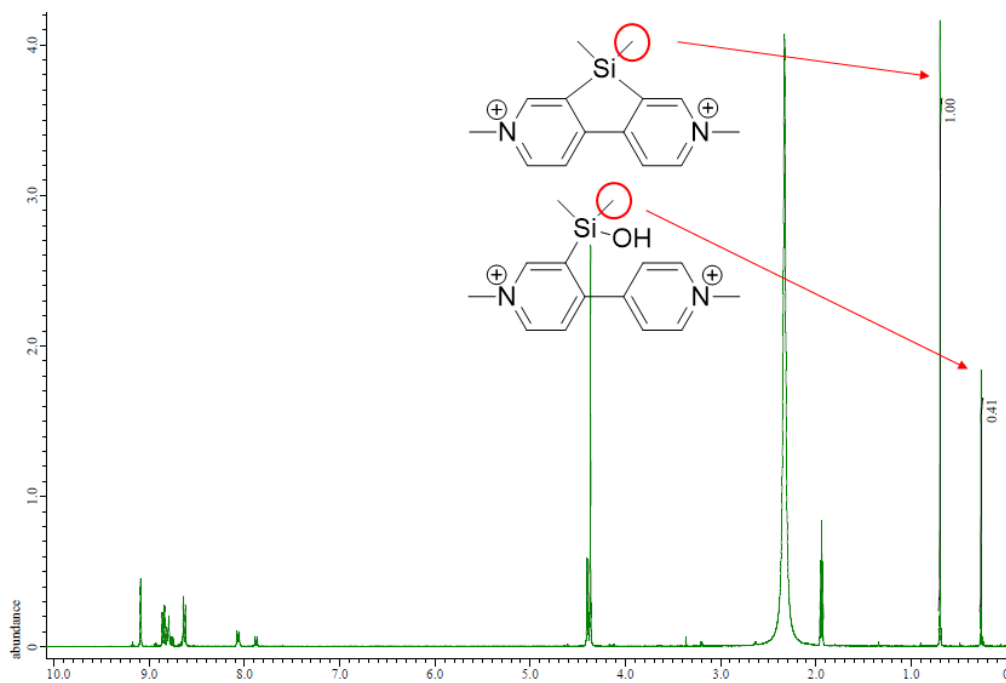


Figure 12: $^1\text{H-NMR}$ of SiMV with H_2O in CD_3CN after 15.5 days, showing methyl peaks integrated for concentration determination.

A similar experiment was carried out in D₂O. 11.7 mg of SiMV was dissolved in 0.571 ml D₂O and monitored overnight by H¹ NMR. Scans were taken at 20 minute intervals at 23.0 °C. Within 5 hours over 97% of the compound had hydrolyzed. The natural log of the SiMV concentration was again plotted as a function of time and found to be linear with an R² = 0.999. The observed rate constant (k') for the hydrolysis of SiMV in D₂O at 23.0 °C was determined to be $2.4 \pm 0.1 \times 10^{-4} \text{ s}^{-1}$. This corresponds to a half life of 49 minutes.

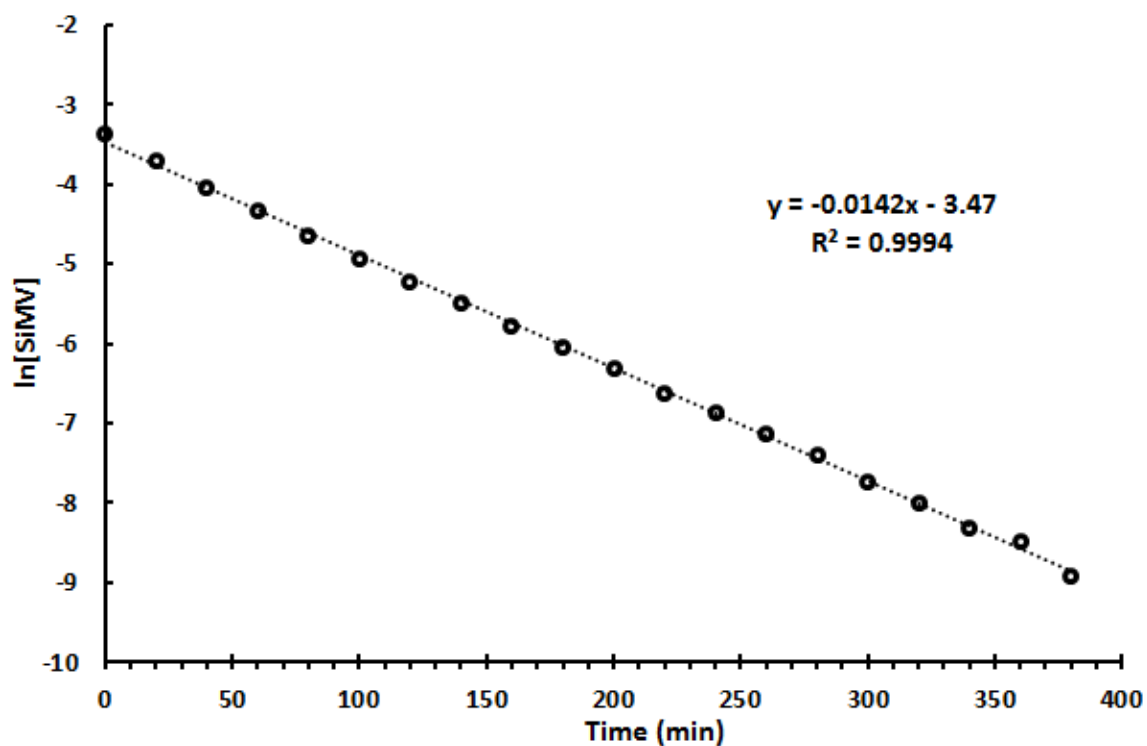


Figure 13: Pseudo first order kinetics plot of the hydrolysis of SiMV in D₂O.

2.3.3 Electrochemistry and Spectroscopy

Cyclic voltammetry of the compound shows two reversible single electron reductions with reduction potentials of -0.829 and -1.31 V vs the ferrocene/ferrocenium redox couple.

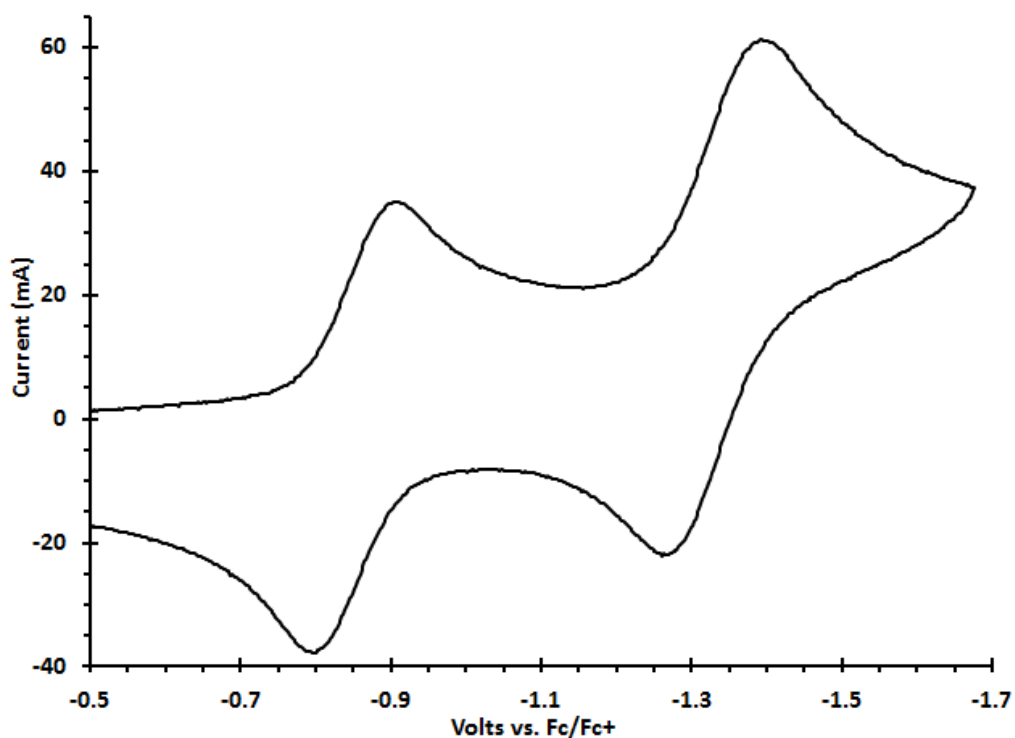


Figure 14: CV of SiMV in CH₃CN. 0.1 M TBAP. Vs. ferrocene, scan rate = 200 mV/s.

For a reversible process, the peak forward current should be proportional to the square root of the scan rate. Voltammograms were obtained at scan rates of 100, 200, 300, 400, 500, and 600 mV/s, and the peak currents plotted against the square root of the scan rates for both of the reduction waves. The R^2 values for the first and second reductions were calculated to be 0.993 and 0.994 respectively, demonstrating the high degree of reversibility under these conditions.

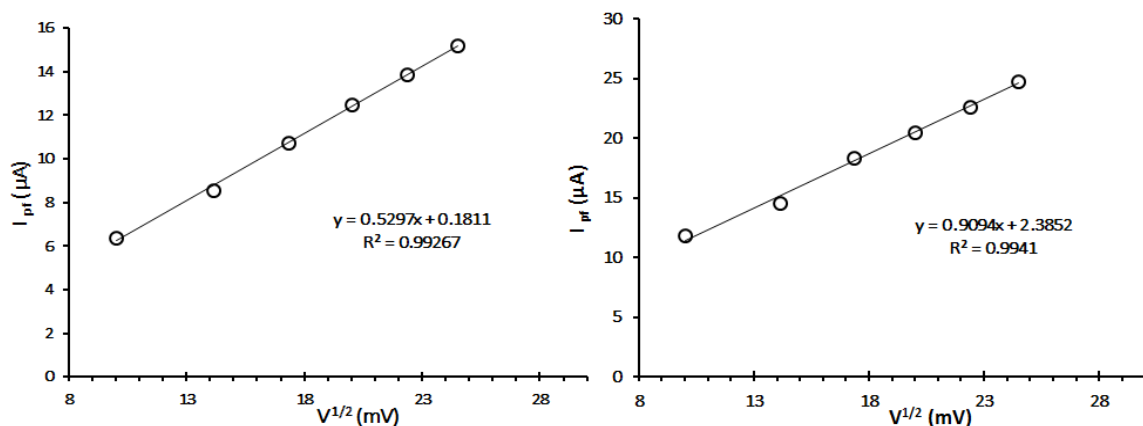


Figure 15: Plots of peak forward current versus scan rate for the first (left) and second (right) reductions of SiMV.

The absorption spectrum of the siloloviologen triflate salt in CH_3CN displayed a peak in the UV region centered around 270 nm with an extinction coefficient of $17500 \text{ cm}^{-1} \text{ M}^{-1}$. Solid state and solution phase samples of the iodide salt were intensely colored, indication of a counter ion charge transfer process.

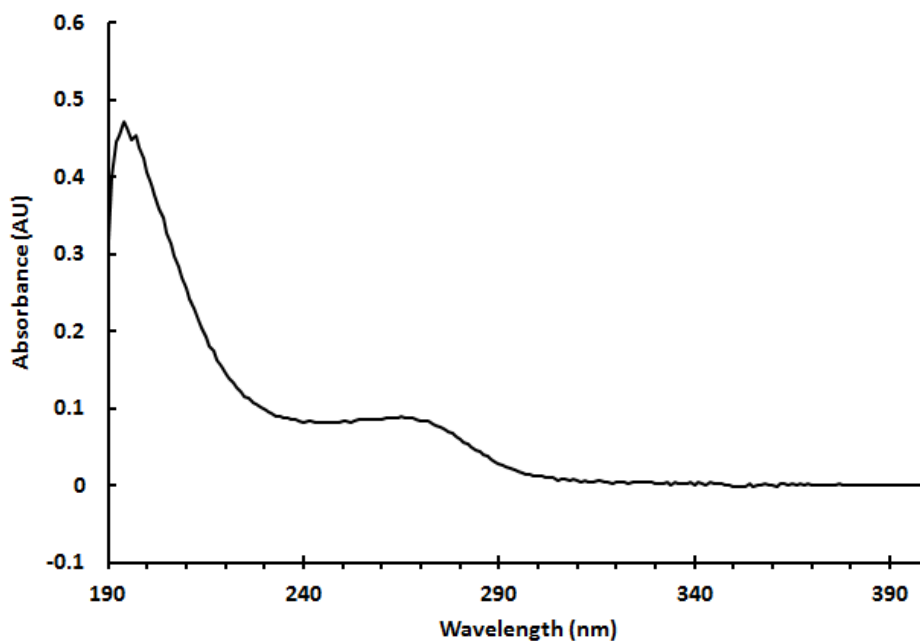


Figure 16: UV-Vis absorbance of 10^{-5} M SiMV in CH_3CN .

Spectroelectrochemical studies were undertaken to investigate the electrochromic properties of the compound. Application of a potential halfway between the first and second reduction potentials (-0.6 V vs Ag/AgCl, about -1.04 vs Fc/Fc⁺) should generate predominately the radical cation and allow qualitative evaluation of its absorption spectrum. A potential beyond the second reduction potential should produce the neutral compound.

The radical cation is characterized by the formation of two new peaks centered at 395 and 606 nm. The former peak is narrow and intense while the latter is broad, extending over much of the visible region. At a potential of -1.0 V (vs Ag/AgCl) the neutral compound should be the primary species at the electrode. The long wavelength absorption completely disappeared, while the peak at 395 nm broadened and decreased in intensity, with a tail stretching nearly all the way to 600 nm. Neutral viologens are often associated with insolubility. In acetonitrile there was no observable precipitation at large negative potentials, although after extended use the working electrode displayed signs of discoloration.

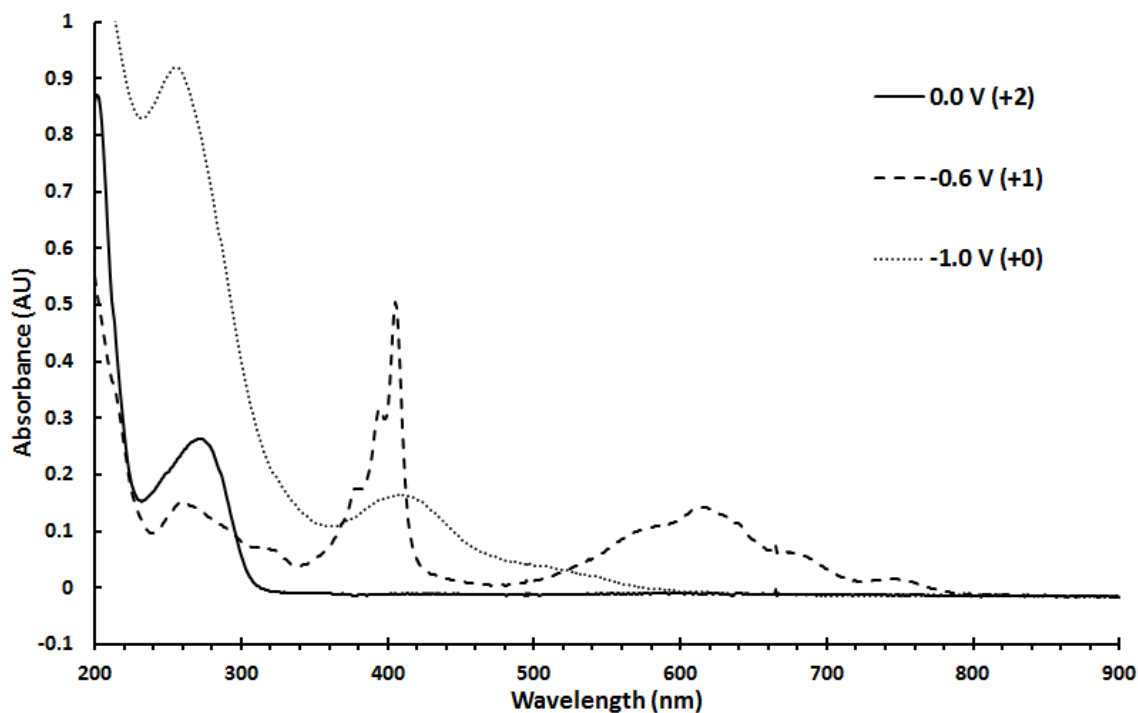


Figure 17: Spectroelectrochemistry of SiMV in CH_3CN . V vs Ag/AgCl.

SiMV was fluorescent in acetonitrile with an emission centered at 350 nm.

Observations of a long wavelength emission at 420 nm were followed by attempts to induce aggregation by addition of diethyl ether, chloroform, dichloromethane, or toluene. In all instances, addition of these antisolvents served to quench the fluorescence.

Attempts were made to induce aggregation by varying the concentration in acetonitrile, but no nonlinear shifts in fluorescence intensity were observed. It was concluded that the long wavelength emission was likely due to some impurity, rather than an aggregation effect. It was observed that fresh samples of SiMV had little to no long wavelength emission, while those which had been subject to repeated irradiation began to have the same emission at 420 nm. In at least one case, emission beyond 500 nm was observed.

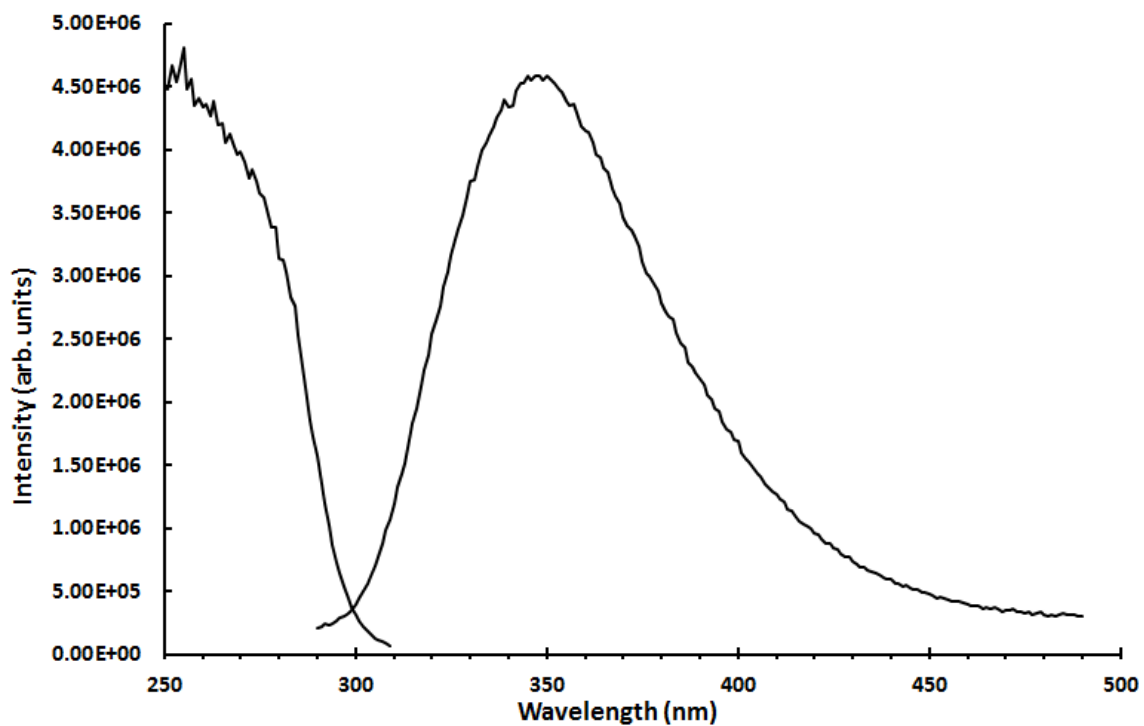


Figure 18: Fluorescence excitation and emission spectra of 10^{-4} M SiMV in CH_3CN .

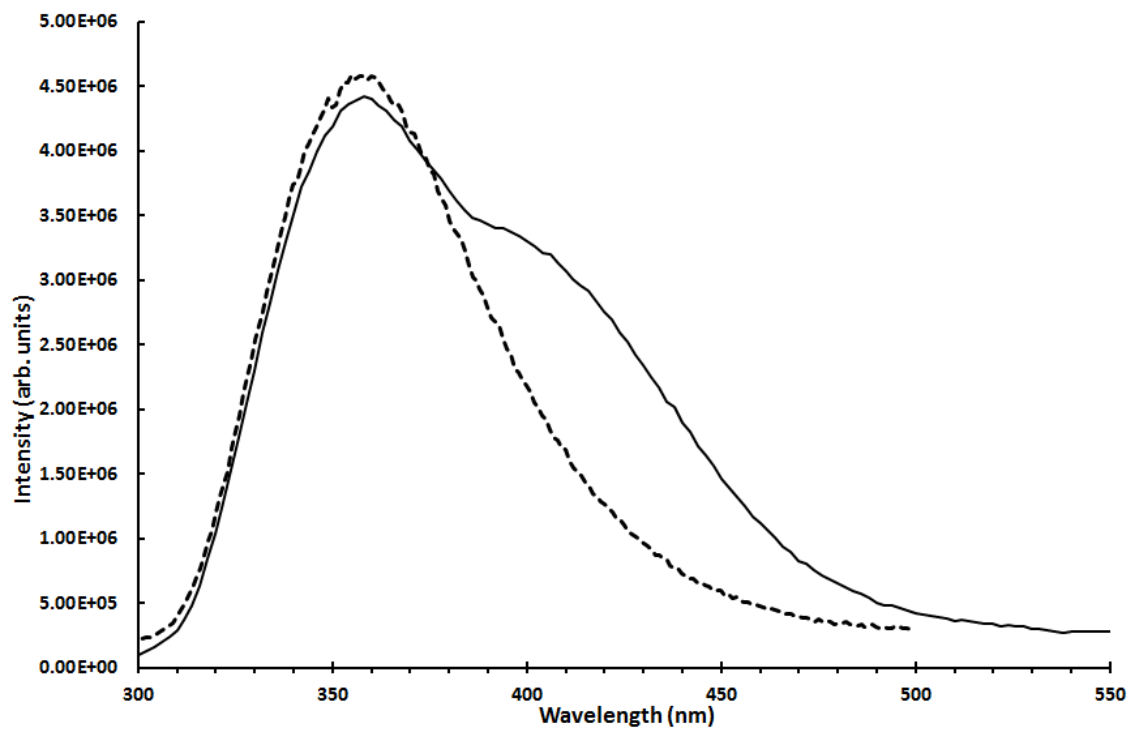


Figure 19: Emission of fresh sample of SiMV (dashed line) superimposed on a sample after repeated irradiation (solid line), showing emergence of long wavelength emission.

2.4 Experimental

2.4.1 Instrumentation and General Methods

Absorption spectra were measured with a Cary 300 UV-Vis spectrophotometer. Spectroelectrochemical measurements were made with an Agilent 8453 diode array UV-Vis spectrophotometer in a Pine Research Instrumentation honeycomb spectroelectrochemical cell. Fluorescence measurements were conducted on a Jobin-Yvon Fluorolog 3 fluorescence spectrometer. ^1H and ^{13}C NMR spectra were acquired using a JEOL 300 MHz NMR spectrometer. For the ^{29}Si spectra a JEOL 500 MHz NMR spectrometer was used. Combustion analysis (C, H, and N) was conducted by Atlantic Microlab, Inc.

Cyclic voltammetry studies were performed using a Princeton Applied Research Model 273A Potentiostat/Galvanostat employing a conventional three-electrode setup consisting of a platinum disk or glassy carbon working electrode, a silver/silver chloride reference electrode, and a platinum wire auxiliary electrode. Positive feedback iR compensation was routinely used. Voltammograms were obtained in 0.1 M tetrabutylammonium hexafluorophosphate (TBAPF₆)/acetonitrile solution using solvent that had previously been purified and dried using a solvent purification system (SPS- 400, Innovative Technologies) and subsequently purged with nitrogen. The supporting electrolyte (TBAPF₆) was recrystallized from ethanol and dried under vacuum prior to use. Ferrocene was used as an internal standard without further purification.

Crystals of suitable size were removed from the mother liquor, coated with a thin layer of paratone-N oil, mounted on the Agilent Gemini A Ultra diffractometer, and flashcooled to 100 K in the cold stream of the Cryojet XL liquid nitrogen cooling device

(Oxford Instruments) attached to the diffractometer. The Gemini A Ultra diffractometer was equipped with a sealed-tube long fine focus X-ray source with Mo target ($\lambda = 0.71073 \text{ \AA}$) and Cu target ($\lambda = 1.5418 \text{ \AA}$), four-circle kappa goniometer, and Kodak CCD detector. CrysAlisPro⁴⁸ software was used to control the diffractometer and perform data reduction. The crystal structure was solved with SHELXS⁴⁹. All non-hydrogen atoms appeared in the E-map of the correct solution. Alternate cycles of model-building in Olex2⁵⁰ and refinement in SHELXL⁴⁹ followed. All non-hydrogen atoms were refined anisotropically. All hydrogen atom positions were calculated based on idealized geometry, and recalculated after each cycle of least squares. During refinement, hydrogen atom – parent atom vectors were held fixed (riding motion constraint). Crystallographic data is provided in appendix A.

2.4.2 Synthetic Details

3,3'-dibromo-4,4'-bipyridine

To a solution of 2.56 g diisopropylamine (25.3 mmol) in 50 mL tetrahydrofuran, 15.8 mL of 1.6 M n-butyl lithium (25.3 mmol) was added dropwise at $-90 \text{ }^\circ\text{C}$. The solution was stirred at this temperature for 45 min. 4.0 g 3-bromopyridine (25.3 mmol) was added dropwise and allowed to stir for 1 h. 8.0 g CuCl_2 (59.5 mmol) was added, air was allowed into the reaction vessel, and the mixture was slowly warmed to room temperature and stirred overnight. The resulting brown solid was taken up in a mixture of 30 mL H_2O , 15 mL 30% w/w NH_4OH , and 15 mL saturated NH_4Cl then extracted three times with chloroform. The combined organic phases were dried with NaSO_4 and the volatiles removed under vacuum. The crude product was purified by column chromatography on silica gel (hexanes/ethyl acetate 2:1) to yield 1.23 g (31%) of 3,3'-

dibromo-4,4'-bipyridine as off-white crystals. ^1H NMR (CDCl_3 , 300 MHz): $\delta = 8.88$ (s, 2 H), 8.64 (d, 2 H), 7.18 (d, 2 H). ^{13}C NMR (CDCl_3 , 300 MHz): $\delta = 152.5$, 148.4, 124.6, 120.7 ppm. MS (EI): $m/z = 313.9$ (M^+), 233.0 ($[\text{M} - \text{Br}]^+$)

3,5-dibromo-4,4'-bipyridine⁴⁷

6.0 g 4,4'-bipyridine (38.5 mmol) was dissolved in 30 ml methanol and cooled to 0 °C. 13 ml HBr (48% w/w) was added dropwise and the mixture stirred at room temperature for 1 h. The volatiles were removed under reduced pressure to yield a yellow powder. The powder was ground with 4.3 ml Br_2 (84 mmol) in a mortar and pestle. This mixture was sealed in a glass ampoule and heated at 185 °C for 72 h. The crude product was added to 100 ml of 2.0 M NaOH and 0.5 M $\text{Na}_2\text{S}_2\text{O}_3$, stirred for 30 min, and extracted with 300 ml CH_2Cl_2 . The volatiles were removed under reduced pressure and the resulting solid purified by column chromatography (SiO_2 , hexanes/ethyl acetate 1:1). Crystals suitable for x-ray analysis were obtained by recrystallization from ethyl acetate. ^1H NMR (CDCl_3 , 300 MHz): $\delta = 8.80$ (d, 2 H), 8.76 (s, 2 H), 7.17 (d, 2 H). ^{13}C NMR (CDCl_3 , 300 MHz): $\delta = 150.7$, 150.3, 147.6, 145.6, 123.1, 121.2 ppm. MS (EI): $m/z = 313.8$ (M^+), 232.9 ($[\text{M} - \text{Br}]^+$)

Dimethyldipyridinosilole

To a solution of 1.0 g 3,3'-dibromo-4,4'-bipyridine (3.18 mmol) in 40 mL THF was added 4.0 mL 1.6 M n-butyl lithium (6.4 mmol) dropwise at -90 °C. The mixture was stirred at this temperature for 1 h. 0.5 mL SiMe_2Cl_2 (4 mmol) was added dropwise and the mixture was allowed to warm to room temperature and stir overnight. The

mixture was taken up in 50 mL 1 M NaHCO₃ and extracted three times with diethyl ether. The combined organic layers were dried over MgSO₄ and evaporated under vacuum to yield a light brown oil. The crude product was purified by column chromatography (SiO₂, hexanes/ethyl acetate, 1:2) followed by recrystallization from hexanes to yield dimethyldipyridosilole as white crystals (0.33 g, 49% yield). Crystals suitable for x-ray analysis were grown via slow evaporation of a filtered diethyl ether solution at room temperature. ¹H NMR (CDCl₃, 300 MHz): δ = 8.90 (s, 2 H), 8.75 (d, 2 H), 7.76 (d, 2 H) 0.56 (s, 6 H). ¹³C NMR (CDCl₃, 300 MHz): δ = 153.9, 153.1, 151.7, 133.3, 116.9, -3.47 ppm. ²⁹Si NMR (CDCl₃, 500 MHz): δ = 3.62 ppm. MS (EI): *m/z* = 212.1 (M⁺), 197.1 ([M - CH₃]⁺)

Methyl siloloviologen iodide

To a solution of 25 mg dimethyldipyridosilole (0.12 mmol) in 1 mL CD₃CN was added 34 mg CH₃I (0.24 mmol). The mixture was allowed to sit overnight, resulting in a red precipitate. The supernatant was decanted and allowed to slowly evaporate in air to yield crystals of the hydrolyzed compound. NMR data (hydrolyzed triflate salt): ¹H NMR (D₂O, 300 MHz): δ = 9.01 (m, 2 H), 8.94 (m, 2 H), 8.21 (d, 1 H), 8.02 (d, 1 H) 4.51 (s, 3 H), 4.47 (s, 3 H), 2.22 (s, 6 H). ¹³C NMR (D₂O, 300 MHz): δ = 157.7, 154.2, 149.7, 145.5, 138.8, 127.8, 121.7, 117.5, 48.5, 48.2 ppm

Methyl siloloviologen triflate

To a solution of dimethyldipyridosilole (0.5 g, 2.4 mmol) in acetonitrile (20 mL) was added methyl triflate (0.79 g, 4.8 mmol) dropwise at 0 °C. The solution was stirred

overnight and diethyl ether allowed to slowly diffuse into the reaction vessel, yielding siloloviologen as white needles (0.78 g, 61% yield). Crystals suitable for x-ray diffraction were via slow ether diffusion into a saturated acetonitrile solution under a nitrogen atmosphere. ^1H NMR (CDCl_3 , 300 MHz): δ = 9.06 (s, 2 H), 8.83 (d, 2 H), 8.61 (d, 2 H), 4.36 (s, 6 H) 0.70 (s, 6 H). ^{13}C NMR (CDCl_3 , 300 MHz): δ = 157.2, 151.0, 148.7, 142.4, 123.9, 49.5, -4.58 ppm. ^{29}Si NMR (CDCl_3 , 500 MHz): δ = 10.0 ppm. Elemental analysis calcd (%) for $\text{C}_{16}\text{H}_{18}\text{N}_2\text{O}_6\text{F}_6\text{Si}_2$: C 35.55, H 3.36, N 5.18; found: C 35.38, H 3.19, N 5.20. MS (MALDI-TOF): m/z = 242.5 (M^+), 227.6 ($[\text{M} - \text{CH}_3]^+$)

2.5 Discussion

The dimethylsilylene-bridged methyl viologen was successfully synthesized via methylation of dimethyldipyridosilole. Crystal structures of each compound show that the silicon bridge indeed enforces a high degree of planarity. This is reflected in the optical properties of each compound. Table 1 compares the absorbance maxima of DMS to 4,4'-bipyridine and other heteroatom bridged derivatives. It can be seen that all of the bridged compounds are significantly red shifted from 4,4'-bipyridine. The siloles demonstrate more conjugation than the germole, but less than the phosphole.

Table 1: Comparison of UV-Vis absorbance maxima of various 4,4'-bipyridines. Structures can be found in Figure 4.

Compound	λ_{max} (nm)	Solvent
4,4'-bipyridine	237	CHCl_3
diphenyl dipyridogermole	269	CHCl_3
dimethyl dipyridosilole (DMS)	273	CHCl_3
diphenyl dipyridosilole	273	CHCl_3
phenyl dipyridophosphole oxide	276	CH_2Cl_2

Both reductions of siloloviologen were found to be reversible, as expected. Table 2 compares these reduction potentials to methyl viologen and other heteroatom bridged methyl viologens found in the literature. The incorporation of the silicon bridge makes the compound about 260 mV easier to reduce for the first reduction and 210 mV easier to reduce for the second, relative to unbridged methyl viologen. This is a more significant LUMO lowering effect than that of a thienoviologen (SMV) reported by Sasse et al. in 1986⁴², but still about 300 mV more negative than that of Baumgartners phosphaviologen (PMV).⁴³ The absorbance maxima follow this general trend as well, with the phosphaviologen being the most red shifted followed by the siloloviologen.

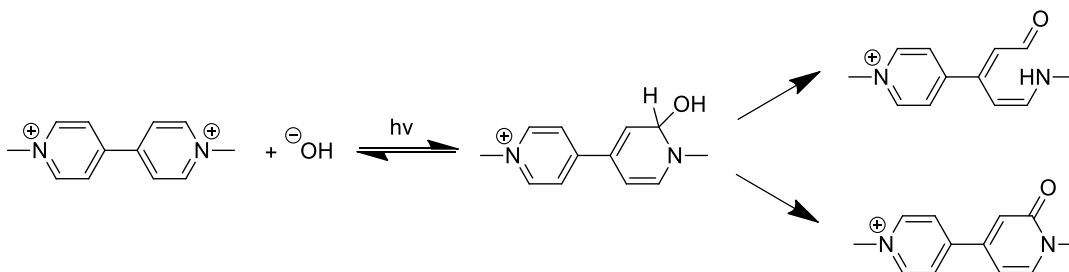
Table 2: Comparison of reduction potentials and absorbance maxima of SiMV to methyl viologen and other heteroatom-bridged methyl viologen derivatives. V vs Fc/Fc⁺. E_{red} for SMV converted from NHE by subtracting 0.64 V. ^a dication ^b radical cation

Compound	E _{red} (+2/+1) (V)	E _{red} (+1/0) (V)	λ _{max} ^a (nm)	λ _{max} ^b (nm)
PMV ²⁺ ⁴³	-0.51	-1.00	288	406, 634
SiMV ²⁺	-0.829	-1.31	270	395, 606
MV ²⁺	-1.09	-1.52	260 ⁵¹	397, 606 ⁵²
SMV ²⁺ ⁴²	-1.05	-	-	

SiMV demonstrated fairly typical viologen fluorescence, with the emission maximum redshifted about 5 nm from MV to 350 nm. Kohler et al. studied the fluorescence of MV in various solvents and found that alcohols and ethereal solvents quenched the emission.⁵³ This is consistent with our experiences with ether, but chloroform did not quench fluorescence in Kohlers paper as it did for us. Kohler determined that the reduction potential of the photoexcited species is +3.65 V (vs NHE),

demonstrating that MV is an extremely potent photooxidant. Even relatively mild electron donors can quench the fluorescence through electron transfer, and the fluorescence quenching by chloroform can be explained by the enhanced electron accepting character imparted by the silicon bridge.

The long wavelength emission we observed at 420 nm, which was followed by attempted studies of aggregation induced emission, was ultimately attributed to photogenerated impurities. The observance of long wavelength emission in viologens is not a novel phenomenon; initially it was attributed to the formation of ion-pair complexes.⁵⁴ Mau et al. studied⁵⁵ the fluorescence of methyl viologens in the 1980's and observed similar green emission. They determined that compounds formed from either base treatment or irradiation were responsible for the detected green fluorescence, and subsequently identified one of them as a pyridone derivative.



Scheme 4: Pyridone formation from methyl viologen as identified by Mau et al.⁵⁵

The spectroelectrochemistry of SiMV, with absorbance maxima at 395 and 606 nm, is strikingly similar to that of methyl viologen which is reported to have absorbance maxima of 397 and 607 nm in CH_3CN .⁵² This shows very little effect of the silicon bridge on the optical absorption of the radical cation, with the peaks even being slightly

blue shifted relative to the parent compound. It may be that since the optical absorption of the radical cation is characterized by charge transfer between +1 and +0 nitrogens,³⁰ the dominant effect on energy levels is the nature of the nitrogen substituent, with little effect from the silicon bridge.

On the other hand, Baumgartners PMV radical cation demonstrates a clear red shift when comparing absorbance maxima.⁴⁴ Another possibility is that the reduced states of SiMV, while stable and reversible on the timescale of the CV experiments, undergo electrolysis in these conditions. In this case the absorbing species may more closely resemble MV and be responsible for the similar absorption spectra. When comparing the shape of the entire spectra rather than only the absorbance maxima, SiMV does demonstrate a longer wavelength shoulder around 680 and a weak local maximum at 740 nm which are absent for PMV. It should be noted that spectroelectrochemistry of a thienoviologen⁴² was shown to have a similar basic profile as MV, albeit with larger shifts, so the similarity in shape itself is not necessarily concerning. Furthermore, the spectrum of neutral SiMV more closely resembles that of PMV⁰ than it does MV⁰.^{44,52}

In any event, it appears that there is little significant variance in colors when comparing the different states of SiMV, PMV, and MV. The dications are colorless, the radical cations blue, and the neutral species yellow. Tuning the spectral properties of the reduced states is better achieved by variation of N-substituent rather than bridging heteroatom. The chief advantages of the bridging atom are therefore the enhanced electron affinity and additional site for functionalization.

CHAPTER 3: SPIROSILABIFLUORENES

3.1 Background

3.1.1 Spirobifluorenes

Organic electronics, in which organic materials are used to perform functions such as charge carrier transport, light emission, and light absorption, have been a major research focus over the past several decades. Major applications include photovoltaics, light emitting diodes, and field effect transistors.⁵⁶ Compared to inorganic semiconductors, organic semiconductors have several potential advantages. The manufacture of high purity silicon is energy intensive, whereas organic materials are solution processable; this allows for the possibility of room temperature device fabrication. Beyond the promise of lower cost, organic materials are lighter and more flexible. They can be processed in thin-film, large-area devices.⁵⁶ These unique properties may allow for new applications that are not possible with traditional inorganic materials.

Despite these potential advantages, in many ways the performance of organic electronics does not match that of silicon-based materials. Hole and electron mobilities of organic semiconductors are several orders of magnitude lower than that of crystalline silicon.⁵⁷ Long term stability of organic materials is often an issue, particularly for applications which subject the materials to regular light or heat exposure. These devices are typically made of thin amorphous layers of organic compounds. The amorphous state is desirable for three primary reasons: it's easy to reproducibly fabricate, it avoids the

grain boundaries characteristic of polycrystalline films which create charge carrier traps, and it has favorable optical properties.^{56,58} When an amorphous material is heated above its glass transition temperature (T_g), the molecules can shift into the more thermodynamically stable crystalline arrangement, resulting in device degradation.

One strategy to increase the morphological stability of small organic molecules is to “spiro” link them, resulting in compounds in which two identical moieties are connected by a tetrahedral center.⁵⁹ This results in a large increase in T_g with minimal effect on electronic and chemical properties.⁶⁰ The increase in T_g is more than simply a function of doubling the molecular weight. The rigid, perpendicular arrangement causes entanglement in the amorphous state and suppresses π - π interactions. This hampers crystallization and also improves solubility.⁵⁸

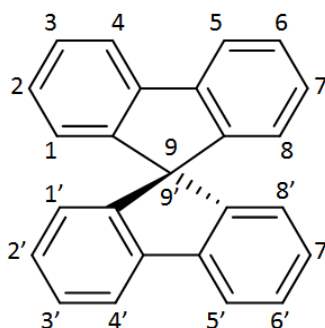


Figure 20: Spirobifluorene. A simple spiro-linked molecule with atom numbering.

Most spiro compounds investigated for electronic applications contain the spirobifluorene core.⁵⁸ This provides a robust framework of conjugated π systems which can be functionalized to obtain the desired properties. Spirobifluorene derivatives have been used for a variety of different functions depending on substituents. Incorporation of electron accepting groups provides n-type transport character and leads to electron

transport materials (ETM).³¹ Conversely, electron donating groups such as amines provide p-type character and are commonly used in hole transport materials (HTM).⁵⁶ One strategy to synthesize ambipolar compounds, those which can transport both electrons and holes efficiently, is to combine both categories of substituent in one compound.^{61,62} Not limited to simply transporting charges, spirobifluorenes have also been extensively studied for their emissive properties,^{59,63,64} and have been successfully incorporated into functioning OLEDs as emitters.^{61,65,66}

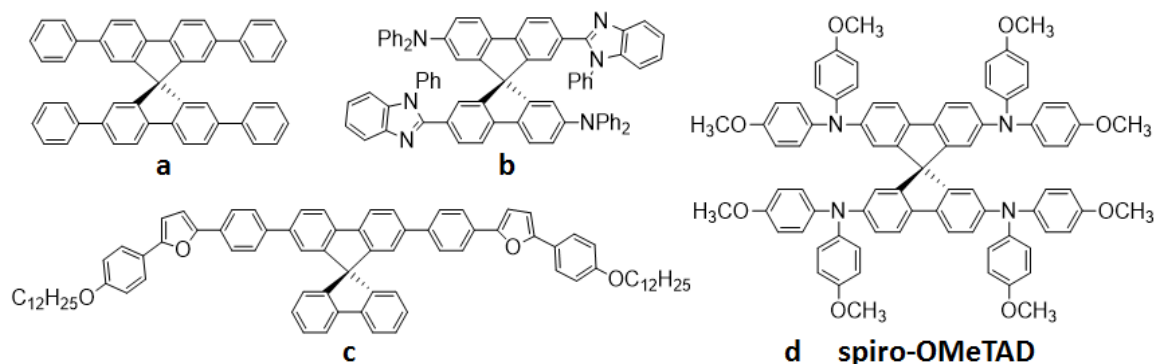


Figure 21: The many uses of spirobifluorene derivatives. a) OLED emitter⁶⁷ b) ambipolar charge transport material⁶¹ c) electron transport material⁶⁸ d) spiro-OMeTAD⁶⁹

The spiro compound which has received the most interest and widespread use is certainly the hole transporting material spiro-OMeTAD. First described in 1998 by Michael Grätzel et al.⁶⁹ it's no surprise that spiro-OMeTAD was born out of the development of the Grätzel cell, or dye-sensitized solar cell (DSSC). DSSCs are one of the most well established alternatives to photovoltaic devices based on crystalline inorganic semiconductors.⁷⁰ A typical DSSC consists of a layer of photosensitizing dye molecules attached to a mesoporous wide bandgap semiconductor, such as TiO₂. When the dye absorbs a photon, an electron is excited from the HOMO into the LUMO. It is

then injected into the TiO_2 conduction band where it can then travel to the electrode. Meanwhile, the oxidized dye is reduced by electron transfer from the HTM. The hole travels through the HTM to the counter electrode where the HTM is reduced and the circuit completed. Current depends on the devices ability to generate and collect charge carries. Recombination losses occur when the electrons in the TiO_2 conduction band combine with oxidized dye molecules or holes in the HTM. The obtainable voltage depends upon the offset between the HTM HOMO and the TiO_2 Fermi level.⁷¹

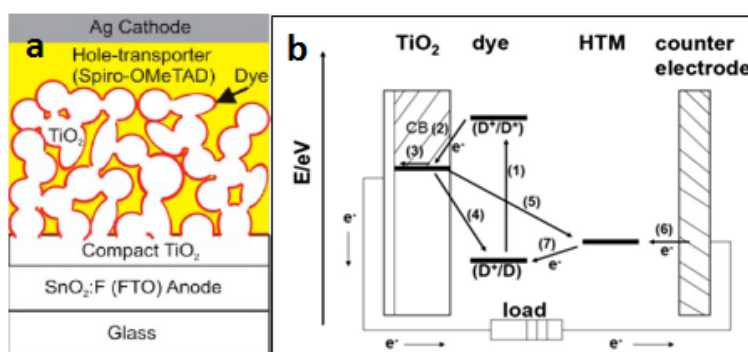


Figure 22: The DSSC. a) Basic structure of a solid state DSSC using spiro-OMeTAD as HTM⁷² b) Energy level diagram of a DSSC illustrating the operation of the device.⁷¹

The first HTMs were based on liquid electrolytes, commonly an iodide/triiodide redox couple. However these are fundamentally limited by the high overpotential required to drive the redox process, reducing the maximum obtainable voltage.⁵⁶ This leads to a theoretical maximum obtainable power conversion efficiency of 13.4%,⁷³ well short of the approximately 30% limit predicted by Shockley and Queisser.⁷⁴ There are also stability issues stemming from the use of volatile organic solvents. These require well sealed devices and their corrosive nature makes them incompatible with many inorganic sensitizers such as quantum dots or perovskites. These

issues have led to the development of solid state HTMs based on organic small molecules or polymers. Use of solid state HTMs should reduce the loss-in-potential found with redox electrolytes and increase the theoretical maximum obtainable efficiency of DSSCs to just over 20%.⁷³ The first effective solid state HTM was spiro-OMeTAD, and it has yet to be surpassed in overall performance.

The success of spiro-OMeTAD largely stems from the good morphological stability provided by its spiro structure, and sufficient hole injection/transport properties provided by its dimethoxydiphenyl amine substituents.⁷⁵ The electron donating methoxy groups in the para positions lower the oxidation potential, and the HOMO level provides a good balance between hole-transfer yield and open-circuit voltage.^{63,76} As a small molecule it is more effective at filling the pores of mesoporous electrodes than polymeric HTMs. The tradeoff is that its hole mobility is adequate at best (10^{-5} - 10^{-3} cm² V⁻¹ s⁻¹) and chemical doping or additives such as LiTFSI are necessary to achieve sufficient conductivity.⁷⁰

Despite the theoretical advantages of solid state DSSCs and the success of spiro-OMeTAD as a HTM, the efficiencies of traditional DSSCs using solid state HTMs lag behind their liquid electrolyte counterparts. The best performing solid state DSSC is reported to have a power conversion efficiency of 7.2%,⁷⁷ well short of the theoretical performance limit of 20%⁷³ and less than the best performing liquid electrolyte DSSCs using photosensitizers based on ruthenium dyes (11.1%)⁷⁸ or porphyrins (12.3%).⁷⁹ While the solid state devices attain a higher photovoltage, their optimized device thickness is only 2 μ m.⁸⁰ This is too thin to provide the surface area necessary for good light absorption and is the limiting factor for solid state DSSC performance.

The origin of this thickness limitation was a matter of some debate. Initially it was attributed to incomplete pore filling of the mesoporous TiO_2 ,⁸⁰ and strategies were developed to increase the pore filling fraction.^{81,82} Further research demonstrated that a pore filling fraction of no more than 60% is sufficient, and that this is attainable for thicknesses of up to 5 μm .^{83,84} The limitation of device thickness is now attributed to parasitic losses resulting from light absorption by the doped spiro-OMeTAD.⁸⁵ Strategies to overcome this involve either making more conductive HTMs which require lower doping levels to achieve adequate hole mobilities, or photosensitizers with greater extinction coefficients which can absorb more light in the thinner devices.

This latter solution has largely been achieved by the development of organometallic mixed halide perovskites of the type $\text{CH}_3\text{NH}_3\text{PbI}_{3-x}\text{Cl}_x$. These materials are strong absorbers have been successfully used in solid state DSSCs.⁸⁶ However the excellent carrier transport properties of perovskites allow for thicker layers of the sensitizer and even allow for highly efficient planar heterojunction solar cells.⁸⁷ Spiro-OMeTAD has followed perovskites and been used in a variety of photovoltaic device architectures beyond DSSCs.⁷⁰ Beyond photovoltaics, spiro-OMeTAD has also been used as a hole transport material in OLEDs.⁸⁸

The simplest OLED consists of an electroluminescent material sandwiched between two electrodes. This requires the material to be able to inject and transport both electrons and holes, in addition to having desirable emissive properties- a demanding set of requirements. More commonly, a p- or n-type emitter is used in conjunction with an ETM or HTM or both. In addition to facilitating charge injection and transport, the charge transport material serves as a blocking layer to confine the carriers to the emissive

layer and improve efficiency.⁸⁹ Despite these advantages, there is still much interest in developing ambipolar compounds capable of transporting both electrons and holes as a path towards efficient single layer OLED devices.⁶²

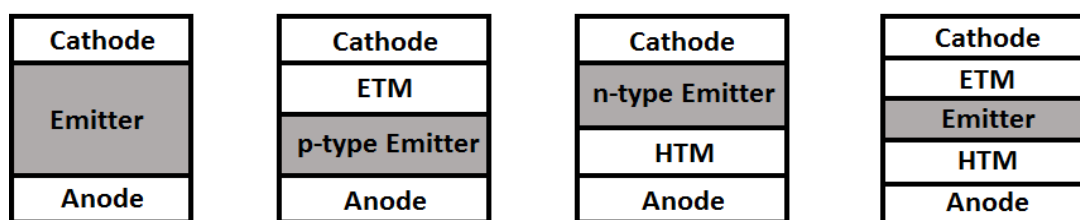


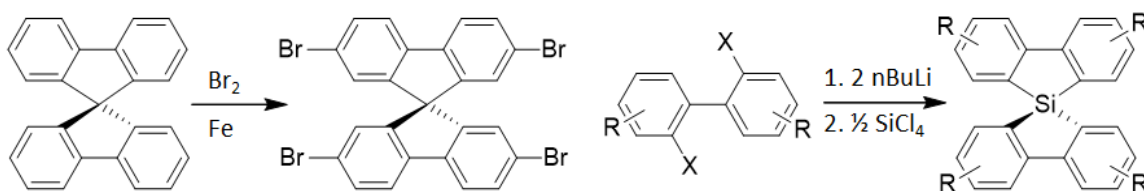
Figure 23: Common OLED architectures.⁸⁹

3.1.2 Spirosilabifluorenes

Despite the extensive interest in spirobifluorenes much less work has been done with the silicon analogs, spirosilabifluorenes, in which the central carbon atom is replaced by a silicon spiro-center. Incorporation of a silicon atom should combine the enhanced electron accepting ability of siloles with the morphological stability of the spiro structure. Spirosilabifluorenes may even have higher T_g 's than their carbon counterparts. This is inferred from the higher melting point of spirosilabifluorene relative to spirobifluorene (227 °C and 198 °C respectively).⁹⁰

In 2004 Kafafi et al. described⁹¹ the synthesis of a series of asymmetric spirosilabifluorenes containing a variety of tert-butyl, phenyl, and pyridine substituents. They studied the optical properties of these compounds and reported solid state photoluminescence with high quantum yields (30-55%). The absorbance spectra were found to be red shifted relative to the carbon analogues, confirming the presence of $\sigma^*-\pi^*$ conjugation in the spirosilabifluorene unit.

An added advantage of studying spiroxilabifluorene derivatives is that they allow for easier access to different substitution patterns. The first step in the synthesis of tetrasubstituted spirobifluorenes is the bromination of spirobifluorene, which results in primarily the 2,2',7,7' isomer. Other substitution patterns are more difficult and require lengthy multistep syntheses.⁹² Spirosilabifluorenes on the other hand are synthesized by lithiation of 2,2'-dihalobiphenyls followed by reaction with SiCl_4 . Any substituents can be included on the biphenyl provided they are less reactive with the organolithium reagent than the aryl halides. Consequently, a variety of symmetric and asymmetric substitution patterns are accessible.



Scheme 5: Comparison of synthetic routes to tetrasubstituted spirobifluorenes (left) and spiroxilabifluorenes (right). $\text{X} = \text{Br}$ or I .

The effects of 3,3',6,6' and 2,2',7,7' substitution patterns for spiroxilabifluorenes have been examined both experimentally and theoretically. In 2010 Kawashima et al.⁹³ synthesized a series of silafluorenes and spiroxilabifluorenes containing electron donating aminostyryl arms at either the 3,6 or 2,7 positions with the aim of elucidating the effects of different substitution patterns as well as the effect of the spiro linkage. They found that the spiro compounds had smaller HOMO-LUMO gaps, attributed to the effect of spiroconjugation increasing the HOMO level and improved $\sigma^*-\pi^*$ conjugation relative to the non-spiro linked siloles further lowering the LUMO. The HOMO-LUMO gap was

smaller for compounds with 2,7 substitution, owing to this being a better π connecting unit than the 3,6 positions. This led to reduced and blue shifted fluorescence for the 3,6 substituted compounds.

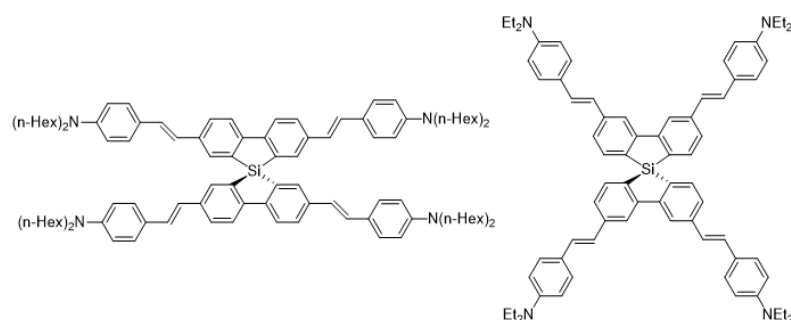


Figure 24: Spirosilabifluorenes studied by Kawashima et al.⁹³
 Left: 2,2',7,7' (or 2,7) substitution. Right: 3,3',6,6' (or 3,6) substitution.

As expected, the spiro compounds displayed improved solubility in organic solvents due to suppressed intermolecular π - π interactions. Interestingly, the 3,6 substituted compounds had greater solubility than the 2,7 despite containing diethyl amines rather than the longer di-n-hexyl amines. This is particularly relevant for solution-processed devices, and in applications containing mesoporous substrates may allow for a higher pore filling fraction without sacrificing the thermal stability associated with a high T_g .

Shortly after this report, Yang and Si⁹⁴ produced a theoretical study on the nonlinear optical properties and reorganization energies of a number of silafluorenes and spiro-silabifluorenes as well as their carbon analogues. The second order polarizabilities and reorganization energies of 3,6- substituted compounds were found to be superior to that of the 2,7- substituted ones. While enhanced second order polarizability makes these

compounds interesting for their NLO properties, the reorganization energy is particularly relevant for charge transport materials.

In contrast to bulk inorganic semiconductors, in which charge carriers are described by plane waves delocalized throughout the crystal lattice, charge transport in amorphous films of small molecules is described as a chain of redox processes in which the charges “hop” from molecule to molecule.⁹⁵ In this situation the charge transfer rate can be described by Marcus Theory. One of the principle variables affecting the rate is the reorganizational energy (λ) which is the energy cost due to molecular geometry modifications to go from the neutral to charged state. A smaller reorganization energy leads to an increased charge transfer rate.

$$k = \frac{4\pi^2}{h} H_{ab}^2 \frac{\exp\left(-\frac{\lambda}{4k_B T}\right)}{\sqrt{4\pi\lambda k_B T}}$$

Equation 4:⁹⁶ Intermolecular hopping rate (k) as a function of temperature (T), overlap integral (H_{ab}), and reorganization energy (λ).

To help predict the effect of isomerism and silicon substitution on charge transport in amine-substituted spirobifluorenes such as spiro-OMeTAD, DFT calculations using the B3LYP method with 6-31G* basis set were carried out. This is the same level of theory used by Yang and Si.⁹⁴ The hole reorganization energy was calculated for the four different spirobifluorenes shown in figure 25. It was determined by calculating the molecular energy at four different states: $E(A)$, the energy of the neutral compound in its ground state geometry; $E(A^+)$, the energy of the neutral compound in the cations most stable geometry; $E^+(A^+)$, the energy of the cation in its most stable geometry; and $E^+(A)$,

the energy of the cation in the neutral compounds most stable geometry. The hole reorganization energy can then be calculated by using equation 5:

$$\lambda_{hole} = [E^+(A) - E^+(A^+)] + [E(A^+) - E(A)]$$

Equation 5: Calculation of hole reorganization energy.

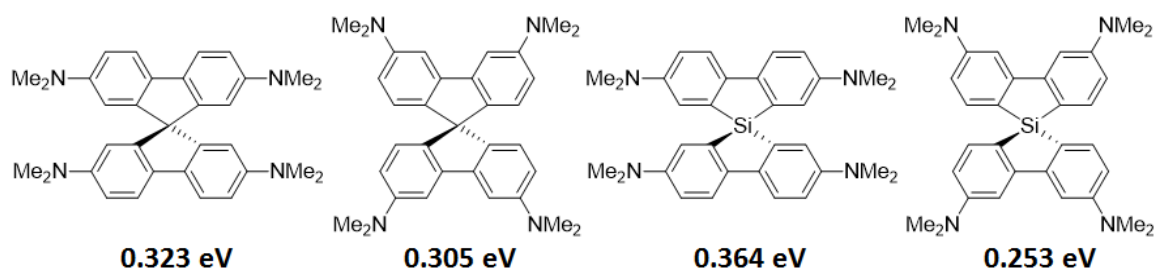


Figure 25: Tetrakis(dimethylamino)spirobifluorenes modeled by DFT and their calculated hole reorganization energies.

The results are consistent with those of Yang and Si. In both cases the 3,6 isomer had a smaller λ_{hole} than the 2,7 analogue. There is not a trend as to the identity of the spiro center; in the instance of the 2,7 isomer the carbon-centered compound has a smaller λ_{hole} , while the 3,6 isomer of the silicon analogue has the smallest hole reorganization energy of all four compounds. These results indicate that 3,6 isomers of spirobifluorenes may have enhanced hole transport properties relative to the more well studied 2,7 isomers.

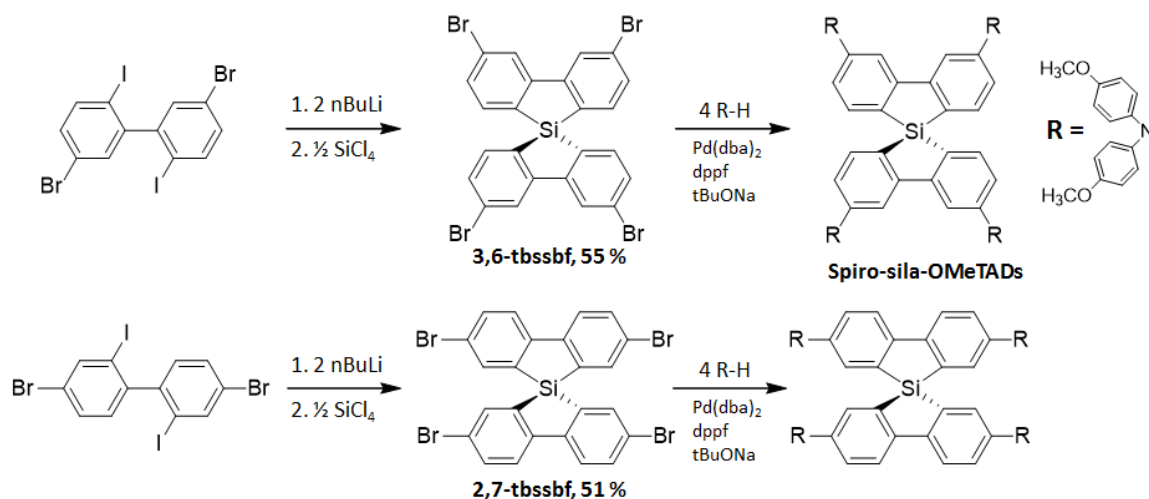
3.2 Spiro-sila-OMeTAD

Considering the potential advantages imbued by the silicon spiro center, the silicon analogue to spiro-OMeTAD was deemed an interesting synthetic target. By synthesizing both the 2,7 and 3,6 isomers, the effect of different substitution patterns as

well as the effect of silicon substitution can be compared. The silicon substitution is expected to increase the compounds electron affinity, possibly affording a degree of ambipolar charge transport. It's also expected to increase the T_g , improving morphological stability. The 3,6 isomer, difficult to obtain for the carbon analogue, should be more soluble and may have improved charge transport properties.

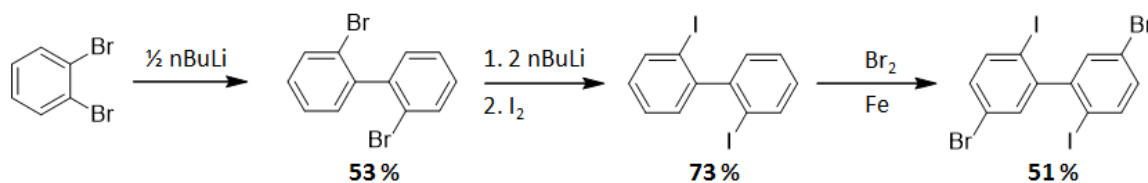
3.2.1 Tetrabromospirosilabifluorenes

Our basic strategy to synthesizing spiro-sila-OMeTAD was to first synthesize the two isomers of tetrabromospirosilabifluorene (tbssbf). As aryl bromides, these compounds were expected to be versatile partners for a variety of cross-coupling reactions beyond aminations. Our approach to synthesizing tbssbf followed the method developed by Henry Gilman:⁹⁷ reaction of biphenyl dilithium derivatives with silicon tetrachloride. This would require symmetric dibromodiiodobiphenyls with iodides in the 2,2' positions owing to their greater reactivity toward lithiation.



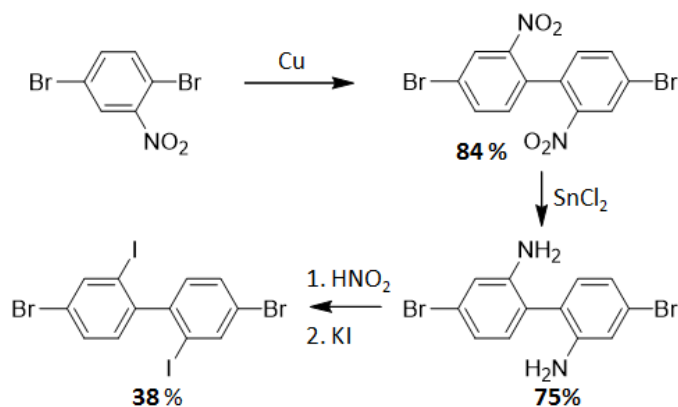
Scheme 5: Synthetic approach toward spiro-sila-OMeTADs starting from dibromodiiodobiphenyls.

5,5'-dibromo-2,2'-diiodobiphenyl and 4,4'-dibromo-2,2'-diiodobiphenyl are known compounds, and our syntheses were adapted from literature sources. Reaction of 1,2-dibromobenzene with half an equivalent of n-butyl lithium at low temperature followed by slowly warming to room temperature yields 2,2'-dibromobiphenyl.⁹⁸ This reaction was found to follow a mechanism in which the monolithiated bromobenzene adds to a transient benzyne species.⁹⁹ Dilithiation of dibromobenzene followed by reaction with iodine produces diiodobiphenyl in a straightforward manner.¹⁰⁰ Finally, the iron catalyzed bromination of diiodobiphenyl affords the desired 5,5'-dibromo-2,2'-diiodobiphenyl.¹⁰¹ The selectivity observed in this electrophilic aromatic substitution arises from the phenyl rings being twisted out of conjugation by steric influences, leading to preferential stabilization of the arenium intermediate by the iodo substituents.



Scheme 6: Synthesis of 5,5'-dibromo-2,2'-diiodobiphenyl from dibromobenzene.

Copper catalyzed Ullman coupling of 1,4-dibromo-2-nitrobenzene leads to 4,4'-dibromo-2,2'-dinitrobiphenyl.¹⁹ Reaction of tin metal with HCl generates SnCl₂ in situ, which reduces the nitro groups to form 4,4'-dibromobiphenyl-2,2'-diamine.¹⁵ Diazotisation conditions followed by addition of potassium iodide afford 4,4'-dibromo-2,2'-diiodobiphenyl in a Sandmeyer-type reaction.¹⁰²



Scheme 7: Synthesis of 4,4'-dibromo-2,2'-diiodobiphenyl from dibromonitrobenzene.

Lithiation of 5,5'-dibromo-2,2'-diiodobiphenyl and 4,4'-dibromo-2,2'-diiodobiphenyl followed by reaction with SiCl_4 successfully led to the corresponding tetrabromospirosilabifluorenes in moderate yields (55% and 51% respectively). It is likely that yields could be improved even further with optimized reaction conditions and work up procedures. The reactions were relatively clean and the crude products could be purified by rinses and recrystallizations, without the use of chromatography.

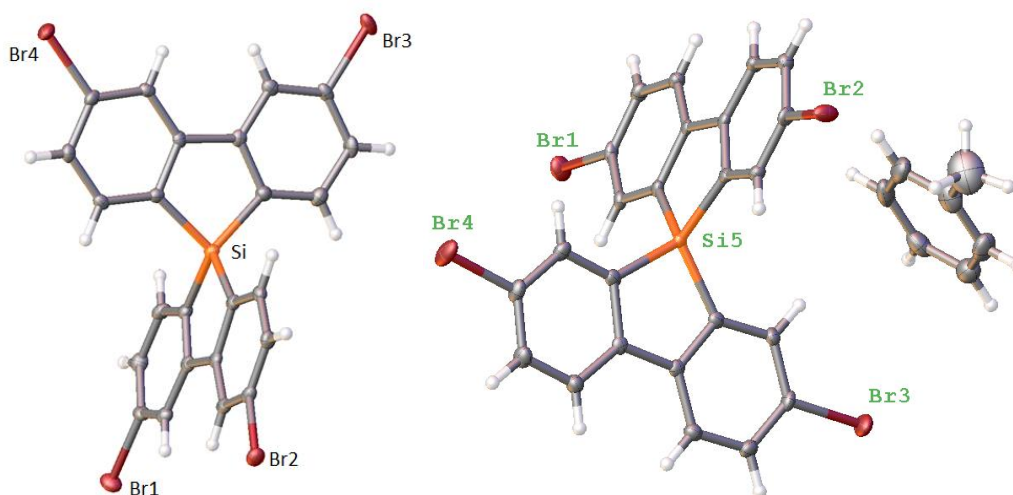


Figure 26: ORTEP representations of 3,3',6,6'-tetrabromospirosilabifluorene (3,6-tbssbf, left, $R = 2.2\%$) and 2,2',7,7'-tetrabromospirosilabifluorene, co-crystallized with solvent toluene (2,7-tbssbf, right, $R = 3.3\%$).

The two tetrabromospirosilabifluorenes had similar UV-vis absorption spectra in CHCl_3 . The 2,7 isomer had local maxima at 304 and 291 nm, while the 3,6 isomer had weaker and slightly shifted absorptions at 301 and 289 nm. The 2,7 isomer also had a weak longer wavelength absorption at 345 nm absent in the 3,6. Both compounds displayed solid state phosphorescence at 77 K.

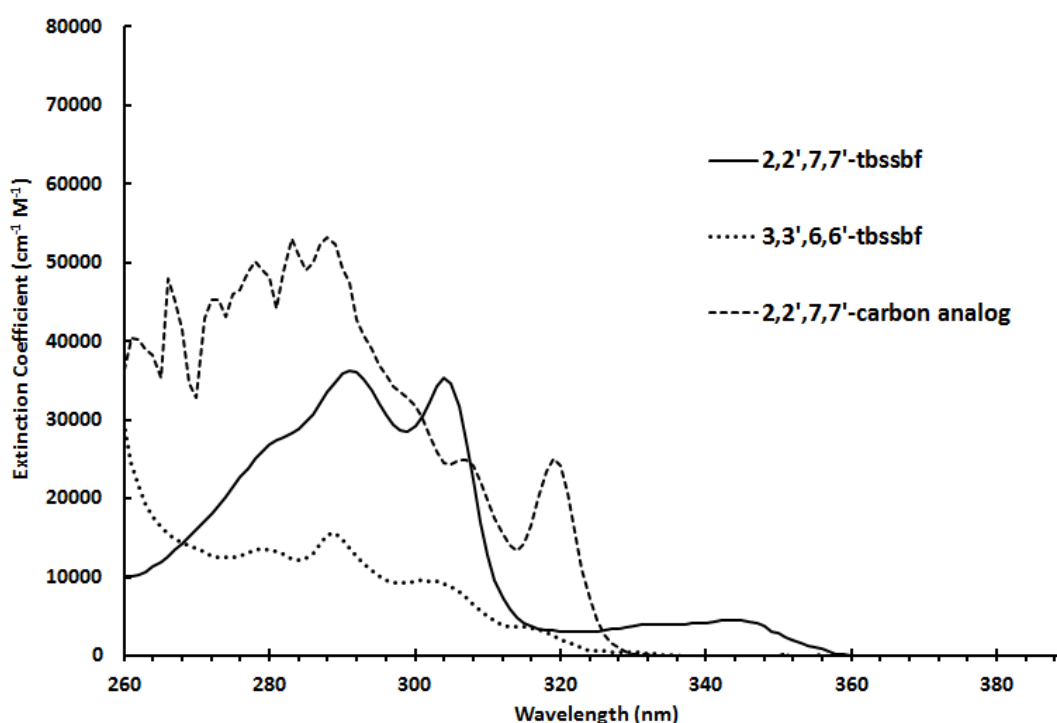


Figure 27: UV-Vis absorbance spectra of tetrabromospirobifluorenes (CHCl_3).

3.2.2 Cross Coupling Reactions

Buchwald-Hartwig amination of tbssbf was expected to proceed analogously to that of the carbon analog and give the corresponding spiro-sila-OMeTADs. Following literature procedures,¹⁰³ neither spiro-sila-OMeTAD nor the starting tbssbf were found in the worked up crude product per $^1\text{H-NMR}$. MALDI-TOF-MS of the product showed no

spiro-sila-OMeTAD (m/z molecular ion = 1240.5), but had a base peak at $m/z = 608.0$. This is consistent with OMe-TAD, the non-spiro linked “half” of the compound. This would indicate that the amination is occurring, but that the silicon linkage is not stable under the reaction conditions.

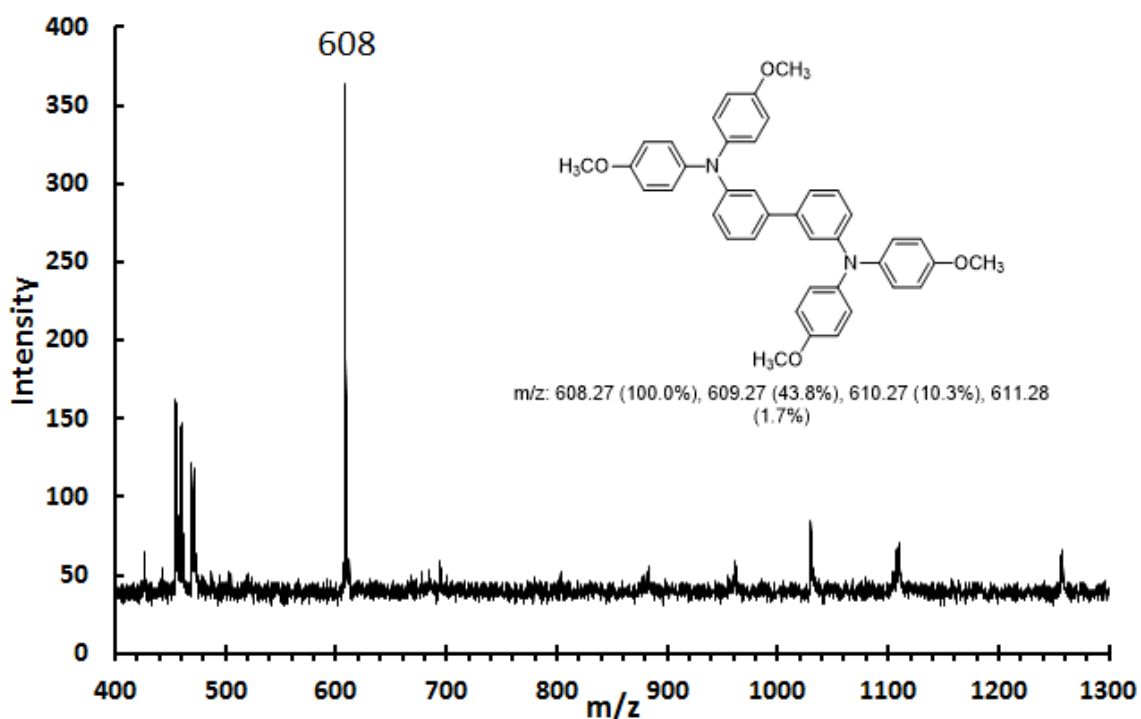
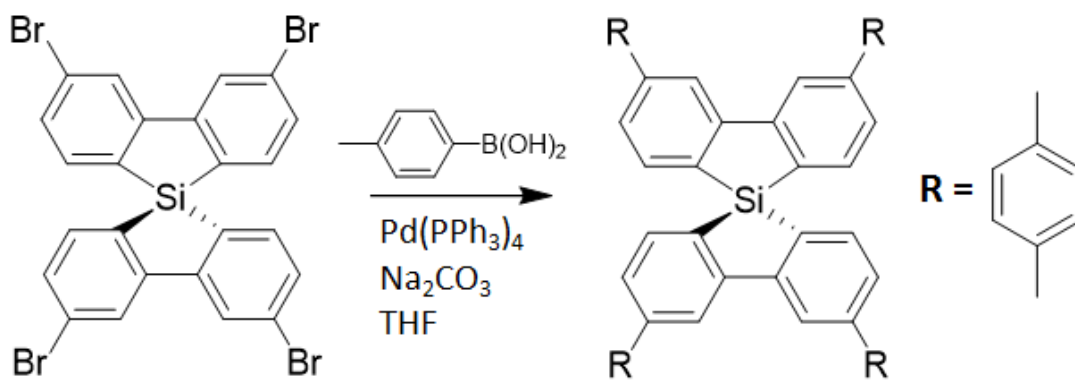


Figure 28: MALDI-TOF-MS of spiro-sila-OMeTAD reaction product. Inset: OMeTAD, assigned to the base peak at 608 m/z .

To ensure that the peak seen in the MALDI mass spectrum was the molecular ion and not a fragment arising from the ionization method, the stability of tbssbf under the reaction conditions was tested by refluxing in toluene with sodium tert-butoxide. After 15 h, the reaction mixture was checked by GC-MS and found to contain predominantly dibromobiphenyl. No starting material was found, the only other peaks in the GC being minor and unidentifiable. This was found to be the case for both isomers. Amination of

2,7-tbssbf was also attempted at 50 °C under otherwise identical conditions; after two days the worked up reaction mixture contained predominantly dibromobiphenyl and dimethoxydiphenylamine per GC-MS and $^1\text{H-NMR}$.

In an effort to use the tetrabromospirosilabifluorenes as starting materials for other electroactive compounds, their suitability toward Suzuki coupling was explored. Suzuki coupling still requires a base, in this case to activate the boronic acid coupling partner, but milder bases such as sodium carbonate are typically used. As a coupling partner, p-tolyl boronic acid was chosen. The desired product, tetratolyl spirosilabifluorene, is expected to have interesting solid-state fluorescence properties.



Scheme 8: Attempted synthesis of 3,3',6,6'-tetratolylspirosilabifluorene.

3,6-tbssbf was reacted with p-tolyl boronic acid in the presence of $\text{Pd}(\text{PPh}_3)_4$ and sodium carbonate. The crude product was analyzed by MALDI-TOF-MS. The only significant peak in the mass spectrum was $m/z = 334.2$. This is consistent with dimethyl tetraphenyl. Again it appears that the coupling reaction is working, but that the spiro-linked compound is not stable in alkaline conditions. In support of this, heating 3,6-tbssbf

in a THF/2 M Na₂CO_{3(aq)} mixture at 80 °C for 6 resulted in dibromobiphenyl as determined by GC-MS.

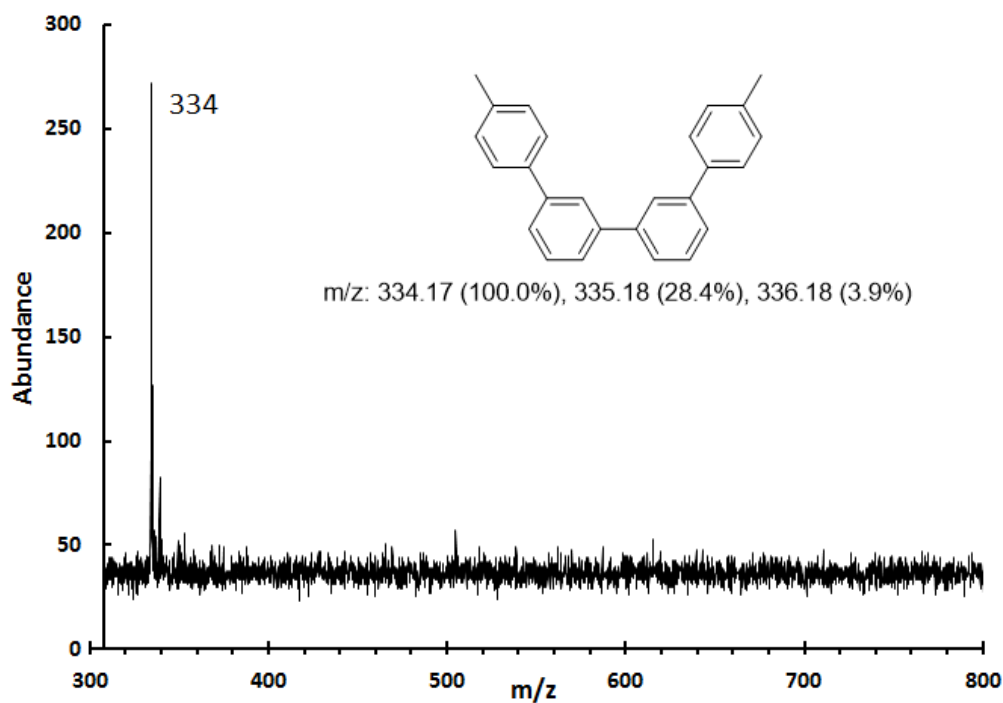


Figure 29: MALDI-TOF-MS of tetratolyl spirobifluorene reaction product. Inset: species assigned to the base peak at 334 m/z.

For comparison, the carbon analog tetrabromospirobifluorene was coupled with p-tolyl boronic acid. The mass spectrum shows a peak at $m/z = 675.9$, consistent with the desired product tetratolyl spirobifluorene. The minor peak at $m/z = 586.1$ appears to show the loss of a tolyl group. This confirms the increased susceptibility of the silicon analogue to decomposition in basic conditions.

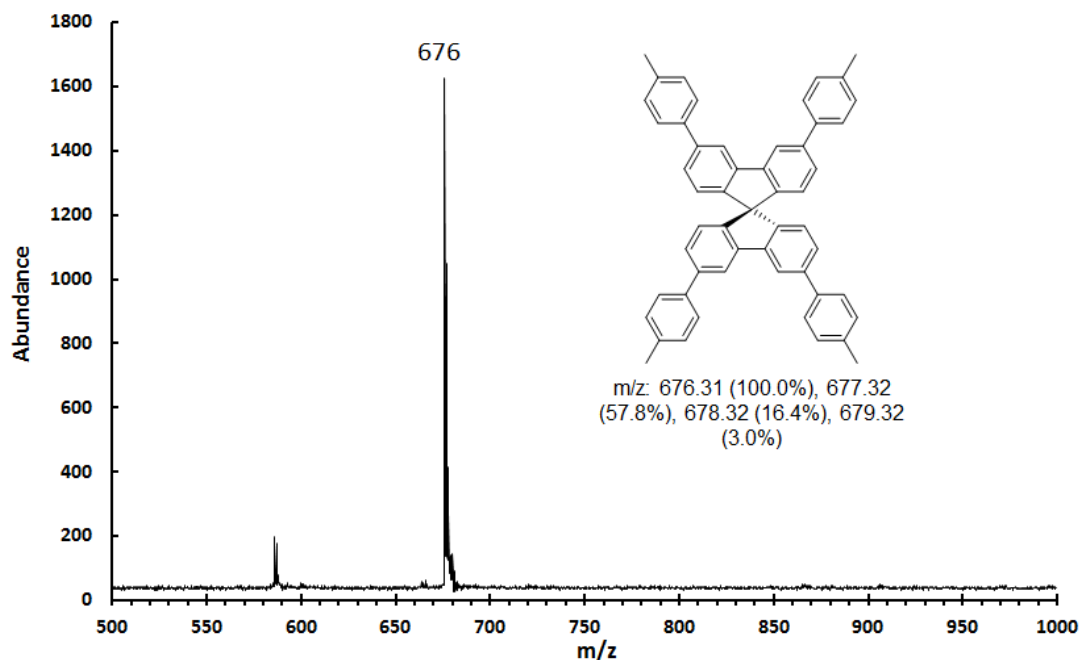


Figure 30: MALDI-TOF-MS of tetratolyl spirobifluorene. Inset: 3,3',6,6'-tetratolyl spirobifluorene.

3.3 Experimental

3.3.1 Instrumentation and General Methods

Absorption spectra were measured with a Cary 300 UV-Vis spectrophotometer. Spectroelectrochemical measurements were made with an Agilent 8453 diode array UV-Vis spectrophotometer in a Pine Research Instrumentation honeycomb spectroelectrochemical cell. Fluorescence measurements were conducted on a Jobin-Yvon Fluorolog 3 fluorescence spectrometer. ^1H and ^{13}C NMR spectra were acquired using a JEOL 300 MHz NMR spectrometer. For the ^{29}Si spectra a JEOL 500 MHz NMR spectrometer was used. Combustion analysis (C, H, and N) was conducted by Atlantic Microlab, Inc.

Cyclic voltammetry studies were performed using a Princeton Applied Research Model 273A Potentiostat/Galvanostat employing a conventional three-electrode setup

consisting of a platinum disk or glassy carbon working electrode, a silver/silver chloride reference electrode, and a platinum wire auxiliary electrode. Positive feedback iR compensation was routinely used. Voltammograms were obtained in 0.1 M tetrabutylammonium hexafluorophosphate (TBAPF₆)/acetonitrile solution using solvent that had previously been purified and dried using a solvent purification system (SPS- 400, Innovative Technologies) and subsequently purged with nitrogen. The supporting electrolyte (TBAPF₆) was recrystallized from ethanol and dried under vacuum prior to use. Ferrocene was used as an internal standard without further purification.

Crystals of suitable size were removed from the mother liquor, coated with a thin layer of paratone-N oil, mounted on the Agilent Gemini A Ultra diffractometer, and flashcooled to 100 K in the cold stream of the Cryojet XL liquid nitrogen cooling device (Oxford Instruments) attached to the diffractometer. The Gemini A Ultra diffractometer was equipped with a sealed-tube long fine focus X-ray source with Mo target ($\lambda = 0.71073 \text{ \AA}$) and Cu target ($\lambda = 1.5418 \text{ \AA}$), four-circle kappa goniometer, and Kodak CCD detector. CrysAlisPro⁴⁸ software was used to control the diffractometer and perform data reduction. The crystal structure was solved with SHELXS⁴⁹. All non-hydrogen atoms appeared in the E-map of the correct solution. Alternate cycles of model-building in Olex2⁵⁰ and refinement in SHELXL⁴⁹ followed. All non-hydrogen atoms were refined anisotropically. All hydrogen atom positions were calculated based on idealized geometry, and recalculated after each cycle of least squares. During refinement, hydrogen atom – parent atom vectors were held fixed (riding motion constraint). Crystallographic data is provided in appendix A.

3.3.2 Synthetic Details

4,4'-Dibromo-2,2'-dinitrobiphenyl¹⁸

34.9 g of 2,5-dibromonitrobenzene (124.2 mmol) was dissolved in 140 mL dry DMF in a 250 mL round bottom flask with stir bar and condenser. 18.9 g activated Cu powder (306 mmol) was added and the resulting mixture stirred and heated in an oil bath at 125 °C for 3 h. The mixture was allowed to cool to room temperature and 100 mL toluene added.

This mixture was filtered through celite and evaporated to dryness. The brown crude product was rinsed twice with H₂O, redissolved in toluene and again filtered through celite. The filtrate was dried with MgSO₄ and evaporated under reduced pressure to yield the title compound as a yellow solid (21.0 g, 84.5%). The δ_{H} data is in agreement with literature values.¹⁰² ¹H NMR (CDCl₃, 300 MHz): δ = 8.38 (s, 2 H), 7.83 (d, 2 H), 7.17 (d, 2 H). MS (EI): m/z = 401.9 (M⁺), 355.9 ([M-NO₂]⁺)

4,4'-dibromobiphenyl-2,2'-diamine¹⁵

15.0 g 4,4'-dibromo-2,2'-dinitrobiphenyl (37.4 mmol) was dissolved in 125 mL EtOH (95%) in a 500 mL round bottom flask with stir bar. 82 mL HCl (32% w/w) and 11.8 g Sn powder (100 mmol) were added and the resulting mixture refluxed for 2 h. The mixture was allowed to cool and poured into approximately 200 ml ice water. NaOH (20% w/w) was added until the pH was greater than 9. This mixture was extracted with 3x100 mL portions of Et₂O, dried over Na₂SO₄ and evaporated under reduced pressure to yield a brown powder (9.6 g, 75%). The δ_{H} data is in agreement with literature values.¹⁰² ¹H NMR (CDCl₃, 300 MHz): δ = 6.93 (m, 6 H), 3.75 (s, b, 4 H). MS (EI): m/z = 342.0 (M⁺), 324.9 ([M-NH₂]⁺)

4,4'-dibromo-2,2'-diiodobiphenyl¹⁰²

5.0 g 4,4'-dibromobiphenyl-2,2'-diamine (14.6 mmol), 45 ml HCl (32% w/w), 160 mL H₂O, and 160 mL CH₃CN were added to a 500 ml three neck round bottom flask. The mixture was cooled to -15 °C and a solution of 4.63 g NaNO₂ (67.1 mmol) in 15 mL H₂O was added dropwise. The reaction was stirred between -10 to -15 °C for 1 h. A solution of 22.2 g KI (134 mmol) in 20 mL H₂O was added dropwise while maintaining this temperature. The reaction was allowed to warm to room temperature and then heated at 80 °C for 15 h. The product was extracted with CHCl₃, washed with Na₂S₂O_{3(aq)}, H₂O, and brine, dried with MgSO₄, and evaporated to dryness. The resulting solid was purified by column chromatography (SiO₂, hexanes) followed by recrystallization from hexane to yield title compound as white crystals (3.1 g, 38%). The δ_H data is in agreement with literature values.¹⁰² ¹H NMR (CDCl₃, 300 MHz): δ = 8.09 (s, 2 H), 7.56 (d, 2 H), 7.03 (d, 2 H). MS (EI): *m/z* = 563.7 (M⁺), 436.8 ([M-I]⁺)

2,2',7,7'-tetrabromospirosilabifluorene

A 100 ml three neck round bottom flask was charged with 3.00 g 4,4'-dibromo-2,2'-diiodobiphenyl (5.32 mmol) and 60 mL dry THF. The solution was subjected to three freeze pump thaw cycles and cooled to -90 °C. 4.84 ml n-BuLi (2.2 M in hexanes, 10.6 mmol) was added dropwise via syringe. The reaction was stirred at this temperature for one hour, and 0.6 ml SiCl₄ (0.5 mmol) was added dropwise. The reaction was allowed to warm to room temperature and stirred overnight. 100 mL H₂O was added to the solution and the resulting mixture was extracted with diethyl ether (3 x 100 ml). The organic layer was dried with MgSO₄, filtered, and evaporated to dryness to yield a yellow/orange solid.

The crude product was rinsed thoroughly with cold dichloromethane to yield 0.95 g product as a white powder (55%). Crystals suitable for x-ray analysis were grown via slow evaporation of a filtered toluene solution at room temperature. ^1H NMR (CDCl_3 , 300 MHz): δ = 7.75 (d, 4 H), 7.65 (d, 4 H), 7.50 (s, 4 H). ^{13}C NMR (CDCl_3 , 300 MHz): δ = 147.8, 137.1, 135.1, 133.7, 123.2, 123.0 ppm. ^{29}Si NMR (CDCl_3 , 500 MHz): δ = -7.32 ppm. MS (EI): m/z = 647.7 (M^+). Elemental analysis calcd (%) for $\text{C}_{24}\text{H}_{12}\text{Br}_4\text{Si}$: C 44.48, H 1.87, N 0; found: C 44.55, H 1.84, N 0.0.

Attempted synthesis of 2,2',7,7'-spiro-sila-OMeTAD⁸¹

0.100 g 2,2',7,7'-tetrabromospirosilabifluorene (0.15 mmol), 0.163 g bis(4-methoxyphenyl)amine (0.71 mmol), 0.066 g sodium tert-butoxide (0.69 mmol), 0.01 g $\text{Pd}(\text{dba})_2$ (0.02 mmol), and 0.01 g 1,1'-Bis(diphenylphosphino) (0.02 mmol) were transferred to a 50 ml schlenk flask. 5 ml anhydrous toluene was added and the mixture stirred for 12 h at 110 °C. DI water was added, and the product was extracted with EtOAc, dried with MgSO_4 , filtered, and evaporated.

2,2'-dibromobiphenyl⁹⁸

22.1 g 1,2-dibromobenzene (93.6 mmol) was dissolved in 150 ml THF in a 250 ml three neck round bottom flask and cooled to -90 °C. 23.0 mL 2.2 M n-BuLi (50.6 mmol) was added dropwise. The reaction mixture was slowly warmed to room temperature and allowed to stir overnight. 100 ml 0.5 M $\text{HCl}_{(\text{aq})}$ was added to neutralize the mixture, which was then extracted with Et_2O , dried with MgSO_4 , and evaporated to dryness. The crude product was recrystallized from ethanol to yield title compound as white crystals

(7.7 g, 53%). The δ_{H} data is in agreement with literature values.¹⁰¹ ^1H NMR (CDCl_3 , 300 MHz): $\delta = 7.67$ (d, 2 H), 7.38 (m, 2 H), 7.29 (m, 2 H), 7.24 (d, 2 H). MS (EI): $m/z = 312.0$ (M^+), 231.0 ($[\text{M}-\text{Br}]^+$)

2,2'-diiodobiphenyl¹⁰⁰

11.25 g 2,2'-dibromobiphenyl (36.1 mmol) was dissolved in 100 ml THF in a 250 ml three neck round bottom flask. The solution was cooled to $-90\text{ }^\circ\text{C}$ and 32.8 ml n-BuLi (2.2 M, 72.2 mmol) was added dropwise. The mixture was stirred at this temperature for 1 h and a solution of 21.4 g I_2 (84.3 mmol) in 40 mL THF was added dropwise via cannula. The mixture was allowed to warm to room temperature and stirred overnight. H_2O was added and the reaction mixture extracted 3 times with diethyl ether. The combined organic phases were dried over MgSO_4 and evaporated to dryness. The resulting solid was recrystallized from hexanes to yield title compound as white needles (10.7 g, 73%). The δ_{H} data is in agreement with literature values.¹⁰¹ ^1H NMR (CDCl_3 , 300 MHz): $\delta = 7.95$ (d, 2 H), 7.43 (m, 2 H), 7.20 (d, 2 H), 7.10 (d, 2 H) MS (EI): $m/z = 405.8$ (M^+), 278.9 ($[\text{M}-\text{I}]^+$)

5,5'-dibromo-2,2'-diiodobiphenyl¹⁰¹

To a solution of 4.06 g 2,2'-diiodobiphenyl (10.0 mmol) in 80 ml CHCl_3 was added 0.080 g iron powder. 2.0 mL Br_2 (39 mmol) was added via syringe and the mixture stirred for 1 h at $55\text{ }^\circ\text{C}$. The mixture was allowed to cool to room temperature, washed with $\text{Na}_2\text{S}_2\text{O}_3$, and extracted three times with CH_2Cl_2 . The combined organic layers were dried with MgSO_4 and evaporated under vacuum. The crude product was rinsed with cold

CH₂Cl₂ to yield title compound as a white powder (2.9 g, 51%). The δ_{H} data is in agreement with literature values.¹⁰² ¹H NMR (CDCl₃, 300 MHz): δ = 7.78 (d, 2 H), 7.32 (s, 2 H), 7.24 (d, 2 H). MS (EI): m/z = 563.7 (M⁺), 436.8 ([M-I]⁺)

3,3',6,6'-tetrabromo-spirosilabifluorene

A 100 ml three neck round bottom flask was charged with 3.00 g 5,5'-dibromo-2,2'-diiodobiphenyl (5.32 mmol) and 60 mL dry THF. The solution was subjected to three freeze pump thaw cycles and cooled to -90 °C. 4.84 ml n-BuLi (2.2 M in hexanes, 10.6 mmol) was added dropwise via syringe. The reaction was stirred at this temperature for 1 h, and 0.6 ml SiCl₄ (0.5 mmol) was added dropwise. The reaction was allowed to warm to room temperature and stirred overnight. 100 mL H₂O was added to the solution and the resulting mixture was extracted with diethyl ether (3 x 100 ml). The organic layer was dried with MgSO₄, filtered, and evaporated to dryness to yield a yellow/orange solid. The crude product was rinsed thoroughly with dichloromethane to yield 0.88 g product as a white powder (51%). Crystals suitable for x-ray analysis were grown via slow evaporation of a filtered ethyl acetate solution at room temperature. ¹H NMR (CDCl₃, 300 MHz): δ = 8.01 (s, 4 H), 7.40 (d, 4 H), 7.24 (d, 4 H). ¹³C NMR (CDCl₃, 300 MHz): δ = 150.6, 135.6, 131.7, 130.3, 127.3, 125.0 ppm. ²⁹Si NMR (CDCl₃, 500 MHz): δ = -6.90 ppm. MS (EI): m/z = 647.7 (M⁺). Elemental analysis calcd (%) for C₂₄H₁₂Br₄Si: C 44.48, H 1.87, N 0; found: C 44.46, H 1.71, N 0.0.

Attempted synthesis of 3,3',6,6'-spiro-sila-OMeTAD²⁰

0.100 g 3,3',6,6'-tetrabromospirosilabifluorene (0.15 mmol), 0.163 g bis(4-methoxyphenyl)amine (0.71 mmol), 0.066 g sodium tert-butoxide (0.69 mmol), 0.01 g Pd(dba)₂ (0.02 mmol), and 0.01 g 1,1'-Bis(diphenylphosphino) (0.02 mmol) were transferred to a 50 ml schlenk flask. 5 ml anhydrous toluene was added and the mixture stirred for 12 h at 110 °C. DI water was added, the product was extracted with EtOAc, dried with MgSO₄, filtered, and evaporated.

Attempted synthesis of 3,3',6,6'-tetratolyl-spirosilabifluorene

0.040 g 3,3',6,6'-tetrabromospirosilabifluorene (0.062 mmol), 0.042 g p-tolylboronic acid (0.31 mmol), 2 mg Pd(dba)₂ (0.004 mmol), and 5 mg triphenylphosphine (0.02 mmol) were combined in a 50 ml round bottom flask with 0.8 ml THF and 0.4 ml 2.2 M Na₂CO₃. The reaction mixture was heated at 80 °C for 18 h. 5 ml ethyl acetate was added and the organic later washed with H₂O. The organic layer was dried with MgSO₄ and evaporated to dryness. The product was analyzed by MALDI-TOF-MS, and the base peak was found to be m/z = 334.2.

Synthesis of 2,2',7,7'-tetratolyl-spirobifluorene

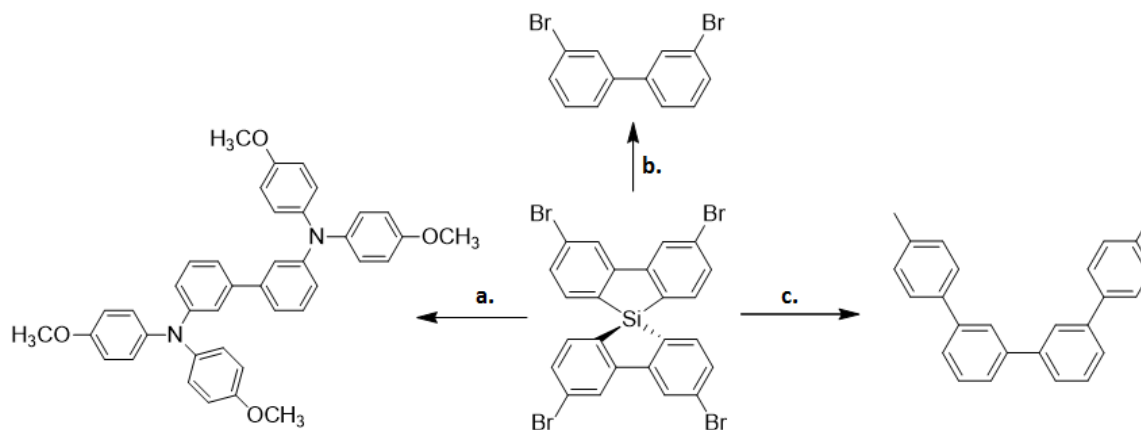
0.025 g 2,2',7,7'-tetrabromospirobifluorene (0.040 mmol), 0.025 g p-tolyl boronic acid (0.18 mmol), approximately 2 mg Pd(dba)₂ (0.004 mmol) and 5 mg PPh₃ (0.019 mmol) were added to a 25 ml round bottom flask equipped with stir bar and condenser. 0.6 ml THF and 0.4 ml 2.0 M Na₂CO_{3(aq)} were added and the mixture degassed. The reaction mixture was heated at 80 °C for 8 h. 10 ml ethyl acetate was added, the organic layer

washed with H₂O, dried with MgSO₄, and evaporated to dryness to yield the title compound. MS (MALDI-TOF): $m/z = 675.9$ (M⁺), 586.1 ([M-tolyl]⁺).

3.4 Discussion

Synthesis of the 2,7 and 3,6 isomers of tetrabromospirobifluorene was successful. While the 2,7 isomer has been reported in the primary literature¹⁰⁴ and the 3,6 isomer in the patent literature¹⁰⁵, characterization was limited to ¹H and ¹³C NMR for the former and was nonexistent for the latter. For both compounds we have successfully obtained ¹H, ¹³C, and ²⁹Si NMR, UV-Vis absorbance, elemental analysis, and crystal structures.

Attempts to couple the tetrabromospirosilabifluorenes to dimethoxydiphenyl amines via Buchwald-Hartwig amination and to p-tolyl boronic acids via Suzuki coupling both failed. Both of these palladium catalyzed coupling reactions are carried out under basic conditions. It appears that while the coupling reactions succeed, the silicon-aryl bonds are broken in basic conditions, leaving the non spiro-linked fragment. Attempts to reduce reaction temperatures and times (50 to 80 °C and 6 to 24 h) failed to prevent complete loss of the spiro linkage.



Scheme 9: Summary of the reactivity of 3,3',6,6' tetrabromospirosilabifluorene. a) Pd(dppf), tBuONa, dimethoxydiphenyl amine, toluene, reflux 12 h. b) tBuONa or Na₂CO₃, reflux 6 h. c) Pd(PPh₃)₄, Na₂CO₃, reflux 8 h.

This result is surprising; while the average Si-C bond enthalpy is less than that of a C-C bond, it is only marginally so (301 vs 348 kJ/mol).¹⁰⁶ While perhaps the larger silicon atom is sterically more vulnerable, similar reactions have been successfully carried out with spiro-silabifluorenes. Tian et al. reported⁹⁰ the synthesis of a triphenylamine-spirosilabifluorene copolymer prepared via Suzuki coupling of 2,2'-dibromo spiro-silabifluorene with triphenylamine diboronic acid. They refluxed the reactants and the palladium catalyst in a THF/K₂CO₃ mixture of unspecified concentration for three days and reported a 75% yield. This a significantly longer reaction time than any of our attempts; perhaps the electron withdrawing effect of two additional bromides makes the silicon center more susceptible to attack.

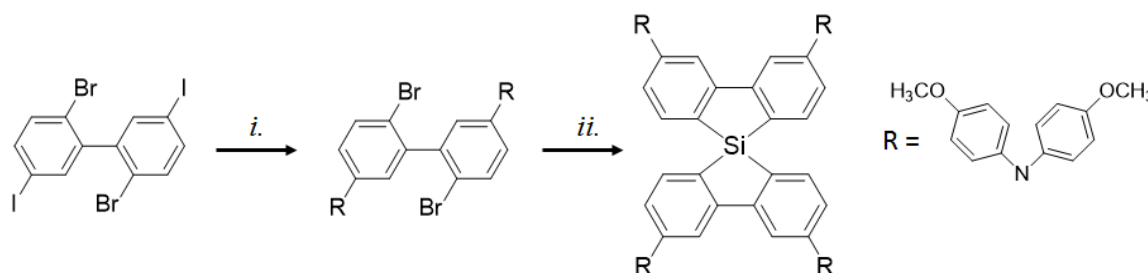
CHAPTER 4: CONCLUSION AND FUTURE WORK

We successfully synthesized the first silylene bridged methyl viologen, or siloloviologen. The silylene bridge increased the conjugation of the molecular π system and demonstrably enhanced its electron affinity. Unfortunately, the compound proved to be susceptible to hydrolysis. This limits its use to non-aqueous systems. While incorporation of the bridge failed to appreciably change the absorption spectrum of the radical cation, it may still be useful for electrochromic applications where its increased electron affinity relative to unbridged viologens would enable color changes to be effected at lower potentials. In addition, through functionalization at the position of the silicon it could be tethered to surfaces or even polymerized. The next step towards the incorporation of siloloviologens into electrochromic devices would be fabrication of a simple proof-of-concept device containing a siloloviologen solution sandwiched between two transparent electrodes.

While we were unable to synthesize spiro-sila-OMeTAD or tetratolyl spiro-silabifluorene in our attempts, these targets may still be obtainable; either via a different synthetic approach or by modification of our cross-coupling conditions. While alkaline conditions are not a requirement for all C-C coupling reactions, they are ubiquitous in Pd-catalyzed aminations.¹⁰⁷ The base is necessary to deprotonate the amine at some point in the catalytic cycle. There are examples¹⁰⁸ of aryl-nitrogen bond formation using copper catalysts in extremely mild bases such as CsF and KHCO_3 .

Therefore one possible approach to synthesizing spiro-sila-OMeTAD from tetrabromo spiro-silabifluorene may be to explore these alternative catalytic systems.

Another, probably more reliable, approach to synthesize spiro-sila-OMeTAD would be to completely assemble the halves of the compound prior to spiro-linking them. This would avoid subjecting the relatively sensitive tetrabromospirosilabifluorene to the alkaline conditions necessary for the Buchwald-Hartwig reaction. This is the approach used by Kawashima et al. to make tetrasubstituted spiro-silabifluorenes.⁹³ The chief requirement is that the functional groups be capable of withstanding exposure to organolithium reagents. A suggested synthetic route to spiro-sila-OMeTADs is outlined below using this alternate route.



Scheme 10: Proposed alternative synthesis of 3,3',6,6'-spiro-sila-OMeTAD. *i.* Pd(dppf), 4 eq. RH, toluene, t-BuONa *ii.* 1) 2 eq. n-BuLi 2) ½ eq. SiCl₄

Starting with the “reverse” dibromodiiodobiphenyls, where the positions of the halogens are reversed from our original approach, the iodine positions could then be selectively aminated owing to their greater reactivity towards the cross-coupling reaction. The bromide positions could then be lithiated and reacted with SiCl₄ to give the corresponding spiro-sila-OMeTADs.

As for tetratolyl spiroilabifluorenes, or more broadly any kind of aryl-substituted spiroilabifluorene, Stille coupling should be a viable route. Unlike Suzuki coupling, in which the boronic acid derivatives must be activated by base, Stille coupling uses more reactive organotin coupling partners and avoids use of basic conditions. The chief drawback of Stille coupling is the greater toxicity of the organotin compounds. Zhu et al.¹⁰⁴ have already demonstrated the suitability of 2,7-tbssbf as a partner for Stille coupling. Utilization of this route could lead to interesting studies comparing the effects of 2,7 vs 3,6 isomerism on aryl-substituted spiroilabifluorenes with promising luminescence and electron transport properties.

REFERENCES

- (1) Siffert, P.; Krimmel, E. *Silicon: Evolution and Future of a Technology*; Springer Science & Business Media, 2004.
- (2) Chandrasekhar, V. *Inorganic and Organometallic Polymers*; Springer Science & Business Media, 2005.
- (3) Richter, R.; Roewer, G.; Boehme, U.; Busch, K.; Babonneau, F.; Martin, H. P.; Mueller, E. *Appl. Organomet. Chem.* **1997**, *11*, 71.
- (4) Acharya, A.; Seki, S.; Saeki, A.; Tagawa, S. *Synth. Met.* **2006**, *156*, 293.
- (5) Acharya, A.; Seki, S.; Saeki, A.; Koizumi, Y.; Tagawa, S. *Chem. Phys. Lett.* **2005**, *404*, 356.
- (6) Suzuki, H.; Hoshino, S.; Furukawa, K.; Ebata, K.; Yuan, C.-H.; Bleyl, I. *Polym. Adv. Technol.* **2000**, *11*, 460.
- (7) Tsuji, H.; Fogarty, H. A.; Ehara, M.; Fukuda, R.; Casher, D. L.; Tamao, K.; Nakatsuji, H.; Michl, J. *Chemistry* **2014**, *20*, 9431.
- (8) Bukalov, S. S.; Leites, L. A.; West, R. *Macromolecules* **2001**, *34*, 6003.
- (9) Tsuji, H.; Michl, J.; Toshimitsu, A.; Tamao, K. *J. Synth. Org. Chem. Japan* **2002**, *60*, 762.
- (10) Hissler, M.; Dyer, P. W.; Réau, R. *Coord. Chem. Rev.* **2003**, *244*, 1.
- (11) Yamaguchi, S.; Tamao, K. *Chem. Lett.* **2005**, *34*, 2.
- (12) Luo, J.; Xie, Z.; Lam, J. W. Y.; Cheng, L.; Tang, B. Z.; Chen, H.; Qiu, C.; Kwok, H. S.; Zhan, X.; Liu, Y.; Zhu, D. *Chem. Commun.* **2001**, *381*, 1740.
- (13) Liu, J.; Lam, J. W. Y.; Tang, B. Z. *J. Inorg. Organomet. Polym. Mater.* **2009**, *19*, 249.
- (14) Wong, W. W. H.; Hooper, J. F.; Holmes, A. B. *Aust. J. Chem.* **2009**, *62*, 393.
- (15) Chan, K. L.; McKiernan, M. J.; Towns, C. R.; Holmes, A. B. *J. Am. Chem. Soc.* **2005**, *127*, 7662.
- (16) Chu, T.-Y.; Lu, J.; Beaupré, S.; Zhang, Y.; Pouliot, J.-R.; Wakim, S.; Zhou, J.; Leclerc, M.; Li, Z.; Ding, J.; Tao, Y. *J. Am. Chem. Soc.* **2011**, *133*, 4250.

- (17) Lorenz, C. R.; Dewald, H. D.; Lemke, F. R. *Electroanalysis* **1997**, *9*, 1273.
- (18) Liu, J.; Yang, X.; Sun, L. *Chem. Commun. (Camb)*. **2013**, *49*, 11785.
- (19) Kane, K. M.; Lemke, F. R. *Inorg. Chem.* **1995**, *34*, 4085.
- (20) Suthar, B.; Aldongarov, A.; Irgibaeva, I. S.; Moazzen, M.; Donovan-Merkert, B. T.; Merkert, J. W.; Schmedake, T. A. *Polyhedron* **2012**, *31*, 754.
- (21) Lee, D. a.; Moon, S. K.; Sizeland, A. N.; Gould, N. W.; Gbarbea, E. M.; Owusu, D.; Jones, D. S.; Schmedake, T. A. *Inorg. Chem. Commun.* **2013**, *33*, 125.
- (22) Maguylo, C.; Chukwu, C.; Aun, M.; Blake Monroe, T.; Ceccarelli, C.; Jones, D. S.; Merkert, J. W.; Donovan-Merkert, B. T.; Schmedake, T. A. *Polyhedron* **2015**, *94*, 52.
- (23) Cahen, D.; Kahn, A. *Adv. Mater.* **2003**, *15*, 271.
- (24) Dandrade, B.; Datta, S.; Forrest, S.; Djurovich, P.; Polikarpov, E.; Thompson, M. *Org. Electron.* **2005**, *6*, 11.
- (25) Harris, D. C. *Quantitative Chemical Analysis*; 2007; Vol. 42.
- (26) Skoog, D.; Holler, F.; Nieman, T. *Principles of Instrumental Analysis*; 2008.
- (27) Kaim, W.; Fiedler, J. *Chem. Soc. Rev.* **2009**, *38*, 3373.
- (28) Mortimer, R. J. *Chem. Soc. Rev.* **1997**, *26*, 147.
- (29) Bird, C. L.; Kuhn, a. T. *Chem. Soc. Rev.* **1981**, *10*, 49.
- (30) Mortimer, R. J. *Annu. Rev. Mater. Res.* **2011**, *41*, 241.
- (31) Takenaka, S.; Ihara, T.; Takagi, M. *J. Chem. Soc., Chem. Commun.* **1990**, 1485.
- (32) Michaelis, L.; Hill, E. S. *J. Gen. Physiol.* **1933**, *16*, 859.
- (33) Du, P.; Schneider, J.; Jarosz, P.; Eisenberg, R. *J. Chem. Soc., Chem. Commun.* **2006**, 7726.
- (34) Fukuzumi, S. *Eur. J. Inorg. Chem.* **2008**, 2008, 1351.
- (35) Sen, S.; Saraidaridis, J.; Kim, S. Y.; Palmore, G. T. R. *ACS Appl. Mater. Interfaces* **2013**, *5*, 7825.
- (36) Mortimer, R. J. *Electrochim. Acta* **1999**, *44*, 2971.

- (37) Bonhôte, P.; Gogniat, E.; Campus, F.; Walder, L.; Grätzel, M. *Displays* **1999**, *20*, 137.
- (38) Sampanthar, J.; Neoh, K.; Ng, S. *Adv. Mater.* **2000**, *12*, 1536.
- (39) Sun, X. W.; Wang, J. X. *Nano Lett.* **2008**, *8*, 1884.
- (40) Sung, Y. C.; Mamak, M.; Coombs, N.; Chopra, N.; Ozin, G. a. *Nano Lett.* **2004**, *4*, 1231.
- (41) Attalla, M. I.; Summers, L. A. *J. Heterocycl. Chem.* **1985**, *22*, 751.
- (42) Launikonis, A.; Mau, A. W.; Sasse, W. H. F.; Summersb, L. A. *J. Chem. Soc., Chem. Commun.* **1986**, 1645.
- (43) Durben, S.; Baumgartner, T. *Angew. Chem. Int. Ed. Engl.* **2011**, *50*, 7948.
- (44) Stolar, M.; Borau-Garcia, J.; Toonen, M.; Baumgartner, T. *J. Am. Chem. Soc.* **2015**, *1*, 3366.
- (45) Ohshita, J.; Murakami, K.; Tanaka, D.; Ooyama, Y.; Mizumo, T. *Organometallics* **2014**, *33*, 517.
- (46) NIST. 4,4'-bipyridine UV/Vis <http://webbook.nist.gov/cgi/cbook.cgi?ID=553-26-4> (accessed Jun 6, 2015).
- (47) D'Souza, D. M.; Leigh, D. A.; Pappmeyer, M.; Woltering, S. L. *Nat. Protoc.* **2012**, *7*, 2022.
- (48) Agilent Technologies (2012). Agilent Technologies UK Ltd., Oxford, UK, CrysAlisPro Software system, Version 1.171.36.28.
- (49) Sheldrick, G. M. *Acta Crystallogr. A.* **2008**, *64*, 112.
- (50) Dolomanov, O. V.; Bourhis, L. J.; Gildea, R. J.; Howard, J. A. K.; Puschmann, H. *J. Appl. Crystallogr.* **2009**, *42*, 339.
- (51) Ballardini, R.; Credi, A.; Gandolfi, M. T.; Giansante, C.; Marconi, G.; Silvi, S.; Venturi, M. *Inorganica Chim. Acta* **2007**, *360*, 1072.
- (52) Watanabe, T.; Honda, K. *J. Phys. Chem.* **1982**, *86*, 2617.
- (53) Peon, J.; Tan, X.; Hoerner, J. D.; Xia, C.; Luk, Y. F.; Kohler, B. *J. Phys. Chem. A* **2001**, *105*, 5768.

- (54) Kuczynski, J. P.; Milosavljevic, B. H.; Lappin, A. G.; Thomas, J. K. *Chem. Phys. Lett.* **1984**, *104*, 149.
- (55) Mau, A. W.-H.; Overbeek, J. M.; Loder, J. W.; Sasse, W. H. F. *J. Chem. Soc. Faraday Trans. 2* **1986**, *82*, 869.
- (56) Shirota, Y.; Kageyama, H. *Chem. Rev.* **2007**, *107*, 953.
- (57) Stolar, M.; Baumgartner, T. *Phys. Chem. Chem. Phys.* **2013**, *15*, 9007.
- (58) Saragi, T. P. I.; Spehr, T.; Siebert, A.; Fuhrmann-Lieker, T.; Salbeck, J. *Chem. Rev.* **2007**, *107*, 1011.
- (59) Johansson, N.; dos Santos, D. A.; Guo, S.; Cornil, J.; Fahlman, M.; Salbeck, J.; Schenk, H.; Arwin, H.; Brédas, J. L.; Salanek, W. R. *J. Chem. Phys.* **1997**, *107*, 2542.
- (60) Saragi, T. P. I.; Fuhrmann-Lieker, T.; Salbeck, J. *Adv. Funct. Mater.* **2006**, *16*, 966.
- (61) Liao, Y. L.; Lin, C. Y.; Wong, K. T.; Hou, T. H.; Hung, W. Y. *Org. Lett.* **2007**, *9*, 4510.
- (62) Duan, L.; Qiao, J.; Sun, Y.; Qiu, Y. *Adv. Mater.* **2011**, *23*, 1137.
- (63) Salbeck, J.; Bauer, J.; Weissgrtel, F.; Bestgen, H. *Synth. Met.* **1997**, *91*, 209.
- (64) Pudzich, R.; Salbeck, J. *Synth. Met.* **2003**, *138*, 21.
- (65) Wu, C. C.; Lin, Y. T.; Chiang, H. H.; Cho, T. Y.; Chen, C. W.; Wong, K. T.; Liao, Y. L.; Lee, G. H.; Peng, S. M. *Appl. Phys. Lett.* **2002**, *81*, 577.
- (66) Thirion, D.; Rault-Berthelot, J.; Vignau, L.; Poriel, C. *Org. Lett.* **2011**, *13*, 4418.
- (67) Steuber, F.; Staudigel, J.; Stössel, M.; Simmerer, J.; Winnacker, A.; Spreitzer, H.; Weissörtel, F.; Salbeck, J. *Adv. Mater.* **2000**, *12*, 130.
- (68) Oyston, S.; Wang, C.; Hughes, G.; Batsanov, A. S.; Perepichka, I. F.; Bryce, M. R.; Ahn, J. H.; Pearson, C.; Petty, M. C. *J. Mater. Chem.* **2005**, *15*, 194.
- (69) Bach, U.; Comte, P.; Moser, J. E.; Weissö, F.; Grätzel, M. *Nature* **1998**, *395*, 583.
- (70) Docampo, P.; Guldin, S.; Leijtens, T.; Noel, N. K.; Steiner, U.; Snaith, H. J. *Adv. Mater.* **2014**, *26*, 4013.
- (71) Zhang, W.; Cheng, Y.; Yin, X.; Liu, B. *Macromol. Chem. Phys.* **2011**, *212*, 15.

- (72) Snaith, H. J. *J. Phys. Chem. Lett.* **2013**, *4*, 3623.
- (73) Snaith, H. J. *Adv. Funct. Mater.* **2010**, *20*, 13.
- (74) Shockley, W.; Queisser, H. J. *J. Appl. Phys.* **1961**, *32*, 510.
- (75) Fantacci, S.; Angelis, F. De; Nazeeruddin, M. K.; Grätzel, M. *J. Phys. Chem. C* **2011**, *115*, 23126.
- (76) Weisspfennig, C. T.; Lee, M. M.; Teuscher, J.; Docampo, P.; Stranks, S. D.; Joyce, H. J.; Bergmann, H.; Bruder, I.; Kondratuk, D. V.; Johnston, M. B.; Snaith, H. J.; Herz, L. M. *J. Phys. Chem. C* **2013**, *117*, 19850.
- (77) Burschka, J.; Dualeh, A.; Kessler, F.; Baranoff, E.; Cevey-Ha, N.-L.; Yi, C.; Nazeeruddin, M. K.; Grätzel, M. *J. Am. Chem. Soc.* **2011**, *133*, 18042.
- (78) Chiba, Y.; Islam, A.; Watanabe, Y.; Komiyama, R.; Koide, N.; Han, L. *Japanese J. Appl. Physics, Part 2 Lett.* **2006**, *45*.
- (79) Yella, A.; Lee, H.-W.; Tsao, H. N.; Yi, C.; Chandiran, A. K.; Yeh, C.-Y.; Zakeeruddin, S. M.; Grätzel, M. *Science*. **2011**, *334*, 629.
- (80) Ding, I. K.; Tétreault, N.; Brillet, J.; Hardin, B. E.; Smith, E. H.; Rosenthal, S. J.; Sauvage, F.; Grätzel, M.; McGehee, M. D. *Adv. Funct. Mater.* **2009**, *19*, 2431.
- (81) Cells, S. D. S.; Leijtens, T.; Ding, I.; Giovenzana, T.; Bloking, J. T.; McGehee, M. D.; Sellinger, A. *ACS Nano* **2012**, *6*, 1455.
- (82) Bailie, C. D.; Unger, E. L.; Zakeeruddin, S. M.; Grätzel, M.; McGehee, M. D. *Phys. Chem. Chem. Phys.* **2014**, *16*, 4864.
- (83) Weisspfennig, C. T.; Hollman, D. J.; Menelaou, C.; Stranks, S. D.; Joyce, H. J.; Johnston, M. B.; Snaith, H. J.; Herz, L. M. *Adv. Funct. Mater.* **2014**, *24*, 668.
- (84) Docampo, P.; Hey, A.; Guldin, S.; Gunning, R.; Steiner, U.; Snaith, H. J. *Adv. Funct. Mater.* **2012**, *22*, 5010.
- (85) Abate, A.; Leijtens, T.; Pathak, S.; Teuscher, J.; Avolio, R.; Errico, M. E.; Kirkpatrick, J.; Ball, J. M.; Docampo, P.; McPherson, I.; Snaith, H. J. *Phys. Chem. Chem. Phys.* **2013**, *15*, 2572.
- (86) Kamat, P. V. *J. Phys. Chem. Lett.* **2013**, *4*, 3733.
- (87) Liu, M.; Johnston, M. B.; Snaith, H. J. *Nature* **2013**, *501*, 395.

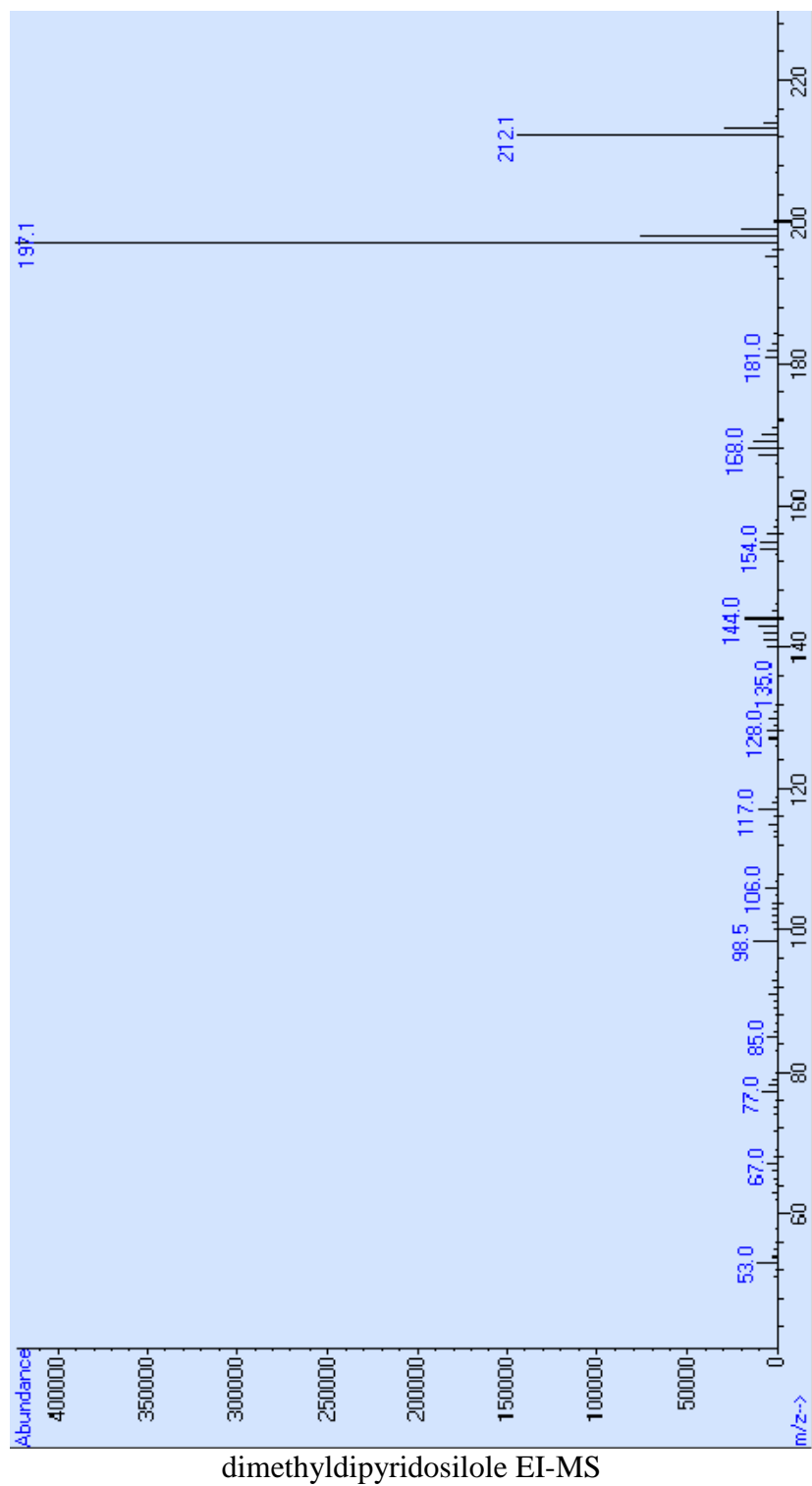
- (88) Jaramillo-Quintero, O. A.; Sánchez, R. S.; Rincón, M.; Mora-Sero, I. *J. Phys. Chem. Lett.* **2015**, *6*, 1883.
- (89) Kulkarni, A. P.; Tonzola, C. J.; Babel, A.; Jenekhe, S. A. *Chem. Mater.* **2004**, 4556.
- (90) Xiao, H.; Leng, B.; Tian, H. *Polymer.* **2005**, *46*, 5707.
- (91) Lee, S. H.; Jang, B. B.; Kafafi, Z. H. *J. Am. Chem. Soc.* **2005**, *127*, 9071.
- (92) Demers, E.; Maris, T.; Wuest, J. D. *Cryst. Growth Des.* **2005**, *5*, 1227.
- (93) Agou, T.; Hossain, M. D.; Kawashima, T. *Chem. Eur. J.* **2010**, *16*, 368.
- (94) Si, Y.; Yang, G. *Theor. Chem. Acc.* **2010**, *128*, 2.
- (95) Coropceanu, V.; Demetrio, A.; Filho, S.; Olivier, Y.; Silbey, R.; Bre, J. *Chem. Rev.* **2007**, 926.
- (96) Marcus, R. A. *Rev. Mod. Phys.* **1993**, *65*, 599.
- (97) Gilman, H.; Gorsich, R. D. *J. Am. Chem. Soc.* **1958**, *80*, 1883.
- (98) Goy, R.; Apfel, U.-P.; Elleouet, C.; Escudero, D.; Elstner, M.; Görls, H.; Talarmin, J.; Schollhammer, P.; González, L.; Weigand, W. *Eur. J. Inorg. Chem.* **2013**, *2013*, 4466.
- (99) Leroux, F. R.; Bonnafoux, L.; Heiss, C.; Colobert, F.; Lanfranchi, D. A. *Adv. Synth. Catal.* **2007**, *349*, 2705.
- (100) Dougherty, T. K.; Lau, K. S. Y.; Hedberg, F. L. *J. Org. Chem.* **1983**, *48*, 5273.
- (101) Chan, K. L.; Watkins, S. E.; Mak, C. S. K.; McKiernan, M. J.; Towns, C. R.; Pascu, S. I.; Holmes, A. B. *Chem. Commun. (Camb)*. **2005**, 5766.
- (102) Keyworth, C. W.; Chan, K. L.; Labram, J. G.; Anthopoulos, T. D.; Watkins, S. E.; McKiernan, M.; White, A. J. P.; Holmes, A. B.; Williams, C. K. *J. Mater. Chem.* **2011**, *21*, 11800.
- (103) Jeon, N. J.; Lee, H. G.; Kim, Y. C.; Seo, J.; Noh, J. H.; Lee, J.; Seok, S. Il. *J. Am. Chem. Soc.* **2014**, *136*, 7837.
- (104) Hou, Q.; Li, N. Y.; Zhang, Y.; Liu, J. G.; Zhu, H. *Adv. Mater. Res.* **2012**, *415-417*, 1364.

- (105) Kreuder, W.; Lupo, D.; Salbeck, J.; Schenk, H.; Stehlin, T. Hetero-spiro compounds and their use as electroluminescence materials. US 6,329,082 B1, 2001.
- (106) Brown, T. L.; LeMay, H. E.; Bursten, B. E.; Murphy, C. J. *Chemistry: The Central Science*; 10th ed.; Prentice Hall: Upper Saddle River, NJ, 2006.
- (107) Beletskaya, I. P.; Cheprakov, A. V. *Organometallics* **2012**, *31*, 7753.
- (108) Phillips, D. P.; Zhu, X.-F.; Lau, T. L.; He, X.; Yang, K.; Liu, H. *Tetrahedron Lett.* **2009**, *50*, 7293.

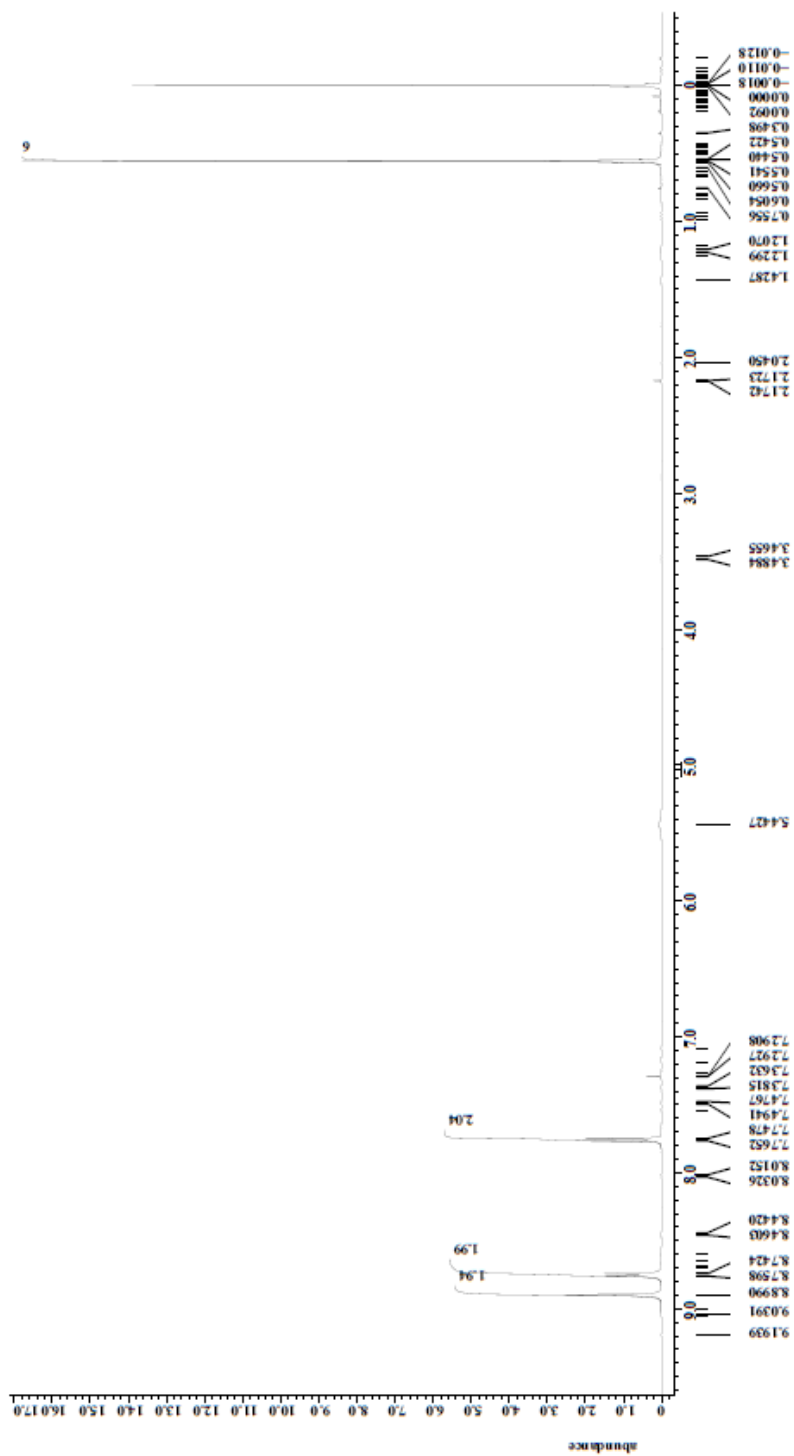
APPENDIX A: CRYSTALLOGRAPHIC DATA

Compound	3,5-dibromobpy	dimethyl DPS	SiMV(OTf) ₂	Si(OH)MV I ₂	2,7-tbssbf	3,6-tbssbf
Formula	C ₁₀ H ₆ Br ₂ N ₂	C ₁₂ H ₁₂ N ₂ Si	C ₁₆ H ₂₀ N ₂ O ₇ F ₆ Si ₂	C ₁₄ H ₂₀ N ₂ SiI ₂ O	C ₃ H ₂₀ SiBr ₄	C ₂₄ H ₁₂ SiBr ₄
Formula weight	313.99	212.33	557.54	514.21	740.21	648.07
T (K)	100(1)	100(1)	100(1)	100(1)	100(1)	100(1)
Crystal system	monoclinic	monoclinic	triclinic	triclinic	triclinic	orthorhombic
Space group	C2/c	P2 ₁ /c	P-1	P-1	P-1	Pbca
a (Å)	10.6457(4)	10.6270(10)	8.0970(5)	8.1622(7)	11.1507(8)	10.3068(1)
b (Å)	13.5666(6)	8.0640(7)	10.0306(7)	9.6383(8)	11.5156(6)	14.7303(2)
c (Å)	6.9808(3)	13.4967(11)	15.7493(8)	13.7442(11)	11.6808(8)	28.6287(4)
α (°)	90	90	102.184(5)	70.496(8)	74.098(5)	90
β (°)	90.118(4)	95.926(8)	97.311(4)	76.927(7)	80.106(6)	90
γ (°)	90	90	110.011(6)	68.934(8)	83.183(5)	90
V (Å ³)	1008.21(7)	1150.43(18)	1146.78(14)	944.14(15)	1416.99(16)	4346.47(10)
Z	4	4	2	2	2	8
D _{calc} (g/cm ³)	2.069	1.226	1.615	1.81	1.735	1.981
μ (mm ⁻¹)	7.998	0.172	3.457	3.392	7.476	9.633
F(000)	600	448	570	492	720	2480
λ (Å)	0.71073	0.71073	1.54184	0.71073	1.54184	1.54184
2θ range for data collection	7.57 to 64.45 °	6.84 to 65.46 °	9.76 to 134.18 °	6.76 to 65.66 °	7.96 to 134.34 °	10.58 to 134.1 °
Reflections collected	2854	7756	10934	20488	14454	17697
Independent reflections	1514 [R _{int} =0.0345]	3830 [R _{int} =0.0389]	4063 [R _{int} =0.0324]	6462 [R _{int} =0.0286]	5027 [R _{int} =0.0388]	3854 [R _{int} =0.0369]
Data/restraints/parameters	1514/0/66	3830/0/138	4063/0/367	6462/0/186	5027/0/326	3854/0/262
Goodness-of-fit on F ²	1.025	1.025	1.067	0.999	1.069	1.052
Final R indexes [I>=2σ (I)]	R ₁ = 0.0322 wR ₂ = 0.0670	R ₁ = 0.0509 wR ₂ = 0.1084	R ₁ = 0.0410 wR ₂ = 0.0932	R ₁ = 0.0325 wR ₂ = 0.071	R ₁ = 0.0326 wR ₂ = 0.0853	R ₁ = 0.0222 wR ₂ = 0.0487
Final R indexes [all data]	R ₁ = 0.0460 wR ₂ = 0.0744	R ₁ = 0.0761 wR ₂ = 0.1273	R ₁ = 0.0578 wR ₂ = 0.1039	R ₁ = 0.0488 wR ₂ = 0.082	R ₁ = 0.0354 wR ₂ = 0.0877	R ₁ = 0.0283 wR ₂ = 0.0512

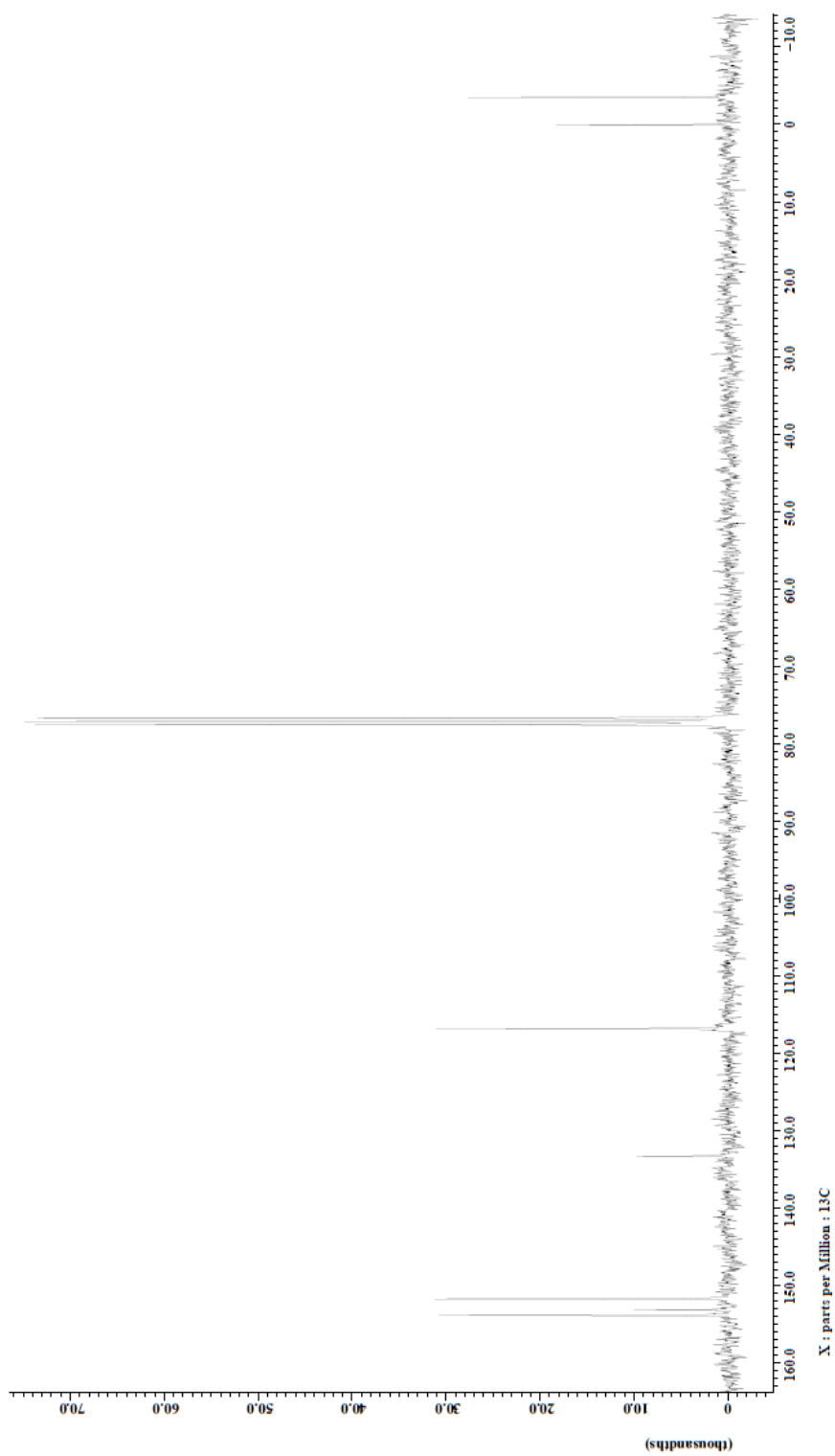
APPENDIX B: DIMETHYLDIPYRIDOSILOLE SPECTRA



APPENDIX B: (Continued)

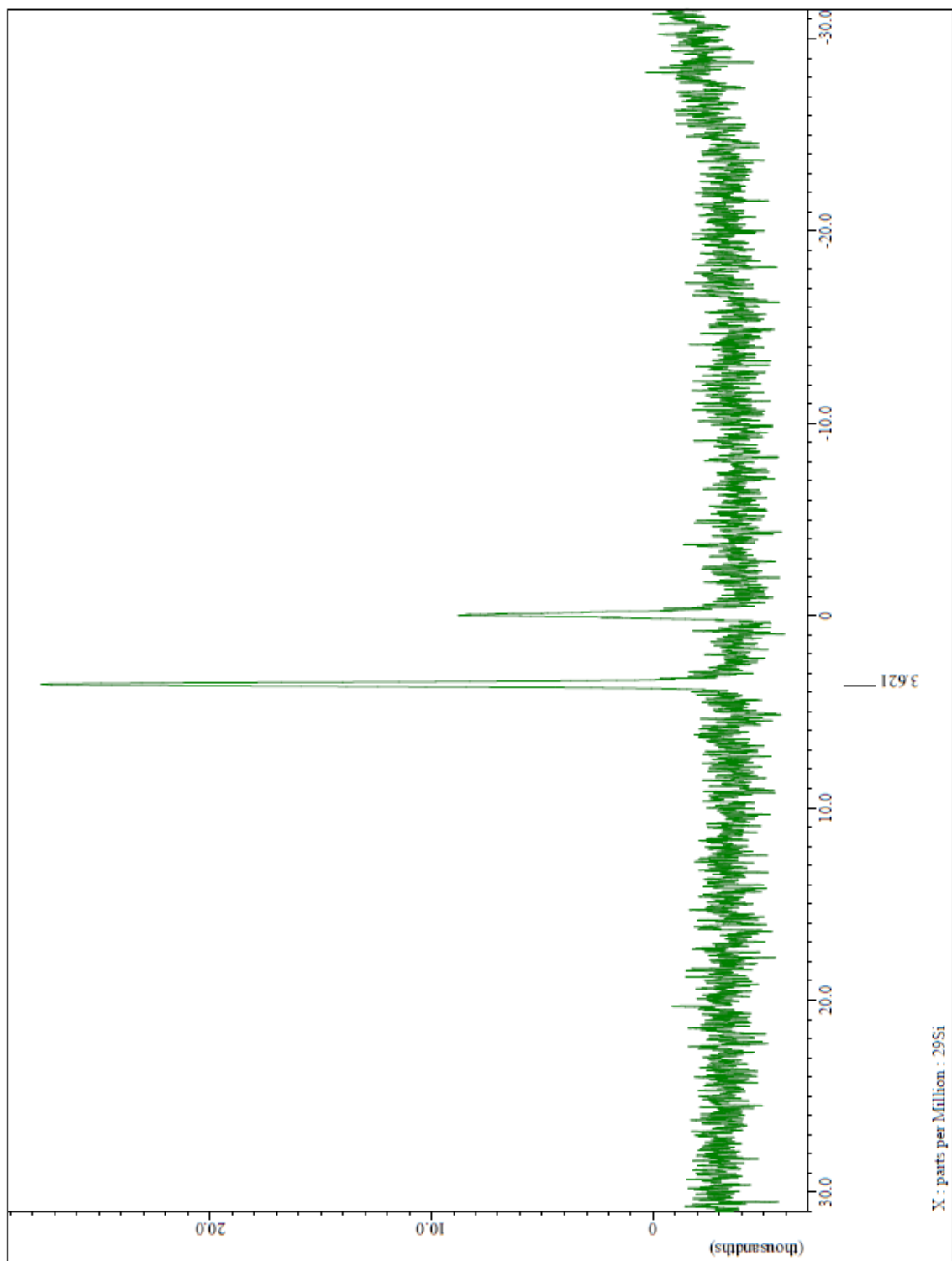
 ^1H NMR spectrum of dimethyldipyridosilole. (300 Mhz, CDCl_3)

APPENDIX B: (Continued)



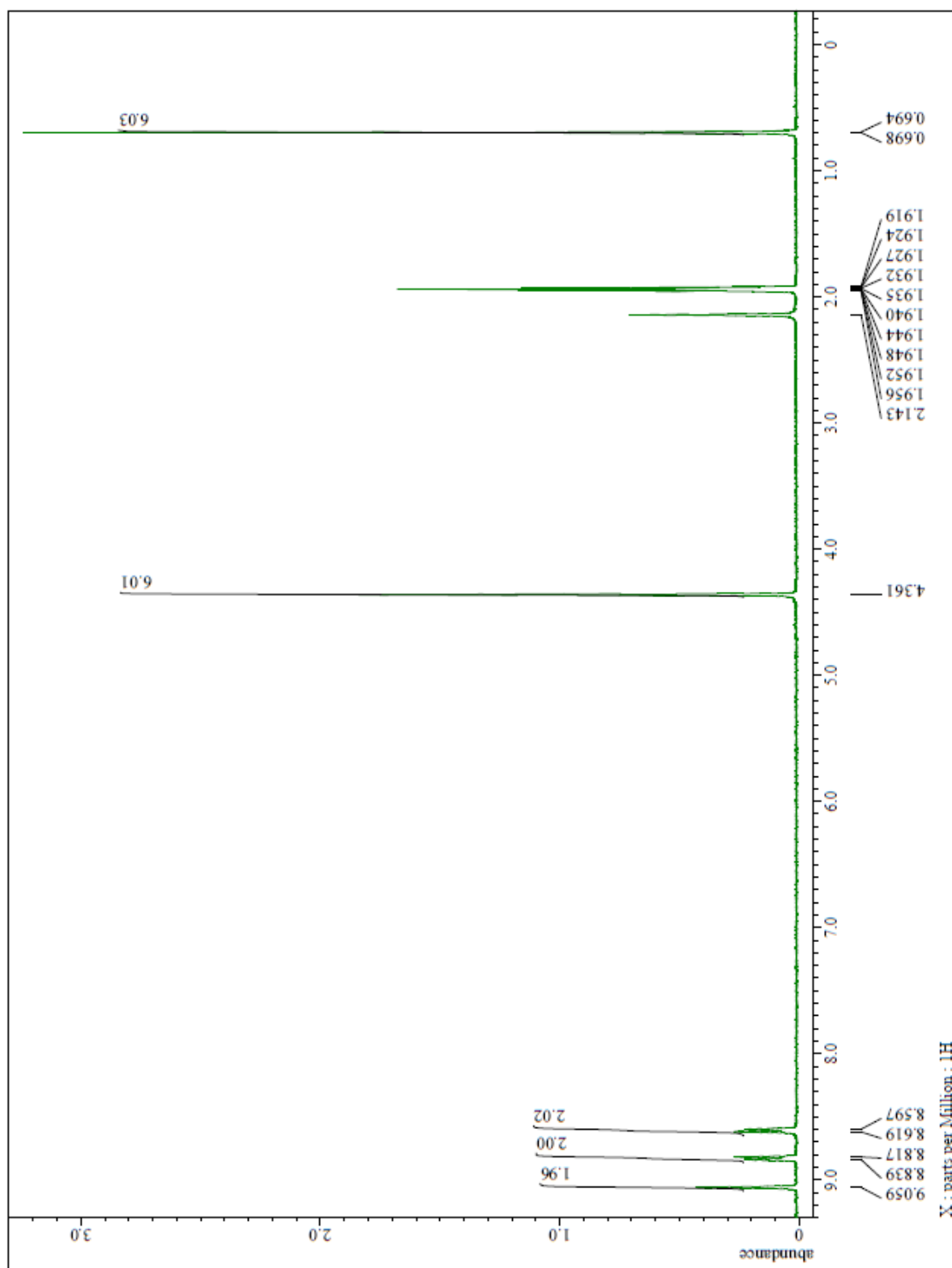
^{13}C NMR spectrum of dimethyl dipyridosilole. (300 Mhz, CDCl_3)

APPENDIX B: (Continued)

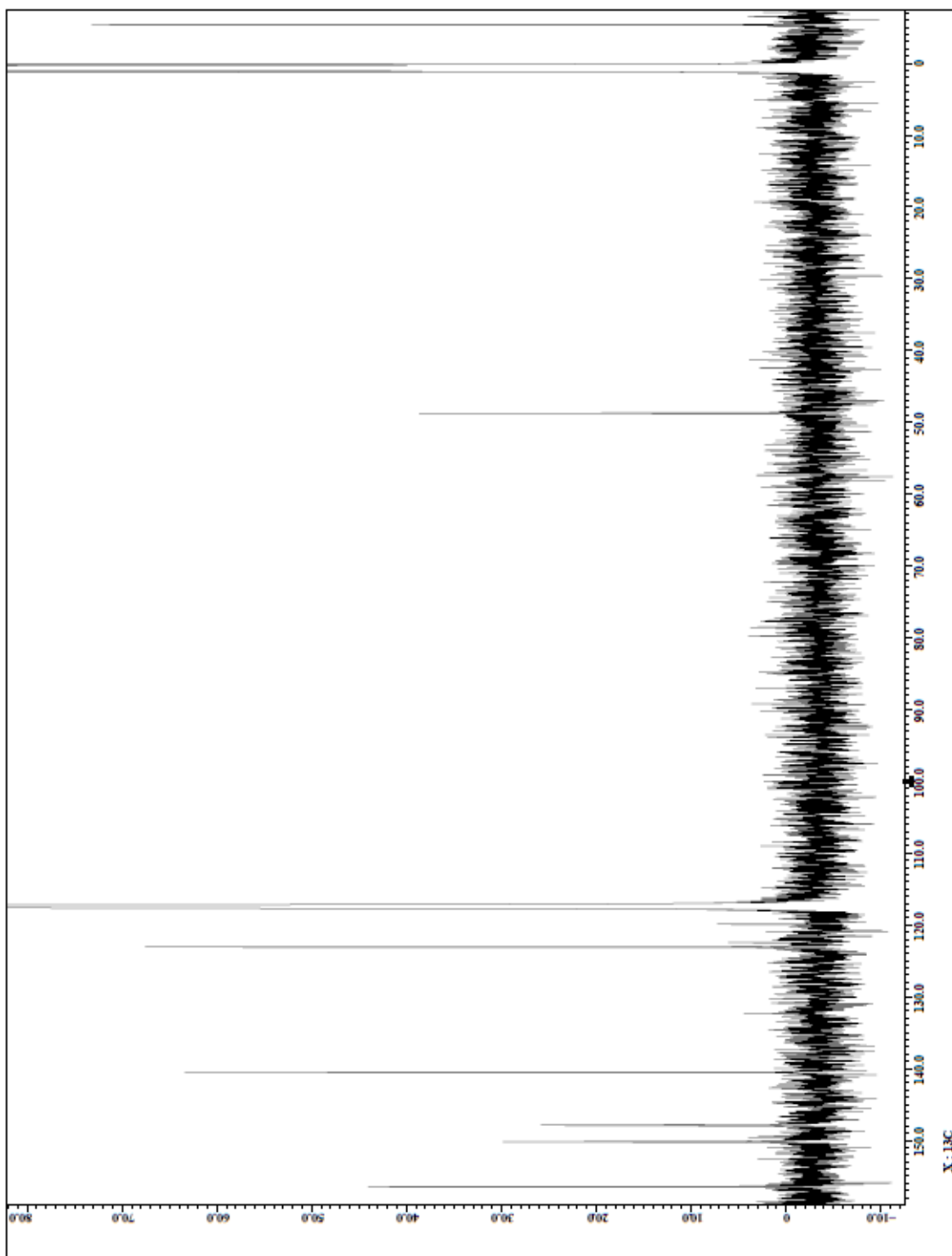


^{29}Si NMR spectrum of dimethyl dipyridosilole. (500 Mhz, CDCl_3)

APPENDIX C: SILOLOVIOLOGEN SPECTRA

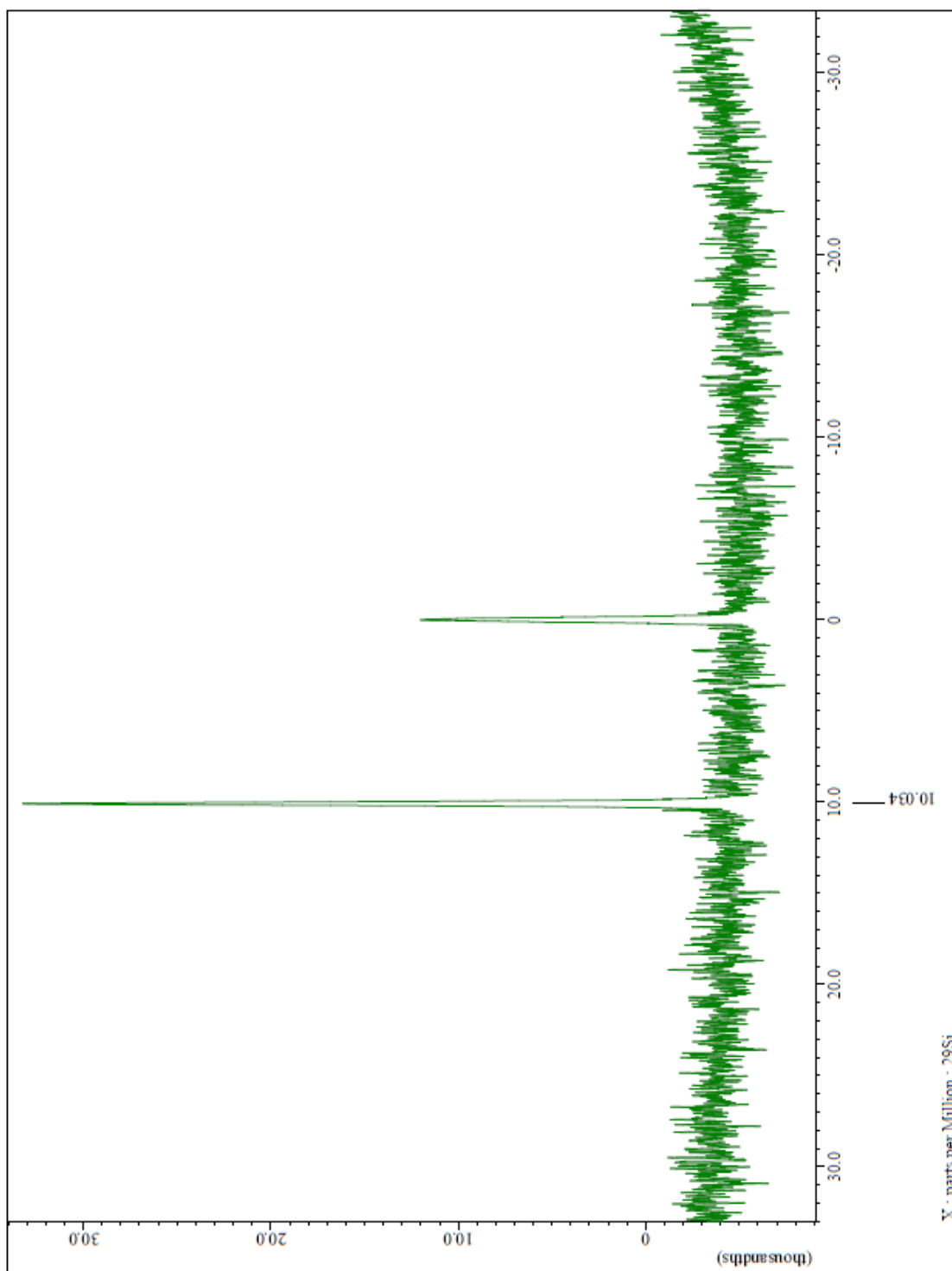
 ^1H NMR spectrum of siloloviologen triflate. (300 Mhz, CD_3CN)

APPENDIX C: (Continued)

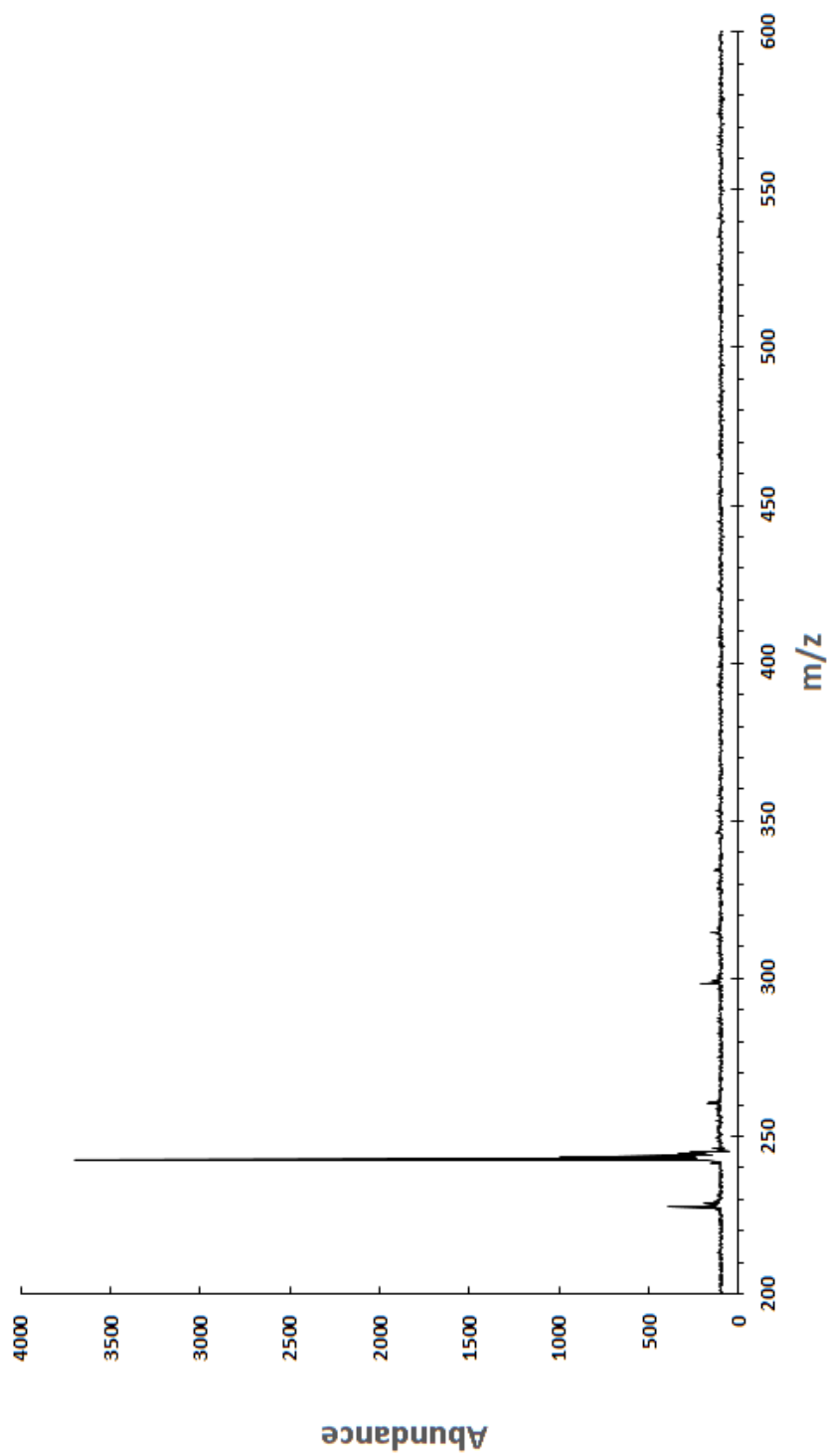


^{13}C NMR spectrum of siloloviologen. (300 Mhz, CD_3CN)

APPENDIX C: (Continued)

 ^{29}Si NMR spectrum of siloloviologen. (500 Mhz, CD_3CN)

APPENDIX C: (Continued)



MALDI-TOF-MS of siloloviogen triflate. Matrix = dithranol.

APPENDIX D: SILOLOVIOLOGEN HYDROLYSIS DATA

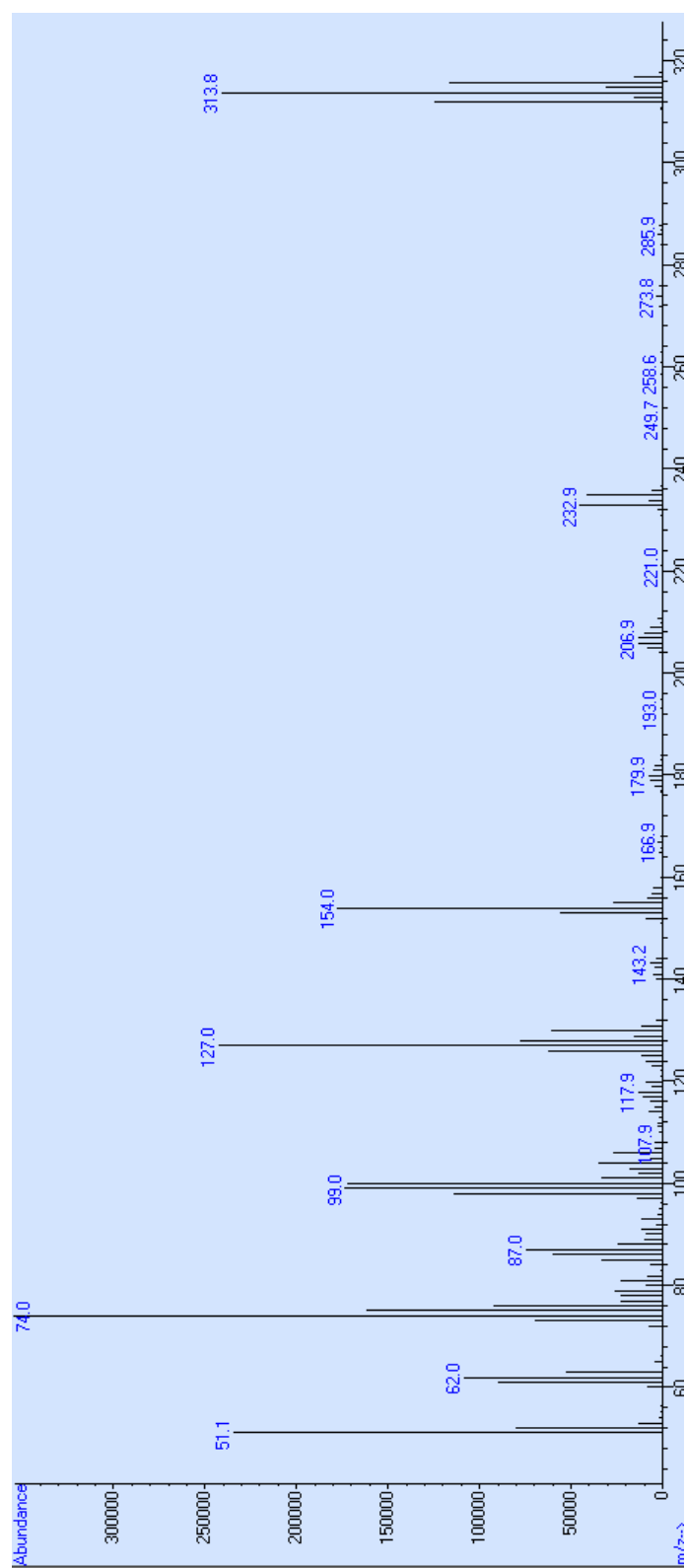
Mass SiMV(g)		0.024	volume (L)		0.00127
Mol SiMV		4.44444E-05	[SiMV] initial (M)		0.034996
time (d)	time (h)	SiMV	Si-OH	[SiMV]	ln [SiMV]
4.5	111	1.11	0.15	0.03082948	-3.47928
6.5	158	1.22	0.25	0.029043989	-3.53894
8.5	208	1.1	0.26	0.028305285	-3.56471
10.5	259	1.09	0.3	0.027442613	-3.59566
12.5	302	1.11	0.36	0.026425268	-3.63343
15.5	380	1.11	0.45	0.024900734	-3.69286
19.5	476	1	0.49	0.023486997	-3.75131
22.5	549	1	0.56	0.022433093	-3.79722

Data for the hydrolysis of SiMV in CD₃CN.

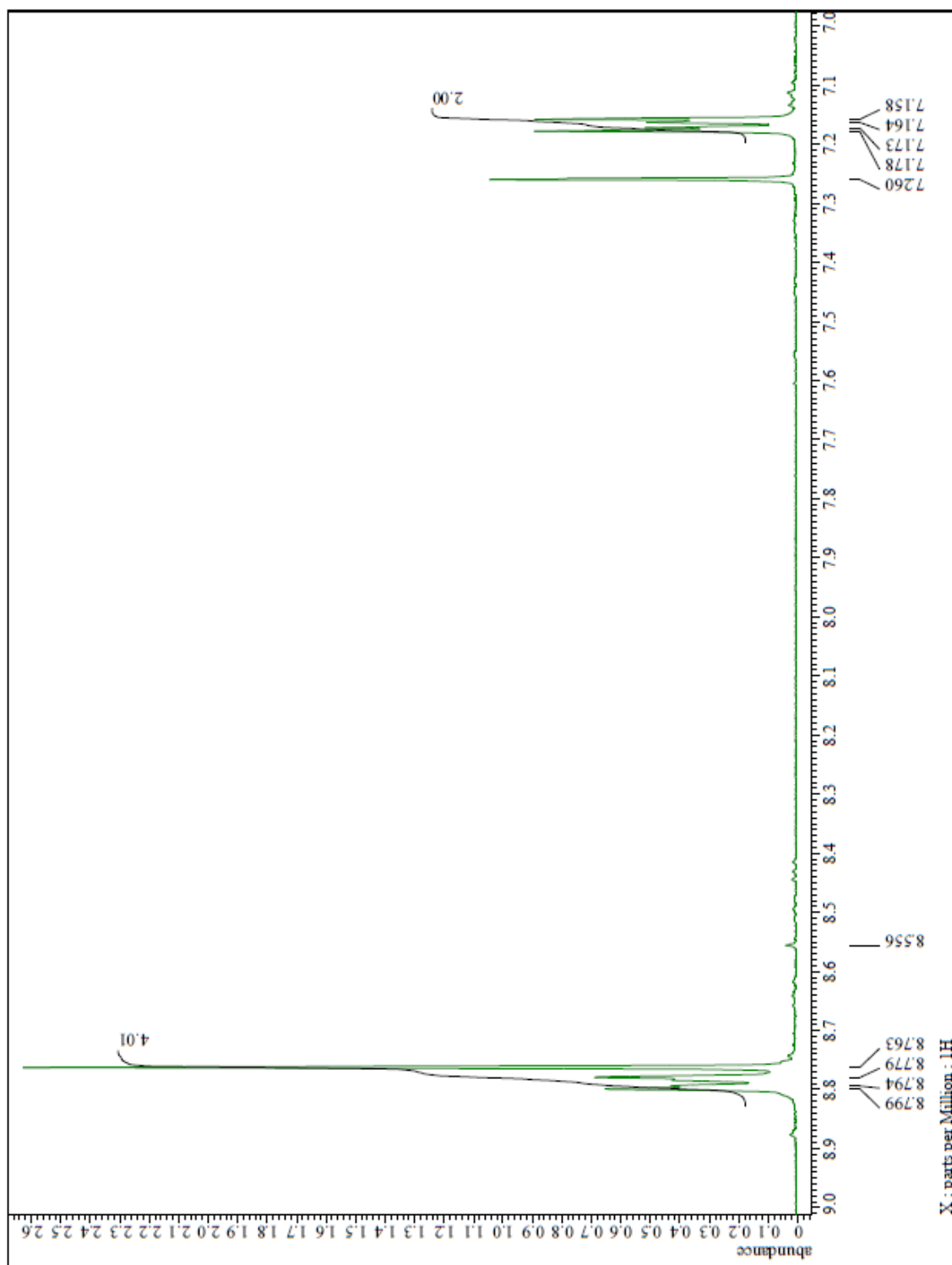
t (min)	A (SiMV)	B (SiOH)	A+B	A/A+B	[SiMV]	ln [SiMV]	[SiOH]
0	18.3055	1.9641	20.2696	0.903101	0.034268	-3.37353	0.003677
20	13.0252	7.1603	20.1855	0.645275	0.024485	-3.70969	0.01346
40	9.4369	10.7781	20.215	0.466827	0.017714	-4.03341	0.020231
60	6.97	13.3101	20.2801	0.343687	0.013041	-4.33964	0.024904
80	5.1633	15.2017	20.365	0.253538	0.009621	-4.64386	0.028325
100	3.8891	16.6026	20.4917	0.189789	0.007202	-4.93346	0.030744
120	2.9335	17.6134	20.5469	0.142771	0.005417	-5.21813	0.032528
140	2.2481	18.3547	20.6028	0.109116	0.00414	-5.48696	0.033805
160	1.6769	18.9568	20.6337	0.08127	0.003084	-5.78159	0.034861
180	1.2886	19.4435	20.7321	0.062155	0.002358	-6.04974	0.035587
200	0.9988	19.8467	20.8455	0.047914	0.001818	-6.30995	0.036127
220	0.7294	20.0458	20.7752	0.035109	0.001332	-6.62091	0.036613
240	0.5739	20.3217	20.8956	0.027465	0.001042	-6.86645	0.036903
260	0.4447	20.498	20.9427	0.021234	0.000806	-7.12376	0.037139
280	0.3355	20.5966	20.9321	0.016028	0.000608	-7.40503	0.037337
300	0.2388	20.7046	20.9434	0.011402	0.000433	-7.74557	0.037512
320	0.1868	20.8637	21.0505	0.008874	0.000337	-7.99626	0.037608
340	0.1355	20.9334	21.0689	0.006431	0.000244	-8.3182	0.037701
360	0.1138	21.0332	21.147	0.005381	0.000204	-8.49643	0.037741
380	0.075198	21.0174	21.0926	0.003565	0.000135	-8.90817	0.03781

Data for the hydrolysis of SiMV in D₂O.

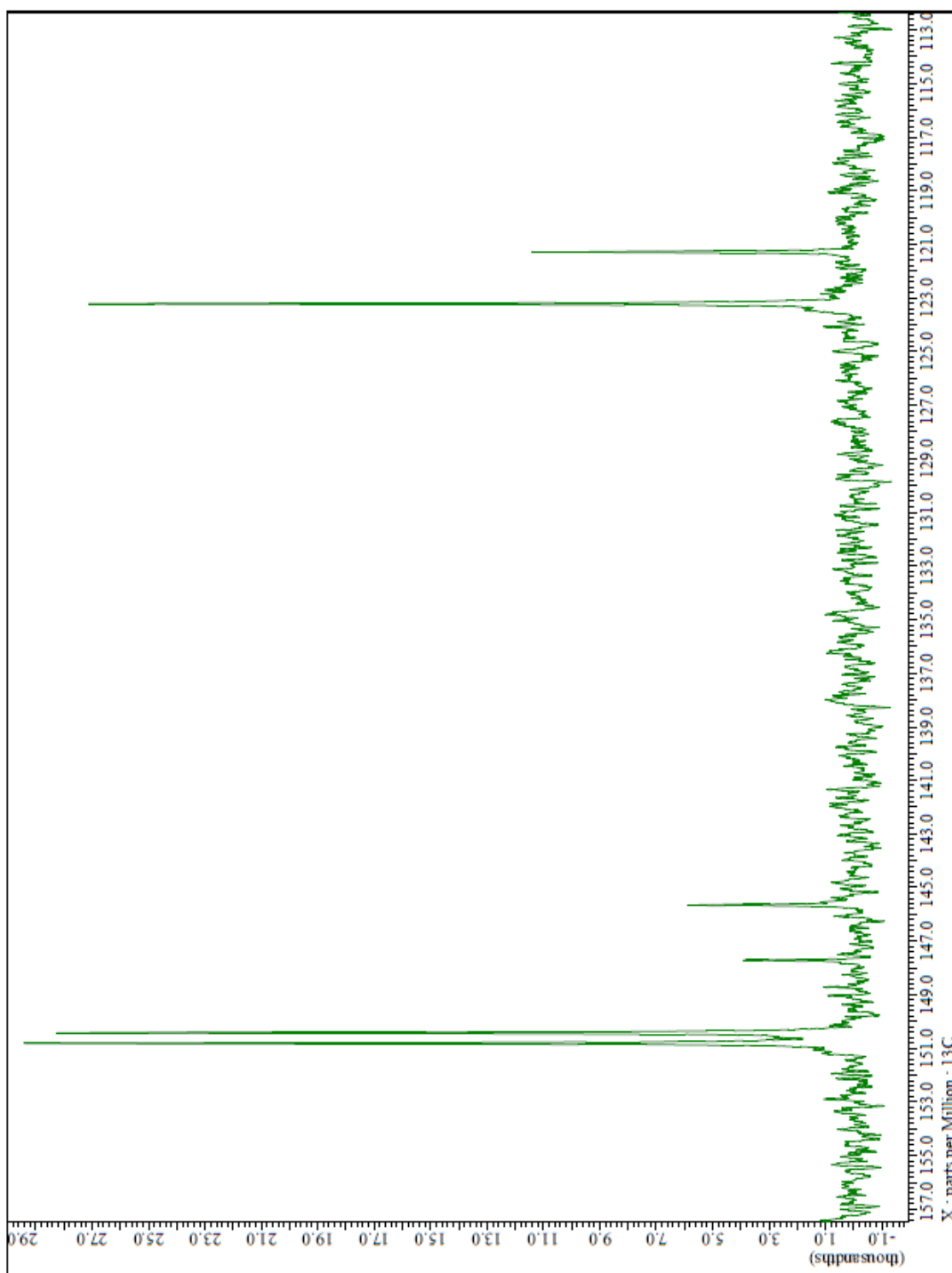
APPENDIX E: 3,5-DIBROMO-4-4'-BIPYRIDINE SPECTRA



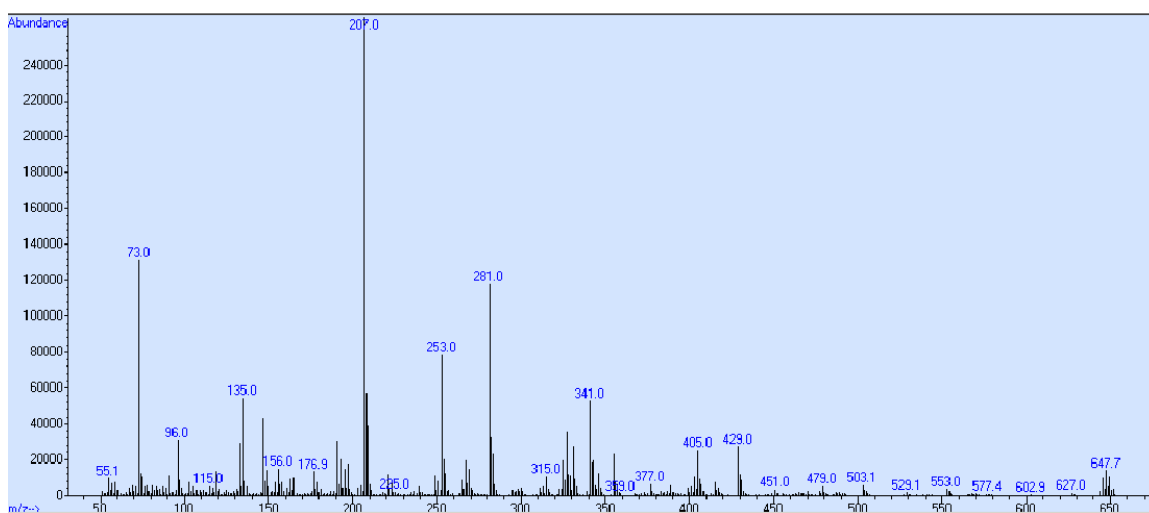
APPENDIX E: (Continued)

3,5-dibromo-4,4'-bipyridine ^1H NMR (300 MHz, CDCl_3)

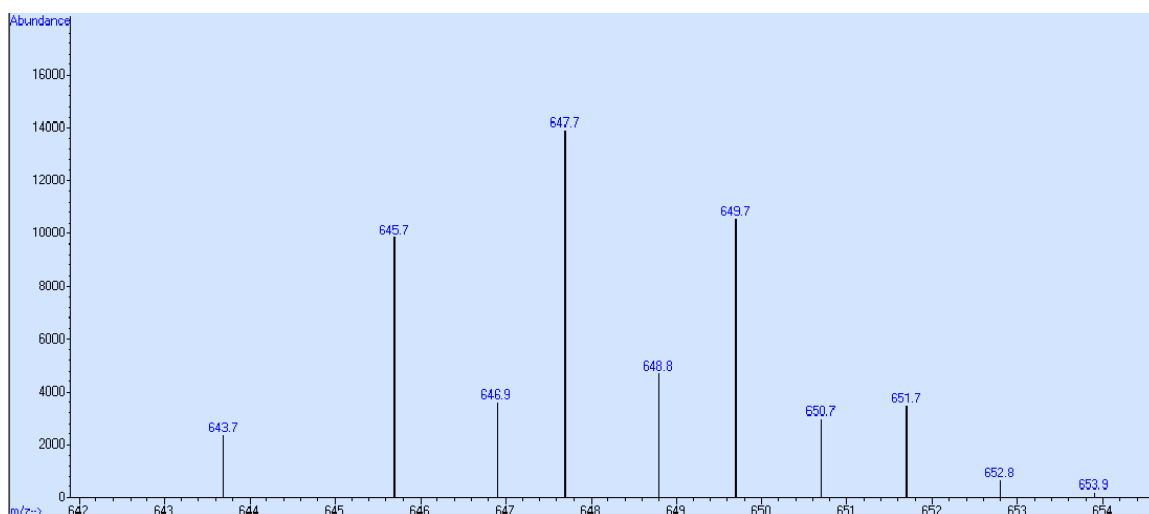
APPENDIX E: (Continued)

3,5-dibromo-4,4'-bipyridine ^{13}C NMR (300 MHz, CDCl_3)

APPENDIX F: 3,3',6,6'-TETRABROMOSPIROSILABIFLUORENE SPECTRA

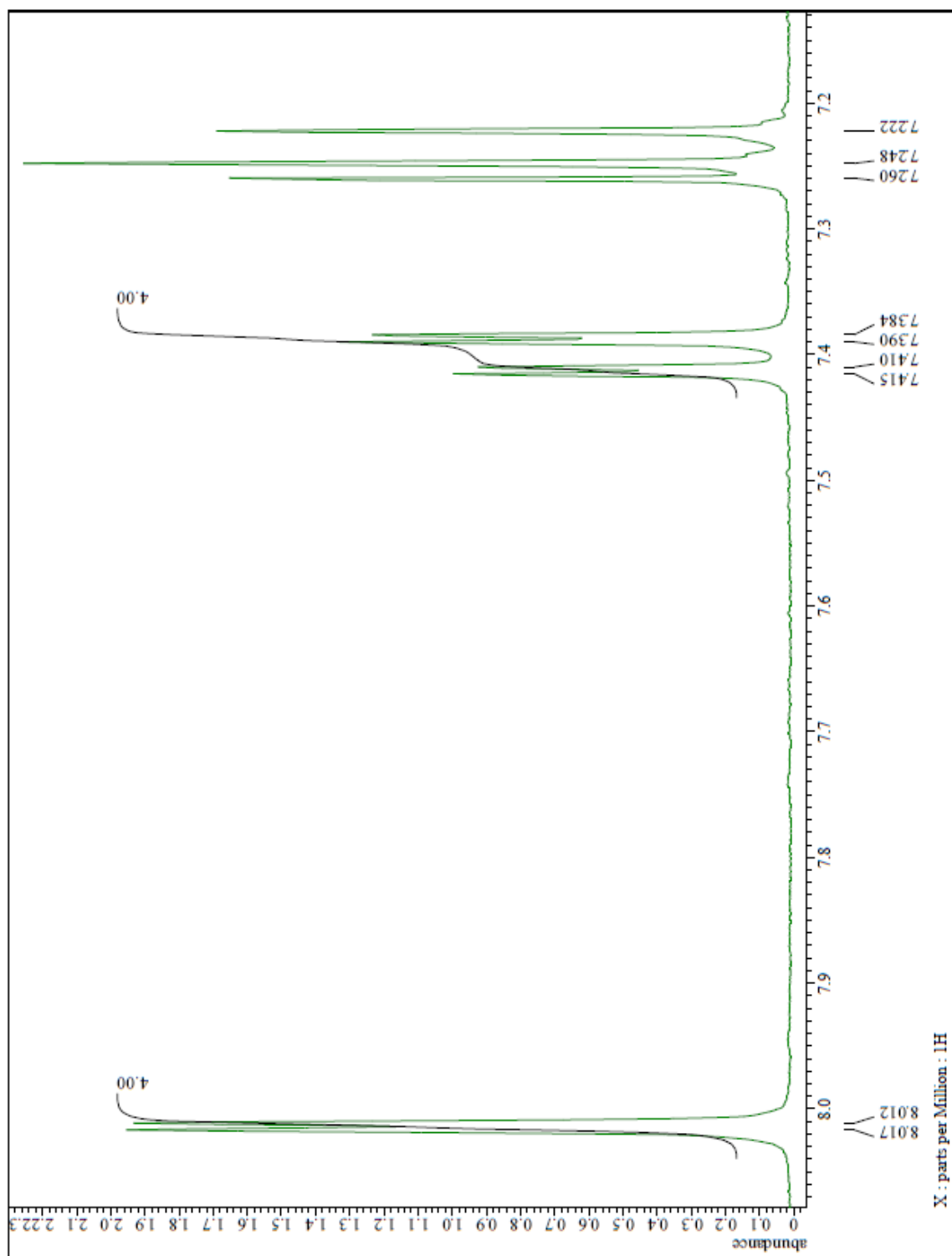


3,3',6,6'-tetrabromospirosilabifluorene EI-MS

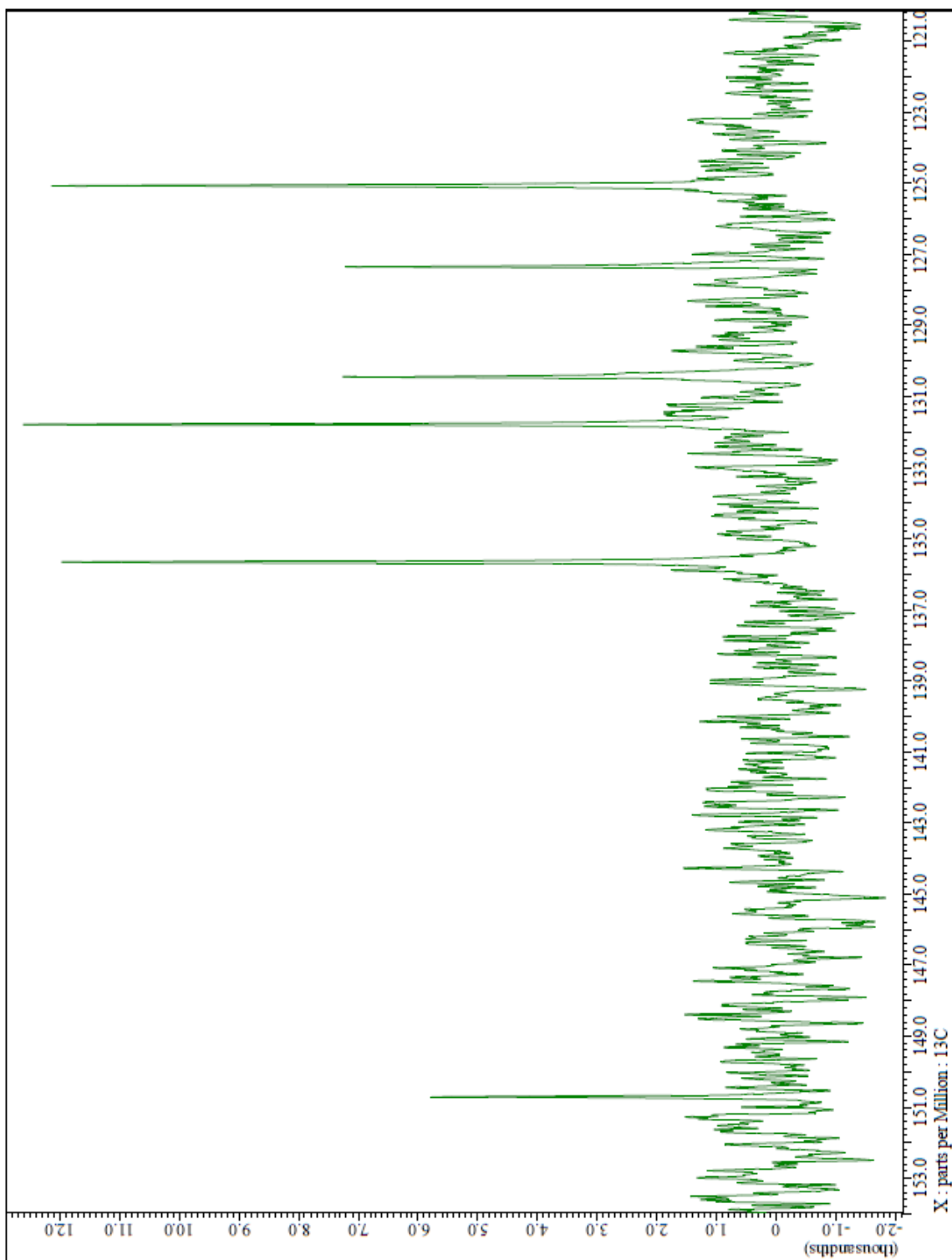


3,3',6,6'-tetrabromospirosilabifluorene EI-MS molecular ion peak

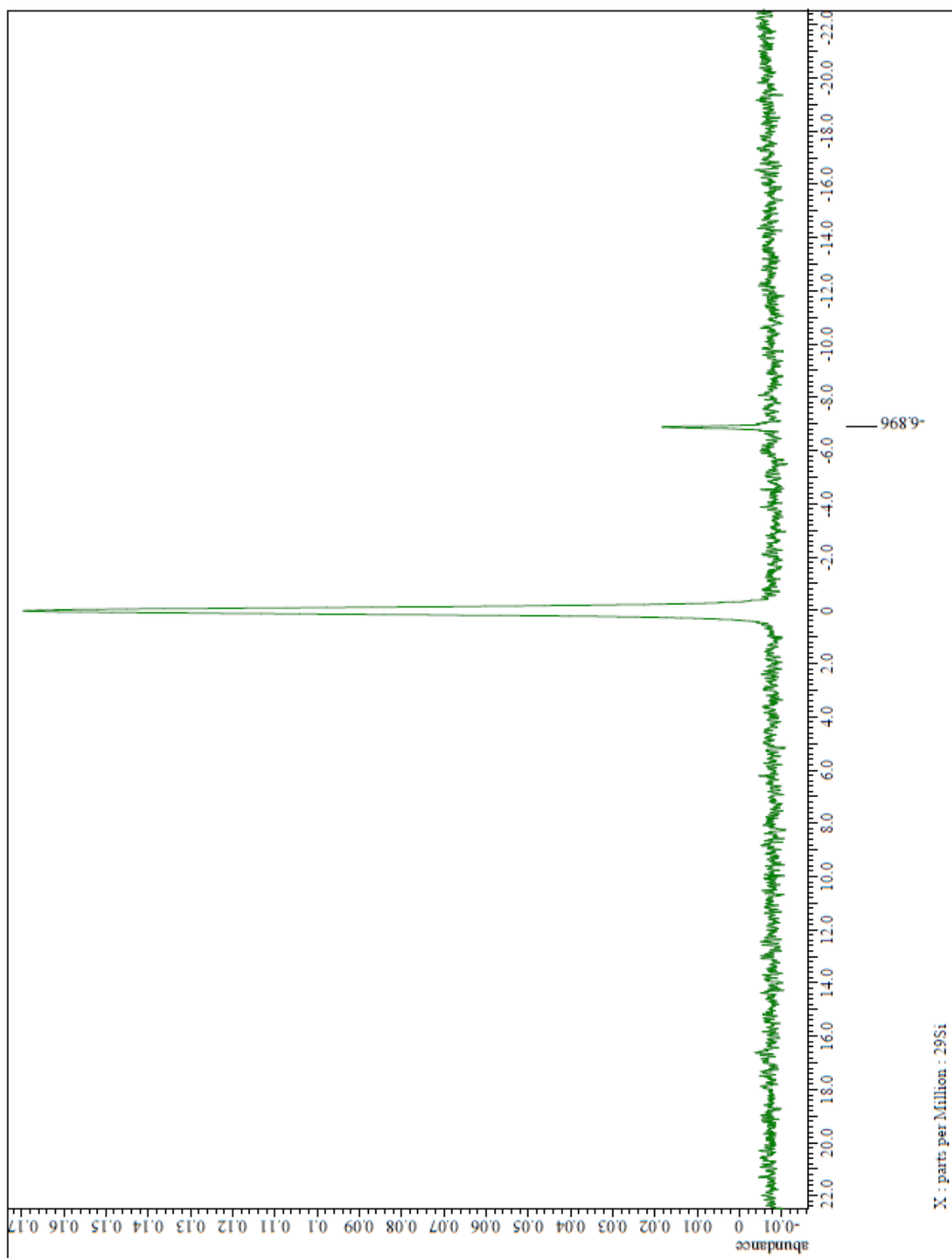
APPENDIX F: (Continued)

3,3',6,6'-tetrabromospirosilabifluorene $^1\text{H-NMR}$ (300 MHz, CDCl_3)

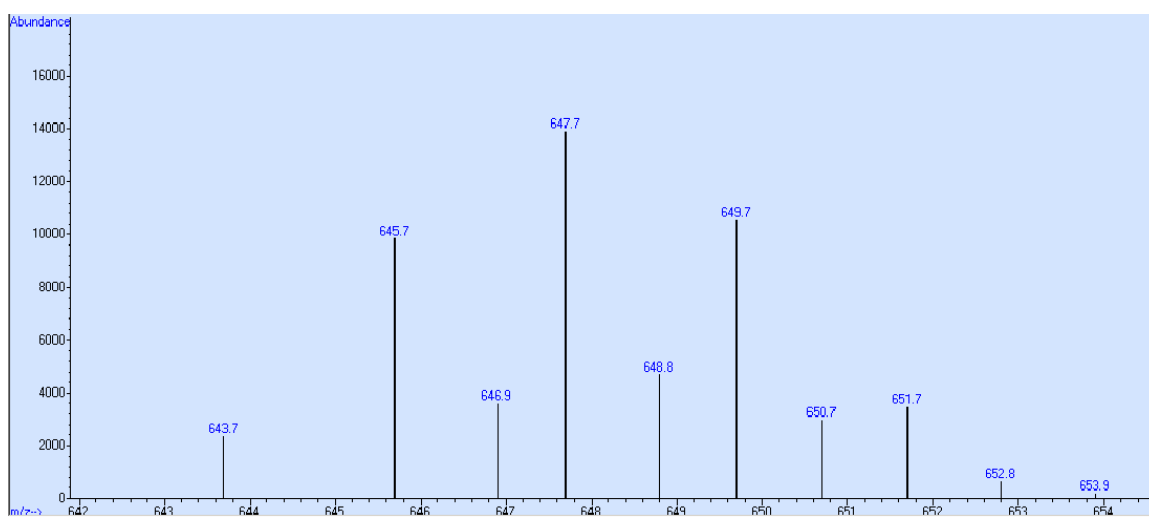
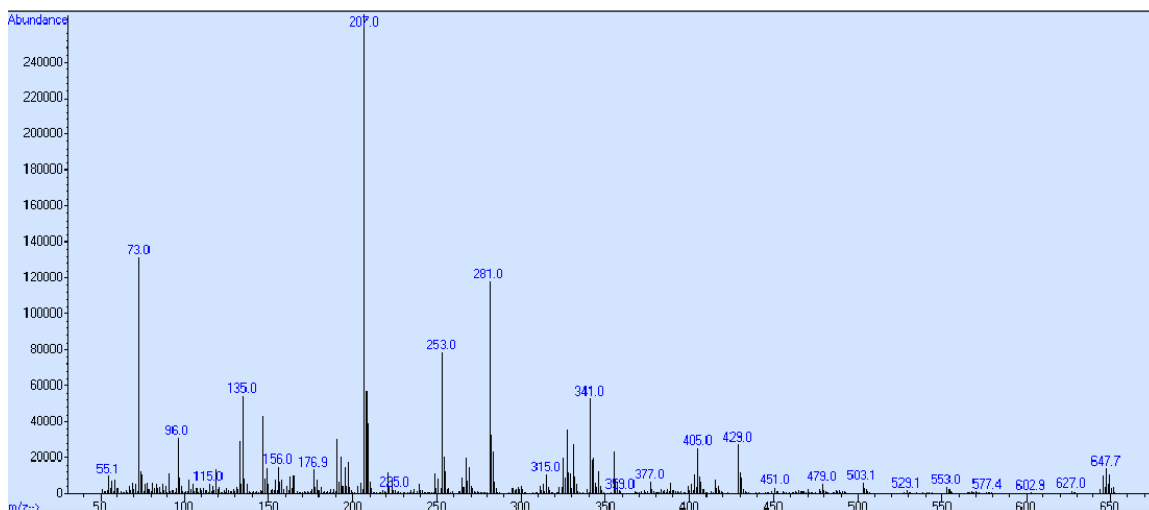
APPENDIX F: (Continued)

3,3',6,6'-tetrabromospirosilabifluorene ^{13}C -NMR (300 MHz, CDCl_3)

APPENDIX F: (Continued)

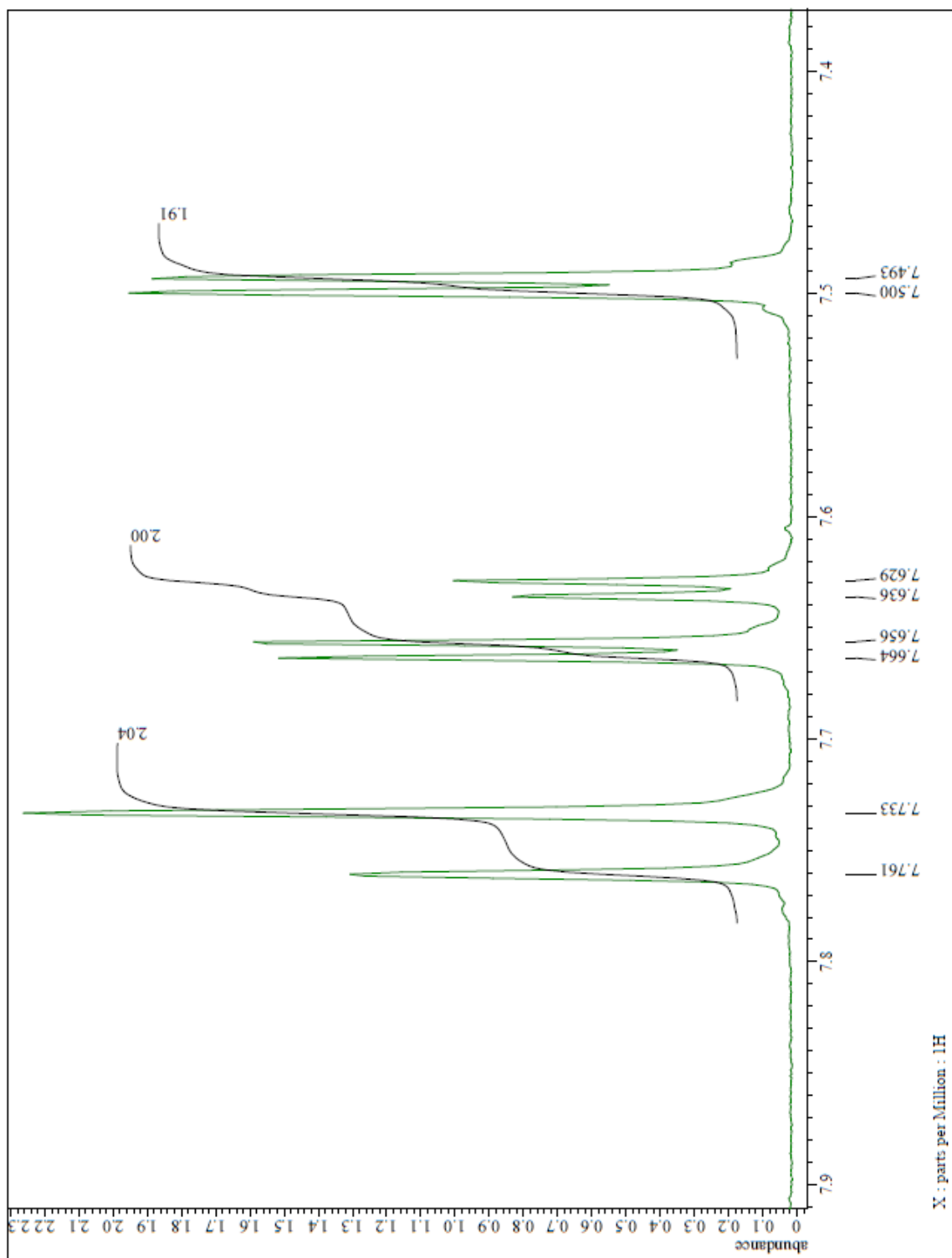
3,3',6,6'- tetrabromospirosilabifluorene ^{29}Si -NMR (500 MHz, CDCl_3)

APPENDIX G: 2,2',7,7'-TETRABROMOSPIROSILABIFLUORENE SPECTRA

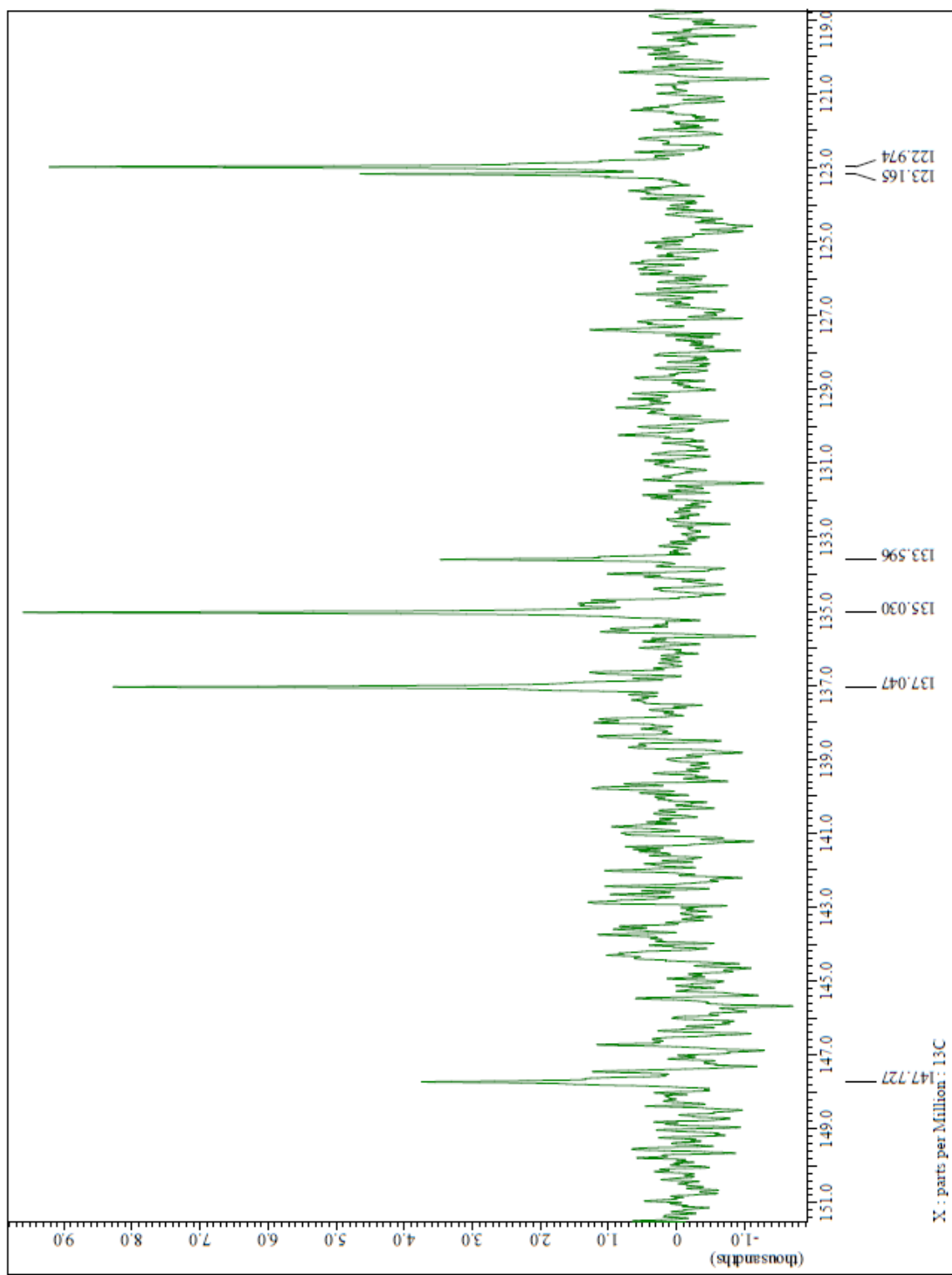


3,3',6,6'- tetrabromospirosilabifluorene EI-MS molecular ion peak

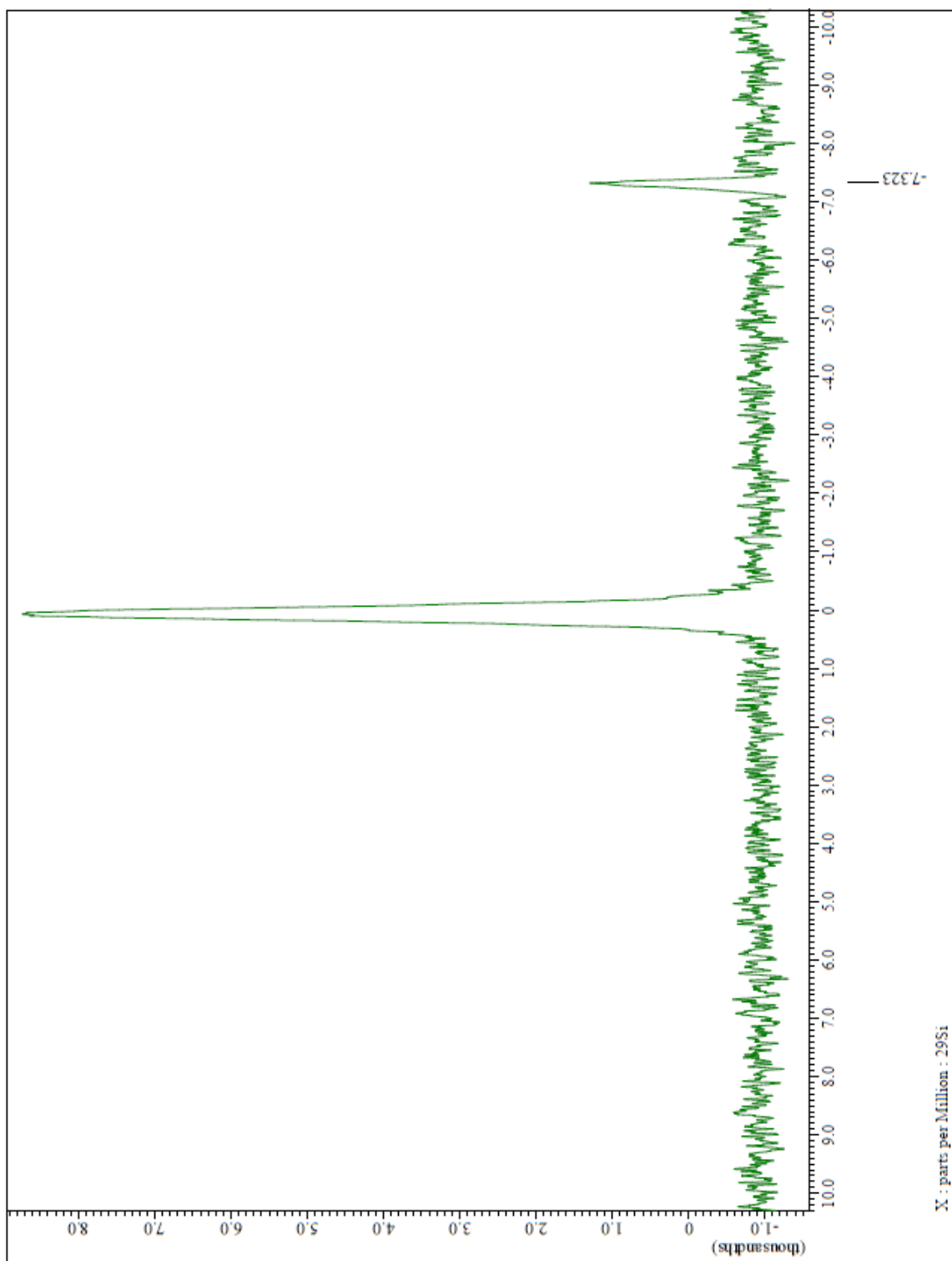
APPENDIX G: (Continued)

2,2',7,7'-tetrabromospirosilabifluorene $^1\text{H-NMR}$ (300 MHz, CDCl_3)

APPENDIX G: (Continued)

2,2',7,7'-tetrabromospirosilabifluorene ^{13}C -NMR (300 MHz, CDCl_3)

APPENDIX G: (Continued)

2,2',7,7'-tetrabromospirosilabifluorene ^{29}Si -NMR (500 MHz, CDCl_3)